EVALUATION OF ALTERNATIVE RESISTANCE MECHANISMS FOR PROGRESSIVE COLLAPSE

A Thesis

presented to

the Faculty of the Graduate School

at the University of Missouri-Columbia

In Partial Fulfillment

of the Requirements for the Degree

Master of Science

---

by

STEPHEN MARTIN STINGER

Dr. Sarah Orton, Thesis Supervisor

MAY 2011

The undersigned, appointed by the dean of the Graduate School, have examined the thesis entitled

EVALUATION OF ALTERNATIVE RESISTANCE
MECHANISMS FOR
PROGRESSIVE COLLAPSE

presented by Stephen Martin Stinger,

a candidate for the degree of Master of Science in Civil Engineering,

and hereby certify that, in their opinion, it is worthy of acceptance.

Professor Sarah Orton

Professor Hani Salim

Professor Sherif El-Gizawy

DEDICATION

I would like to thank my Mom, Dad and the rest of my family for always supporting me.

ACKNOWLEDGEMENTS

I would like to express my gratitude to everyone in the Civil & Environmental Engineering Department at the University of Missouri. I would especially like to thank my graduate advisor Professor Sarah Orton and my undergraduate advisor Professor Hani Salim for allowing me to work for them.

I wish to express my appreciation to Rex Gish and Richard Oberto from Engineering Technical Services for sharing their knowledge and expertise. Also, I want to extend gratitude to my fellow graduate students Joe Kirby, Stephen Older, and Aaron Saucier for helping me out. Lastly, I would like to thank my undergraduate research assistants Matthew Brune, Jeremiah Kasinger, Matthew Muenks, Russell Voss, Todd Witt, and Matthew Wombacher for all their time and efforts.

TABLE OF CONTENTS

ACKNOWLEDGEMENTS ii

LIST OF FIGURES v

LIST OF TABLES xii

ABSTRACT xiii

Chapter

1. INTRODUCTION 1

1.1. Problem 2

1.2. Objectives and Research Approach 3

1.3. Outline 4

2. LITTERATURE REVIEW 5

2.1. Progressive Collapses 5

2.2. Non-Collapsed Buildings 7

2.3. Resistance Mechanisms 9

2.3.1. Catenary Action 10

2.3.2. Vierendeel Action 12

2.3.3. Compressive Arch Action 13

2.4. Previous Research 13

2.5. Standards 22

3. EXPERIMENT SETUP 27

3.1. Design of the Full Scale Reinforced Concrete Frames 27

3.2. Design of the Discontinuous Reinforcement Test Frame 34

3.3. Design of the Continuous Reinforcement Test Frame 38

3.4. Design of the Infill Wall Test Frame 40

3.5. Construction of the Reinforced Concrete Test Frames 41

3.6. Design and Construction of Test Setup 53
3.7. Instrumentation 64
3.8. Material Properties 71
4. TEST RESULTS 77
4.1. Discontinuous Reinforcement Frame 77
4.2. Continuous Reinforcement Frame 89
4.3. Infill Wall Frame 101
4.4. Combined Results and Discussion 115
5. CONCLUSION 122
REFERENCES 128

LIST OF FIGURES

Figure Page

Figure 2.1.1: Ronan Point Tower after collapse (Nair, 2004) 6

Figure 2.1.2: Murrah Building after explosion (Crawford, 2002) 7

Figure 2.2.1: Pentagon Building after the crash (Mlakar et al., 2003) 8

Figure 2.2.2: Office building damaged by system boiler explosion (Sucuoglu et al., 1994) 9

Figure 2.3.1: Change in moment diagram due to loss of column (Orton, 2007) 10

Figure 2.3.1.1: Catenary tension forces throughout a building (Orton, 2007)..... 11

Figure 2.3.1.2: Transfer of catenary forces through stirrups (Orton, 2007) 12

Figure 2.4.1: Catenary tests of precast floor strips (Regan, 1975) 14

Figure 2.4.2: Results of catenary tests of precast floor strips (Regan, 1975) 15

Figure 2.4.3: Force vs. displacement graph (Sasani and Kropelnicki, 2007) 16

Figure 2.4.4: Vertical and axial loads vs. center displacement for beams with discontinuous reinforcement (Orton, 2007). 18

Figure 2.4.5: Photo of test NR-2 under catenary action (Orton, 2007) 18

Figure 2.4.6: Vertical and axial loads vs. center displacement for beams with continuous reinforcement (Orton, 2007). 19

Figure 2.4.7: A reinforced concrete four-bay by three-story one-third scale model frame (Yi and Kunnath, 2008) 20

Figure 2.4.8: Middle column load vs. unloading displacement (Yi and Kunnath, 2008) 21

Figure 2.5.1: System of tie forces (DoD, 2004)..... 24

Figure 2.5.2: Forces on structure due to catenary loads (NIST, 2007)..... 25

Figure 3.1.1: RISA model of a typical office building 29

Figure 3.1.2: Column cross-section for full scale frame 30
Figure 3.1.3: Beam cross-section for full scale frame 30
Figure 3.1.4: Transverse reinforcement detailing for full scale frame 31
Figure 3.1.5: Longitudinal reinforcement layout for full scale discontinuous frame 33
Figure 3.1.6: Transverse reinforcement layout for full scale discontinuous frame 33
Figure 3.2.1: Column cross-section for quarter scale frame 35
Figure 3.2.2: Beam cross-section for quarter scale frame 35
Figure 3.2.3: Transverse reinforcement detailing for quarter scale frame 36
Figure 3.2.4: Design of discontinuous reinforcement test frame 37
Figure 3.2.5: Transverse reinforcement layout for discontinuous reinforcement test frame 37
Figure 3.3.1: Design of continuous reinforcement test frame 39
Figure 3.3.2: Transverse reinforcement layout for continuous reinforcement test frame 40
Figure 3.4.1: Test frame with infill wall 41
Figure 3.5.1: Design of formwork 42
Figure 3.5.2: Construction of formwork 42
Figure 3.5.3: Construction of formwork 43
Figure 3.5.4: Construction of formwork 43
Figure 3.5.5: Construction of formwork 43
Figure 3.5.6: Bending of beam stirrup 44
Figure 3.5.7: Bending of column stirrup 44
Figure 3.5.8: Bending of longitudinal bar 45
Figure 3.5.9: Beam stirrup 45
Figure 3.5.10: Column stirrup 45
Figure 3.5.11: Bent longitudinal bars 46
Figure 3.5.12: Bars grinded and scrubbed clean 46

Figure 3.5.13: Strain gages on bars 47
Figure 3.5.14: PCP pipe in pedestals 48
Figure 3.5.15: Hooked #4 end-threaded bars 48
Figure 3.5.16: Lifting insert in the top of each column 48
Figure 3.5.17: Middle column of the frame 49
Figure 3.5.18: Outer column of frame 49
Figure 3.5.19: Reinforcement tied into formwork 50
Figure 3.5.20: Pouring and vibrating concrete 51
Figure 3.5.21: Smoothing out the concrete 51
Figure 3.5.22: Poured concrete frame 51
Figure 3.5.23: Compression test cylinders 52
Figure 3.5.24: Lifting insert and end-threaded bars 52
Figure 3.5.25: PCP pipes in pedestals 53
Figure 3.5.26: Finished concrete frame 53
Figure 3.6.1: RISA model with missing column 54
Figure 3.6.2: Design of reaction frame 56
Figure 3.6.3: Reaction frame 56
Figure 3.6.4: Reaction frame 57
Figure 3.6.5: Reaction frame bolted into the structural floor 57
Figure 3.6.6: Reaction frame tied into the concrete frame 57
Figure 3.6.7: Design of anchors for the pedestals 58
Figure 3.6.8: Anchor for the pedestal 59
Figure 3.6.9: Pedestal anchored to the floor 59
Figure 3.6.10: Design of the collar for the center column 60
Figure 3.6.11: Details of the collar 61

Figure 3.6.12: Details of the linear ball bearings 61
Figure 3.6.13: Collar for the center column 62
Figure 3.6.14: Collar for the center column 62
Figure 3.6.15: Design of the connection to the actuator 63
Figure 3.6.16: Connection to the actuator 64
Figure 3.6.17: Connection to the actuator 64
Figure 3.7.1: Data acquisition system 65
Figure 3.7.2: Strain gage layout for test frames with discontinuous reinforcement 66
Figure 3.7.3: Strain gage layout for test frame with continuous reinforcement 67
Figure 3.7.4: Load cells 68
Figure 3.7.5: Load cell 68
Figure 3.7.6: LVDT's 69
Figure 3.7.7: LVDT 69
Figure 3.7.8: String pot 70
Figure 3.7.9: Load actuator 70
Figure 3.8.1: Stress vs. strain graph for column #3 bar 73
Figure 3.8.2: Stress vs. strain graph for beam #2 bar 74
Figure 4.1.1: Discontinuous frame before loading 78
Figure 4.1.2: Discontinuous frame forming cracks 78
Figure 4.1.3: Discontinuous frame forming hinges 78
Figure 4.1.4: Discontinuous frame at failure 79
Figure 4.1.5: Initial cracking 80
Figure 4.1.6: Crack at end of negative reinforcement 80
Figure 4.1.7: Formation of hinge 80
Figure 4.1.8: Formation of cracks at the center column 81

Figure 4.1.9: Formation of hinges at the center column 81
Figure 4.1.10: Longitudinal bars breaking out of the stirrups 82
Figure 4.1.11: Diagram of compressive arch action (Orton, 2007) 82
Figure 4.1.12: Vertical load vs. displacement graph 84
Figure 4.1.13: Load cell vs. displacement graph 85
Figure 4.1.14: LVDT vs. vertical displacement graph..... 86
Figure 4.1.15: Strain gages in negative moment region of top beam 87
Figure 4.1.16: Strain gages in positive moment region of top beam 87
Figure 4.1.17: Strain gages in negative moment region of bottom beam 88
Figure 4.1.18: Strain gages in positive moment region of bottom beam 88
Figure 4.2.1: Continuous frame before loading 89
Figure 4.2.2: Continuous frame forming cracks 90
Figure 4.2.3: Continuous frame forming hinges 90
Figure 4.2.4: Continuous frame at failure 90
Figure 4.2.5: Initial cracking..... 91
Figure 4.2.6: Widening of cracks..... 92
Figure 4.2.7: Formation of hinge 92
Figure 4.2.8: Concrete falling off 92
Figure 4.2.9: Failure of beam..... 93
Figure 4.2.10: Crack forming near center column 93
Figure 4.2.11: Hinge forming near center column..... 94
Figure 4.2.12: Bars fracturing near center column 94
Figure 4.2.13: Vertical load vs. displacement graph 95
Figure 4.2.14: Load cell vs. displacement graph 96
Figure 4.2.15: LVDT vs. vertical displacement graph..... 97

Figure 4.2.16: Strain gages in negative moment region of top beam 99
Figure 4.2.17: Strain gages in positive moment region of top beam 99
Figure 4.2.18: Strain gages in negative moment region of bottom beam 100
Figure 4.2.19: Strain gages in positive moment region of bottom beam 100
Figure 4.3.1: Side view of infill wall 101
Figure 4.3.2: Top view of infill wall 101
Figure 4.3.3: Diagonal LVDT 102
Figure 4.3.4: Infill wall frame forming cracks 103
Figure 4.3.5: Infill wall frame cracks widening 103
Figure 4.3.6: Infill wall frame forming hinges 103
Figure 4.3.7: Infill wall separating from beam 104
Figure 4.3.8: Infill wall frame at failure 104
Figure 4.3.9: Crack forms in infill wall 105
Figure 4.3.10: Crack propagates through beam 105
Figure 4.3.11: Crack widens and forms hinge 106
Figure 4.3.12: Infill wall is separated from beam 106
Figure 4.3.13: Crack formed where negative moment bars end 106
Figure 4.3.14: Negative moment bars have break through stirrups 107
Figure 4.3.15: Initial crack near the center column 107
Figure 4.3.16: Crack propagates through beam and forms a hinge 108
Figure 4.3.17: Vertical load vs. displacement graph 109
Figure 4.3.18: Load cell vs. displacement graph 110
Figure 4.3.19: LVDT vs. vertical displacement graph 111
Figure 4.3.20: Diagonal LVDT vs. vertical displacement graph 111
Figure 4.3.21: Strain gages in negative moment region of top beam 113

Figure 4.3.22: Strain gages in positive moment region of top beam 113

Figure 4.3.23: Strain gages in negative moment region of bottom beam 114

Figure 4.3.24: Strain gages in positive moment region of bottom beam 114

Figure 4.4.1: Combined vertical load vs. displacement graph 116

Figure 4.4.2: Combined top load cell vs. displacement graph 117

Figure 4.4.3: Combined bottom load cell vs. displacement graph 117

Figure 4.4.4: Combined top LVDT vs. vertical displacement graph 118

Figure 4.4.5: Combined bottom LVDT vs. vertical displacement graph 119

Figure 5.1: Moment diagram for frame 124

LIST OF TABLES

Table Page

Table 2.5.1: Static load combinations for alternate load path analysis 24

Table 3.1: Test Frame Matrix 27

Table 3.8.1: Concrete cylinder compression tests 72

Table 3.8.2: Column #3 bar tension tests 72

Table 3.8.3: Beam #2 bar tension tests 73

Table 3.8.4: Mortar cubes compression tests 75

Table 3.8.5: Single prisms compression tests 75

Table 3.8.6: Dual-layer prisms compression tests 75

Table 3.8.7: Stacked prisms flexural tests 76

Table 4.4.1: Combined MTS load results 119

Table 4.4.2: Combined load cell results 120

Table 4.4.3: Combined LVDT results 120

Table 4.4.4: Combined strain gage results 121

ABSTRACT

The purpose of this research is to better understand the collapse resistance mechanisms of reinforced concrete buildings. A building must have sufficient strength, ductility and redundancy to resist collapse and ensure life safety. Extreme loading events, such as earthquakes and explosions, may cause severe local damage that triggers a chain reaction of large-scale structural failure or progressive collapse such as in the Oklahoma City building and the World Trade Center. Currently, resisting progressive collapse is generally outside the design considerations for ordinary buildings due to a lack of information on how to economically provide that resistance. Reinforced concrete frame structures, however, may possess inherent structural redundancy and ability to withstand collapse if the structure is properly detailed to provide alternative resistance mechanisms. A more accurate progressive analysis procedure that takes into account alternative collapse resisting mechanisms will lead to the identification of detailing requirements that could be implemented economically on new buildings (regardless of whether a progressive collapse analysis was conducted) or retrofit measures for existing buildings and therefore ensure a limited ability to resist collapse and save lives.

Collapse resisting mechanisms studied in this research include catenary action, Vierendeel action, compressive arch action, and contributions from infill walls. Typical progressive collapse analysis procedures do not usually consider these mechanisms because they are not well understood. This research tested a series of three quarter scale two bay by two story frames. The column between the two bays was removed to

simulate a collapse scenario. The design of the three frames consisted of discontinuous reinforcement, continuous reinforcement, and infill walls placed in the bays. Although a typical flexural analysis of the frame with discontinuous reinforcement would indicate that it had little load capacity, it was able to reach a load of 2.34 kips under compressive arch action and 8.19 kips under catenary tension. The frame with continuous reinforcement reached a load of 5.81 kips under the flexural action. However, due to limited rotational capacity of the hinge regions, the reinforcement fractured and continuity was lost. Upon further loading, the frame reached 8.30 kips under catenary tension. The frame with the infill wall did not perform significantly different than the discontinuous reinforcement frame indicating that the partial height infill wall did little to improve the collapse resistance of the frame. The results show that both compressive arch and catenary action are viable resistance mechanisms in frames under a collapse loading, and if incorporated into design guidelines could reduce the required sizes and reinforcement of structural members.

1. INTRODUCTION

Most reinforced concrete buildings have not been designed for the loads that can result in a progressive or disproportionate collapse such as those from an earthquake, explosion, or vehicle/aircraft collision. Although these are rare occurrences, they can lead to severe consequences such as huge losses of life. This has been demonstrated by the collapse of several buildings such as the Ronan Point Apartment Building in England in 1968, the Murrah Building in Oklahoma City in 1995 and the World Trade Center towers in New York in 2001. Due to these infamous events, research on progressive collapse has gained a lot of momentum over the last decade.

The General Services Administration defines progressive collapse as an event when a "local failure of a primary structural component leads to the collapse of adjoining members" which results in further collapse (GSA, 2003). Therefore, a "domino" effect takes place and the eventual destruction is disproportionate to the original cause.

Typically only resistance from flexural action (bending in the beams) is considered in collapse design. However, reinforced concrete buildings can resist progressive collapse through a variety of mechanisms. These alternate resistance mechanisms include catenary action, Vierendeel action, compressive arch action, and contributions from infill walls. Catenary action, or membrane action, is the resisting of vertical forces through horizontal tension in members undergoing extreme deflection. Vierendeel action, or frame action, is the resisting of forces through moment connections at beams and

columns. Compressive arch action uses axial restraint of the surrounding structure to keeps beams from rotating and thus forming a compressive arch. Infill walls create additional stiffness to help resist vertical forces.

Alternative collapse resistance mechanisms have been given little regard in current progressive collapse guidelines due to limited information on their effectiveness and the inability to calculate capacities (DoD, 2009; GSA, 2003). There are provisions requiring general structural integrity such as those in ASCE 7 (2005) and ACI 318 (2005), but there is no specific mention of progressive collapse resistance. However, alternative mechanisms may provide enough extra capacity to the building to prevent a complete collapse or at least delay the inevitable so that lives can be saved. This has been demonstrated by the fact that a number of reinforced concrete buildings have been able to withstand progressive collapse after the loss of one or several supports due to accidental loads because of these actions (Sasani and Kropelnicki , 2007; Sucuoglu et al., 1994). Therefore, research needs to be done to better understand the effect of alternate resistance mechanisms and hopefully save lives in the future.

1.1. Problem

Currently, there is a very limited amount of information and research on alternative resistance mechanisms of reinforced concrete buildings. Because of this lack of information, there are very few guidelines on how to resist progressive collapse. Therefore, the goal of this research is to better understand the effects of various resistance

mechanisms of reinforced concrete buildings. The ultimate goal is to one day create a set of guidelines on how to best resist progressive collapse.

1.2. Objectives and Research Approach

The main objective of this research is to better understand the collapse resistance mechanisms of reinforced concrete buildings. The effects of these resistance mechanisms need to be studied because they are often not considered in analysis, there is evidence of their effectiveness, and there is a lack of understanding on how to determine their capacities.

The alternative collapse resisting mechanisms to be evaluated in this research include catenary action, Vierendeel action, compressive arch action, and contributions from infill walls. Each of these mechanisms was described in the introduction part of this thesis. This research tested a series of three quarter scale two bay by two story frames. The column between the two bays was removed to simulate a collapse scenario. The three frames were the discontinuous reinforcement frame based on the 1971 ACI 318 code, the continuous reinforcement frame based on the 2008 ACI 318 code, and the discontinuous reinforcement frame with infill walls placed in the top bays. These test frames were placed in a reaction frame and loaded at the center over the location of the removed column.

1.3. Outline

This research is organized into 5 chapters. Following the introduction, Chapter 2 reviews the relevant literature pertaining to progressive collapse in reinforced concrete buildings, historical examples of progressive collapse, design methods and approaches to resisting progressive collapse, types of collapse resistance mechanisms, and previous research performed on progressive collapse. Chapter 3 describes the setup of the experiment including design considerations for the reaction frame, instrumentation and design details of the reinforced concrete frames. Chapter 4 goes into detail over the results of the all the tests performed and compares the various designs while chapter 5 presents the overall conclusions of this research. The document concludes with a list of the references cited in this research.

2. LITTERATURE REVIEW

Previous studies have been performed to better understand progressive collapse. They include analysis of actual building collapses and laboratory testing. This chapter will review relevant literature pertaining to progressive collapse in reinforced concrete buildings, alternative mechanisms resisting progressive collapse, and laboratory testing of reinforced concrete. Furthermore, this chapter will look at the current design guidelines for progressive collapse.

2.1. Progressive Collapses

A number of reinforced concrete structures have suffered from progressive collapse in recent history. The collapse of the Ronan Point Tower in 1968 in the Canning Town area of London, England is probably one of the most famous cases. This accident was started by a gas stove leak in apartment 90 on the 18th floor. The end result was a collapse of the southeast corner bay of the building from top to bottom as shown in Figure 2.1.1. The Ronan Point Tower was a 22-story residential apartment building that consisted of precast panels joined together without a structural frame. Due to poorly designed connections between the walls and floor, there were no alternate load paths to redistribute the forces in the event of a partial collapse. Since the collapse of the southeast corner of the Ronan Point Tower, there have been changes to building codes of the United Kingdom and other parts of the world to help prevent such tragedies from happening again (Pearson and Delatte, 2005). An example of these changes is that precast concrete structures in the United Kingdom are required to be tied together so that they can either

provide an alternative load path or a specific local resistance to withstand an abnormal load (NIST, 2007; Breen, 1975).

Figure 2.1.1: Ronan Point Tower after collapse (Nair, 2004)

Another example of progressive collapse was the Alfred P. Murrah Building in Oklahoma City, Oklahoma. The Murrah building was destroyed by a bomb in a truck at the base of the building on April 19, 1995. The bomb destroyed or severely damaged three columns. The loss of support from these columns led to a failure of the transfer girder. This failure of the transfer girder caused the collapse of the above columns and floor areas (Nair, 2004). The result was a collapse of one side of the building as shown in

Figure 2.1.2. The Murrah building was designed with discontinuous reinforcement for both the positive and negative moment regions of the beams. If the building had been detailed as a special moment frame (with continuous reinforcement), the collapsed area of the structure could have been reduced 50% to 80% (Corley, 2004). The extent of the damage prompted studies of progressive collapse and the development of new design guidelines for important buildings (Nair, 2004).

Figure 2.1.2: Murrah Building after explosion (Crawford, 2002)

2.2. Non-Collapsed Buildings

While the Ronan Point Tower and the Murrah Building are some of the more famous examples reinforced concrete structures that suffered from progressive collapse, there are many other structures that suffered severe damage but were able to resist a disproportionate collapse. One example of this was the partial collapse of the Pentagon Building in Washington D.C. on September 11th, 2001. A plane was flown into the first

floor of the building destroying 30 of the first-floor columns and damaging 20 others along a path that encompassed a 75 ft. wide by 230 ft. long section (Mlakar et al., 2003). Despite extensive damage to many of the columns on the first floor, the upper stories remained intact for more than 20 minutes before they collapsed due to fire as shown in Figure 2.2.1. According to the Pentagon Building Performance Report (Mlakar et al., 2003), the reasons for the performance of the building are "redundant and alternative load paths of the beam and girder framing system, short spans between columns, substantial continuity of beam and girder bottom reinforcement through the supports, design for 150 psf warehouse live load in excess of service load, significant residual load capacity of damaged spirally reinforced columns."

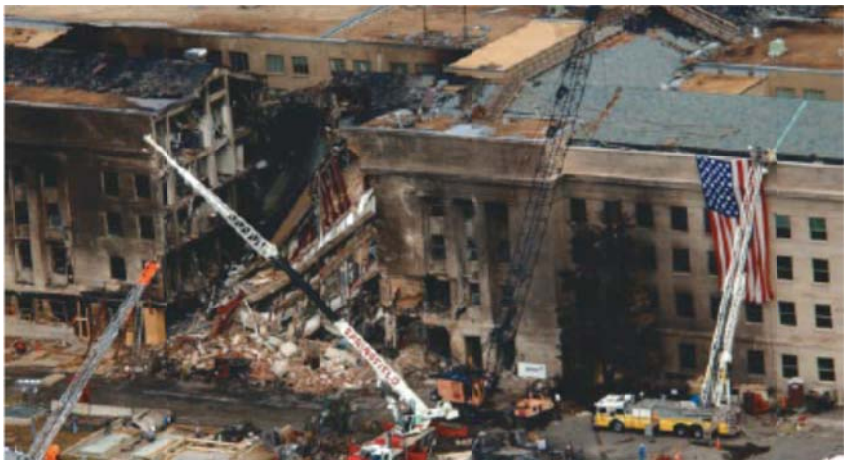

Figure 2.2.1: Pentagon Building after the crash (Mlakar et al., 2003)

Another example was a typical reinforced concrete six-story office building (Figure 2.2.2) that was damaged by a steam boiler explosion (Sucuoglu et al., 1994). Sucuoglu et al. investigated the redistribution paths of forces resulting from a column failure and identified the basic structural defense mechanisms developed in the damaged building

frame. One of the findings of the study showed that non-load-bearing infill walls provide can reserve strength and help prevent the progressive failure of the structure.

Figure 2.2.2: Office building damaged by system boiler explosion (Sucuoglu et al., 1994)

2.3. Resistance Mechanisms

In order to resist progressive collapse, a structure must be able to survive the loss of a primary structural component without further collapse. Besides flexural action (bending in beams), mechanisms for resisting such a collapse include catenary action, Vierendeel action, compressive arch action, and contributions from infill walls. For this research, the loss of an exterior non-corner column in a reinforced concrete building is studied. In this case, the resulting forces due to the double span condition created by the loss of a column can be difficult to accommodate. As shown in Figure 2.3.1, the moment increases by about 4 times due to the double span. Also, the moment over the missing column

reverses direction and thus a positive moment now exists where the beam reinforcement was designed for negative moment. This reversal and increase in moment can be very difficult for the beam to resist.

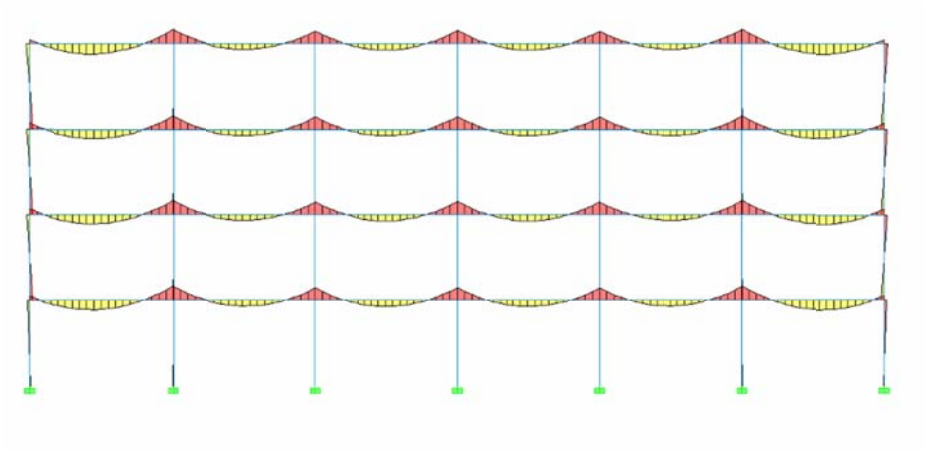

Typical Structure

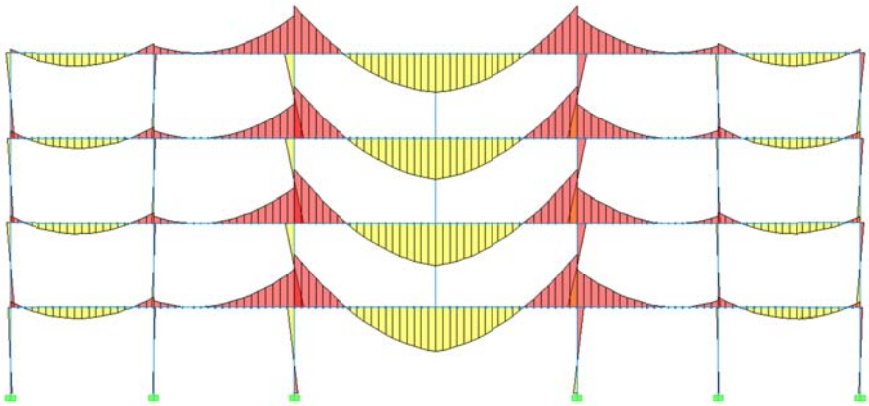

Missing Column

Figure 2.3.1: Change in moment diagram due to loss of column (Orton, 2007)

2.3.1. Catenary Action

As stated before, one method to provide increased capacity to resist progressive collapse is through catenary action. This is similar to the catenary action used in long-span bridges. This action resists the load by transferring axial tension throughout the beam. The tension is then transferred throughout the building as shown in Figure 2.3.1.1.

However, the catenary tension only becomes effective at large levels of displacement, usually around 7 to 10% of the span length (Wong, 2002). Based on a typical 20 ft span, the deflection could be as much as 3 to 4 feet. Even though this is a rather large deflection for a floor, the catenary action prevents a complete collapse of the floor.

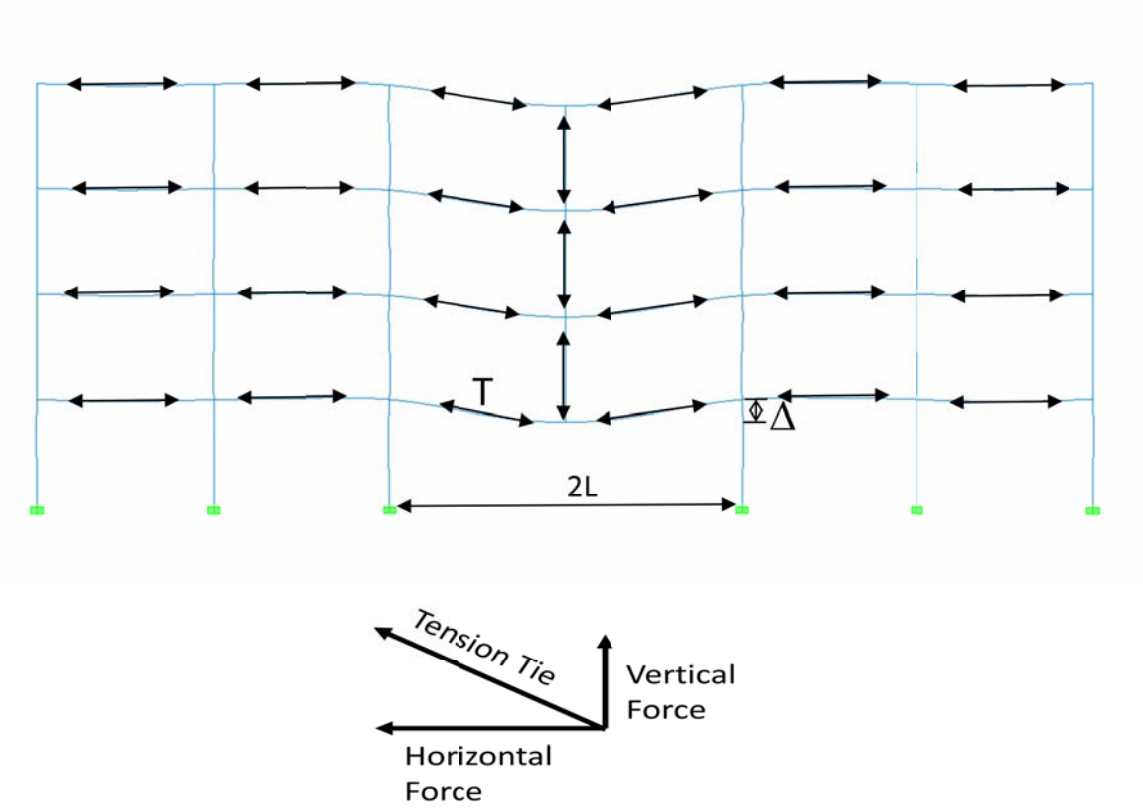

Figure 2.3.1.1: Catenary tension forces throughout a building (Orton, 2007)

In order to develop the needed catenary tension forces to resist progressive collapse, the reinforced concrete beam must have an uninterrupted line of tension for the force to act along. This line of tension can be supplied by continuous reinforcement, either through the positive or negative moment reinforcement. Even if the beam does not have continuous reinforcement, the line of tension can act through both the negative and positive moment reinforcement if there are enough stirrups to transfer the tension force as

shown in Figure 2.3.1.2. But this transfer of tension from one side of the beam to the other is not as efficient and depends on the size, spacing and design of the stirrups.

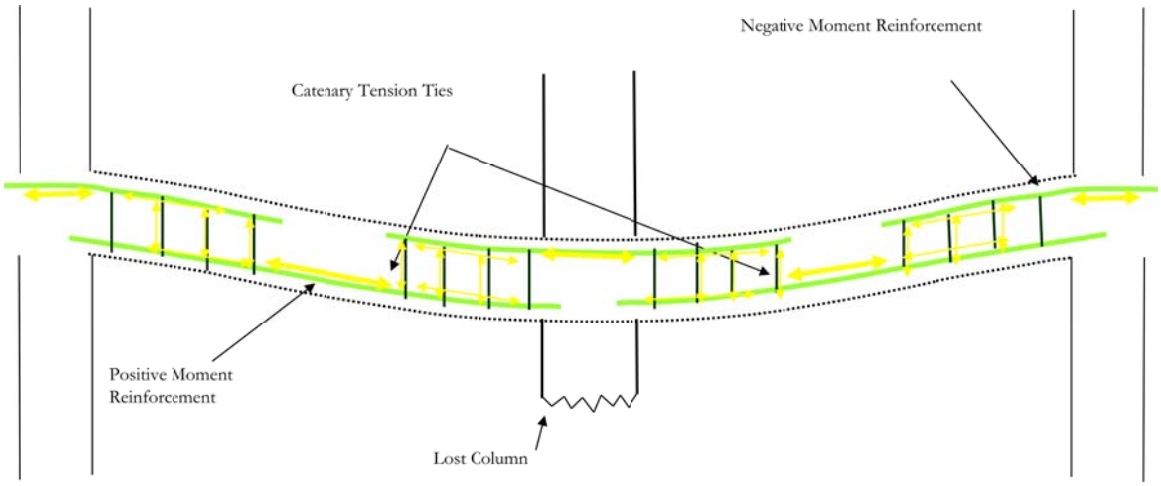

Figure 2.3.1.2: Transfer of catenary forces through stirrups (Orton, 2007)

2.3.2. Vierendeel Action

Another mechanism for resisting progressive collapse is Vierendeel action. As stated before, Vierendeel (frame) action is the resisting of forces through moment connections at beams and columns.

Vierendeel action can also be characterized by the relative vertical displacement the between beam ends and the corresponding double curvature deformations of beams. Such action was demonstrated in the Hotel San Diego building in San Diego, California where Sasani and Sagiroglu (2007) performed an experimental evaluation following predefined initial damage of the structure. The initial damage was caused by the simultaneous explosion (removal) of two adjacent exterior columns, one of which was a corner column. The above mentioned deformation patterns developed in the beams

because of the existence of moment connections and the interaction of beams with columns and infill walls. Based on experimental data, the development of bidirectional Vierendeel action was identified as a major mechanism in the redistribution of loads in the building. Furthermore, infill walls provided the beams with constraints and supports to help carry additional loads. Thus, the Vierendeel mechanism, along with the increased stiffness from infill walls, contributed to the resistance of a building collapse (Sasani and Sagiroglu, 2007).

2.3.3. Compressive Arch Action

Another mechanism for resisting progressive collapse is compressive arch action. Compressive arch action is formed when an in-plane compressive force develops because the axial restraint from the surrounding structure keeps the beams from rotating. This can be increased with contributions from infill walls which provide additional stiffness. Su et al. (2009) performed research on compressive arch action in beams and found that the additional load provided by the compressive arch action in the beams was between 1.53 and 2.63 times that of the flexural capacity of the beams with the greatest increases being for the specimens with the lower span to depth ratios.

2.4. Previous Research

There is not much previous research on progressive collapse of reinforced concrete structures. Most of this research is focused on catenary action in reinforced concrete beams. In the 1970s, research was conducted by Regan (1975) at Imperial College in London, England. He tested precast floor strips that were 14 in. to 28 in. wide and 18 ft.

long with a central joint between two 9 ft. planks representing a lost support, Figure 2.4.1. The specimens were comprised of a 2 in. thick precast panel and a 2 in. thick cast-in-place topping. Details of the ties between the panels varied according to the specimens' width.

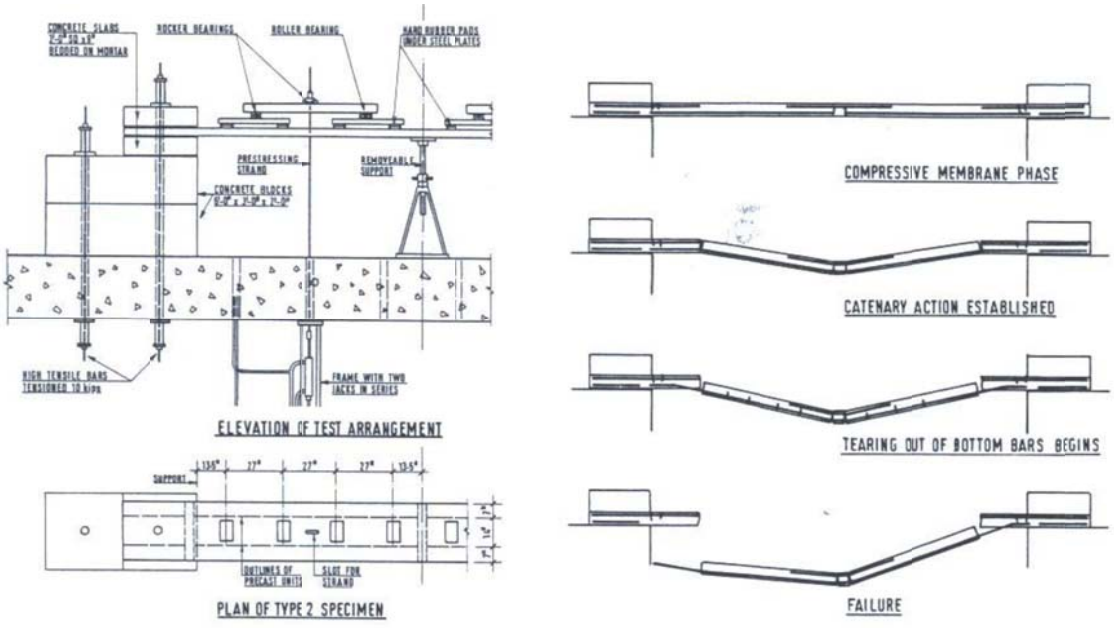

Figure 2.4.1: Catenary tests of precast floor strips (Regan, 1975)

In all the tests, it was observed that an initial compressive arch phase took place followed by a catenary action phase. The majority of the beams failed when the bottom bars near the supports tore out at a deflection of 5 to 7% of the double span length as documented in test #5 in Figure 2.4.2. However, in some cases, the end cantilevers yielded before there was any tearing of the bottom bars. In these cases, the maximum deflections were about 10% of the doubled span, but the collapse was caused by the fracturing of the end ties which was due to limited rotation between the specimen and its supports (test #3 in Figure 2.4.2).

Based on these test results, Regan (1975) concluded that the "successful development of a catenary action requires that the members in question posses not only tensile strength but also ductility, which is largely determined by the detailing of the longitudinal reinforcement." The ductility he mentions partly pertains to the ability of the concentrated rotation locations (hinges) to not fracture the reinforcement before catenary action is developed.

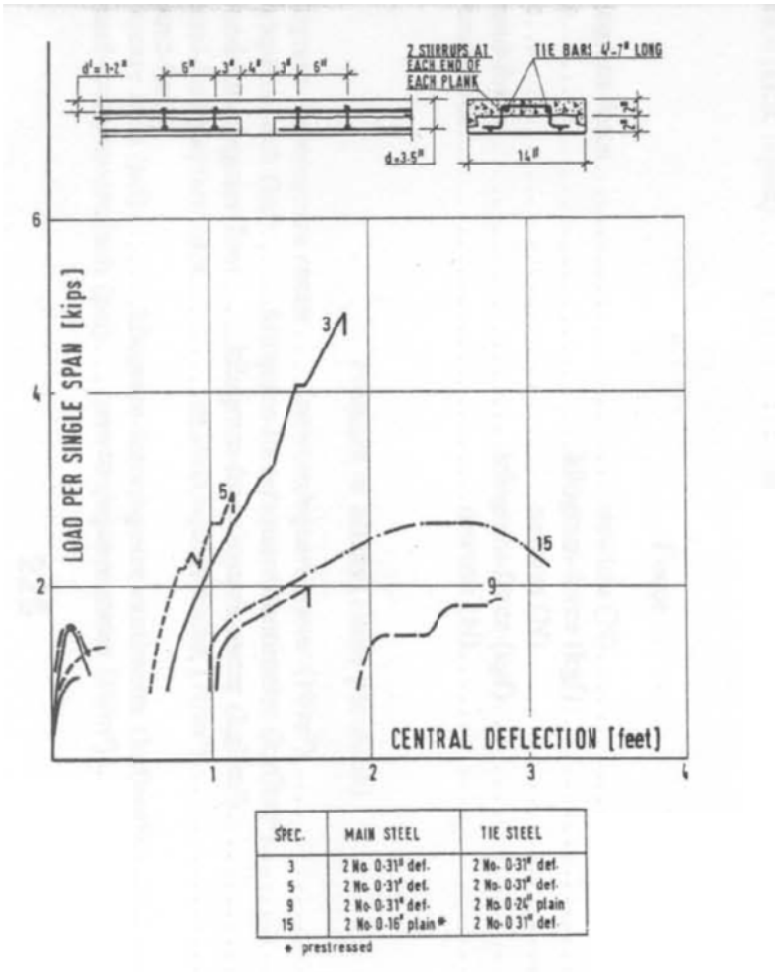

SPEC.	MAIN STEEL	TIE STEEL
3	2 No. 0·315" def.	2 No. 0·315" def.
5	2 No. 0·315" def.	2 No. 0·315" def.
9	2 No. 0·315" def.	2 No. 0·276" plain
15	2 No. 0·196" plain*	2 No. 0·315" def.

* prestressed

Figure 2.4.2: Results of catenary tests of precast floor strips (Regan, 1975)

Sasani and Kropelnicki (2007) carried out another experiment program to evaluate the behavior of a 3/8 scaled model of a continuous reinforced concrete exterior beam that suffered from the removal of a supporting column. The beam was 13 ft. - 8¼ in. long by 12 in. wide by 20 in. deep. It was constructed with fixed boundary conditions. Grade 75 ksi bars were used with a concrete compressive strength of 6 ksi. The test was conducted using displacement control at the center span (Sasani and Kropelnicki, 2007).

As shown in Figure 2.4.3, the two bottom bars fractured at vertical displacements of about 6.0 in. and 7.5 in. They also found that catenary action developed in the top bars following the bottom bar fractures. Finally, the end of the beam rotated to about 11 degrees (Sasani and Kropelnicki, 2007).

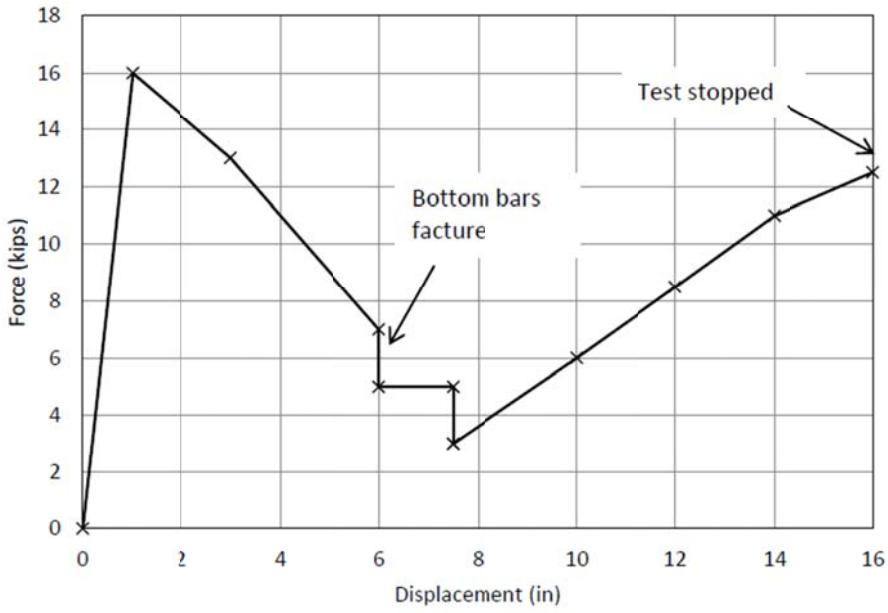

Figure 2.4.3: Force vs. displacement graph (Sasani and Kropelnicki, 2007)

In 2007, Orton tested eight beams to evaluate different load paths in order to develop continuity and catenary action in reinforced concrete beams. The specimens were half-scale reinforced concrete beams that were 30 ft. long, 6 in. wide by 12 in. deep. The reinforcement consisted of #3 and #4 bars which is almost equivalent to half-scale versions of the prototype beam. One test found that beams with discontinuous reinforcement were able to transfer tension forces for catenary action from the positive moment bars to the negative moment bars through the stirrups (Orton, 2007).

The axial load and vertical load vs. displacement response (Figure 2.4.4) shows a compressive arch phase until about 14 in. of deflection followed by a catenary tension phase. Although with discontinuous reinforcement the beam would have little or no flexural capacity, it was able to reach a load of 2.3 kips per loading point in compressive arch action and 5.2 kips in catenary action. The test was then stopped at 25 in. of deflection due to limitations in the test setup (Figure 2.4.5).

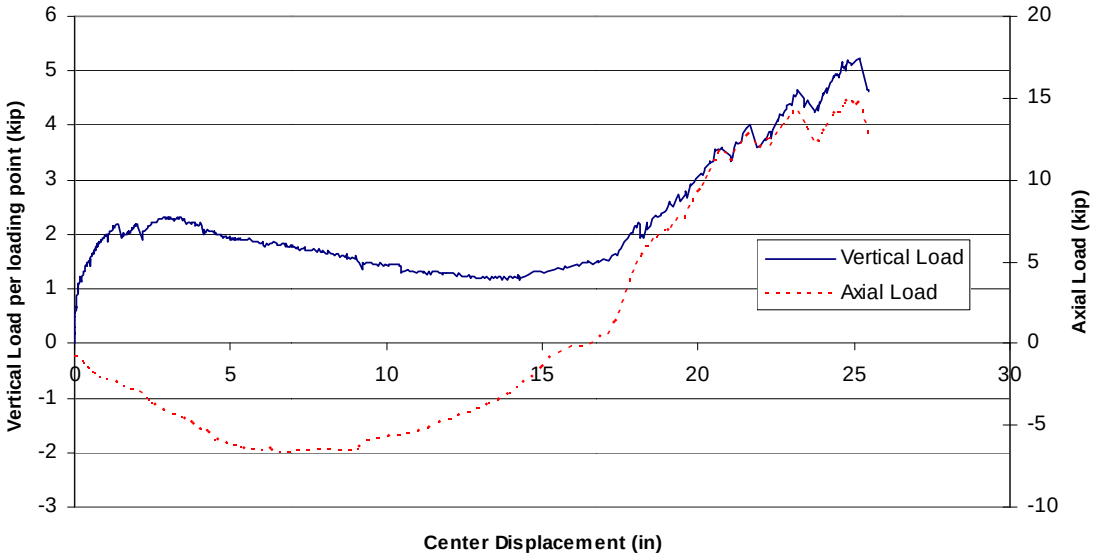

Figure 2.4.4: Vertical and axial loads vs. center displacement for beams with discontinuous reinforcement (Orton, 2007).

Figure 2.4.5: Photo of test NR-2 under catenary action (Orton, 2007)

Another test found that a beam with continuous reinforcement was not able to carry a tension force before the bars fractured due to limited ductility in the beam in the positive hinge region. After fracture of the positive moment bars, the negative moment bars

fractured as well. After the loss of continuity, the beam was still able to carry increasing load through catenary tension.

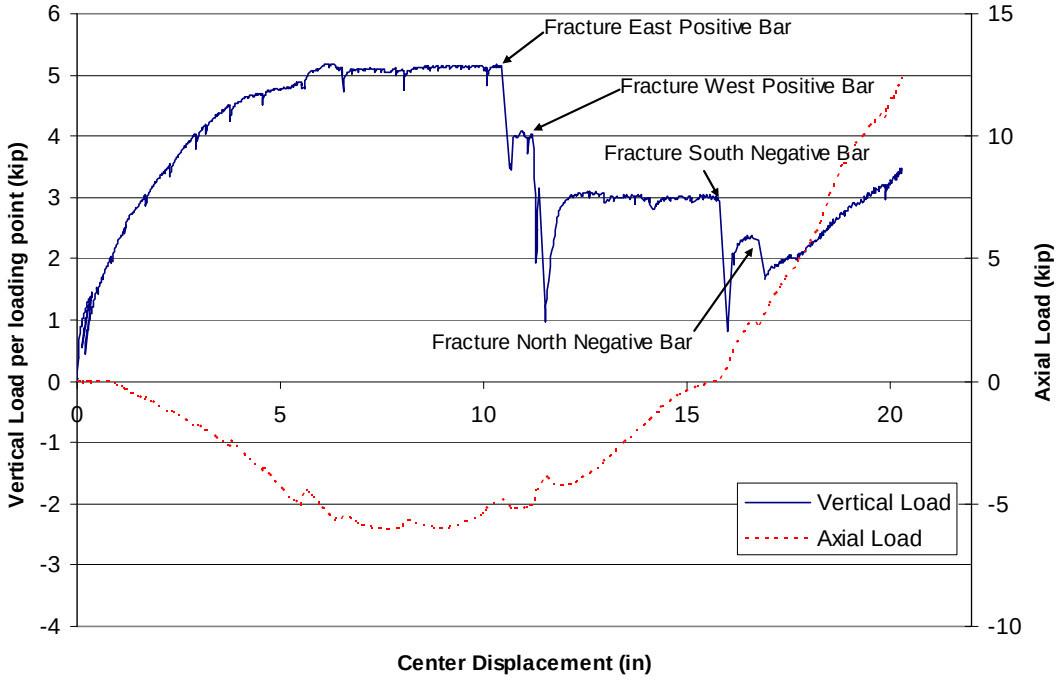

Figure 2.4.6: Vertical and axial loads vs. center displacement for beams with continuous reinforcement (Orton, 2007).

Orton concluded that the catenary action begins after the beam has formed a failure mechanism, or that the beam is no longer able to sustain additional vertical loads in a flexural manner. Orton further mentioned that a reinforced concrete beam can be modeled as rigid rectangular blocks between the hinge locations and that the deflection at which catenary action begins is directly dependent on the height of the beam. Finally, Orton found that the stiffness is dependent on the axial elongation of the beam, which is largely dependent on the length of the beam and yielding in the beam (Orton, 2007).

In other research, Yi and Kunnath (2008) conducted a static experiment to study the progressive collapse of a reinforced concrete frame due to the loss of a bottom story column. They tested a one-third scale model of a four-bay by three-story frame with continuous positive reinforcement as shown in Figure 2.4.7.

Figure 2.4.7: A reinforced concrete four-bay by three-story one-third scale model frame (Yi and Kunnath, 2008)

The test results indicated that three phases were experienced during the progressive collapse process: elastic, plastic and catenary phases, Figure 2.4.8. Based on observations and findings, it was concluded that the catenary action depends on uniform extension of the reinforcing bars; the calculated capacity of the frame based on the plastic limit state was approximately 70% of the tested failure capacity if catenary effects are

also included; the beam catenary mechanism can be considered as an alternative load path and can resist additional loads (Yi and Kunnath, 2008).

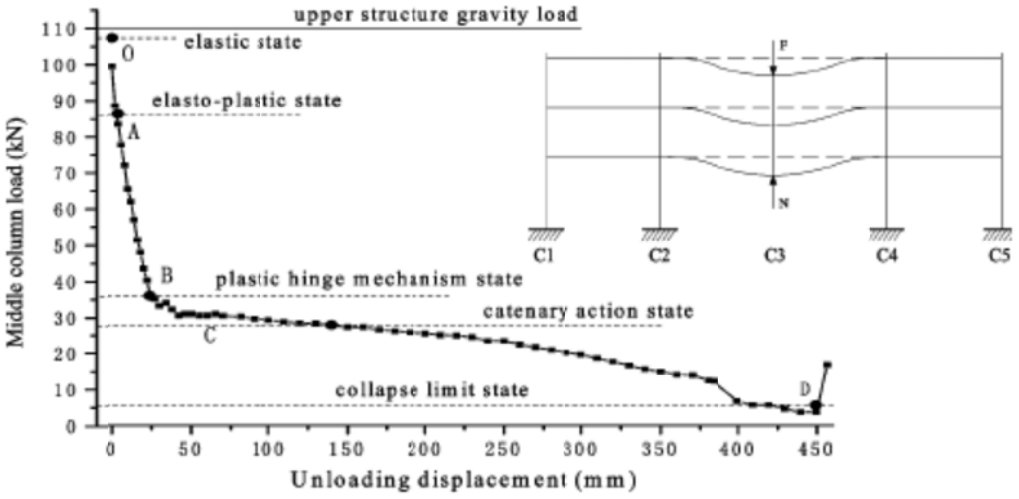

Figure 2.4.8: Middle column load vs. unloading displacement (Yi and Kunnath, 2008)

What lacks in the research so far is the ability to determine the capacities of the different alternative resistance mechanisms for a reinforced concrete building. That means no one has compared the results of similar model buildings that have different alternative resistance mechanism designs. This would include a control (discontinuous reinforcement) building, a modern (continuous reinforcement) building, a building with infill walls, and so on. Regan (1975) performed such research for precast floor strips and Orton (2007) did it for beams. Yi and Kunnath (2008) tested a frame, but it was only one frame with continuous reinforcement. They had no other frames to compare it to. The goal of this research is to help fill the gaps of previous research. By doing multiple frames with different details, the capacities of these alternative resistance mechanisms can helped be determined.

2.5. Standards

The first implementation of standards for progressive collapse was introduced in the U.K. after the 1968 collapse of Ronan Point (NIST, 2007). The British Standards required consideration of progressive collapse in buildings taller than five stories and provisions for structural ties. In the 1970's, the U.S. Department of Housing and Urban Development's Operation Breakthrough examined the problem of progressive collapse in the U.S., focusing on concrete panel structures. Starting in the 1980's, design standards in the U.S., such as the ACI code, began to implement structural integrity provisions. Additionally, ASCE 7 implemented some provisions for general structural integrity. However, these standards did not include specific provisions for resistance against progressive collapse (NIST, 2007).

Agencies of the U.S. government, Department of Defense (DoD) and General Services Administration (GSA), have developed some design requirements for progressive collapse (DoD, 2009; GSA, 2003). Generally, standards for progressive collapse consider three types of approaches:

- Indirect Design: emphasizes strength, continuity, redundancy and ductility; relies on integrated system of tie forces
- Direct Design – Alternate Load Path: analyze structure for instantaneous loss of a vertical load bearing member, and provide redundant or alternate load path to bridge over failed member; analysis can account for plastic or large deformations including catenary or membrane action

- Direct Design – Specific Local Resistance: each member is designed to resist a specific threat

The DoD document *Design of Buildings to Resist Progressive Collapse* (2009) considers both indirect and direct design approaches. For buildings requiring a low level of protection, a system of minimum tie forces is required (Figure 2.5.1). For example, in reinforced concrete buildings the peripheral ties are required to have the strength of:

Tie Force = Lesser of (4.5 + 0.9*number of stories) or 13.5 kips

Similar requirements exist for other types of ties, and more information can be found in the DoD document.

The direct design approach appears both in the DoD document and the GSA *Progressive Collapse Analysis and Design Guidelines* (2003). Both require the structure to survive the removal of a primary structural component, such as an external column. For static analysis, the loads placed on the structure include a factor for dynamic amplification due to the falling nature of the structure. The static load combinations are given in Table 2.5.1. For the GSA guidelines, this amplification factor is 2 while the DoD factor of Ω_N was calculated to be 1.09 for these particular test frames. Some research has indicated that the amplification factor could be 1.5 (Ruth et al., 2006). The increased loads must be placed in a tributary area surrounding the removed element.

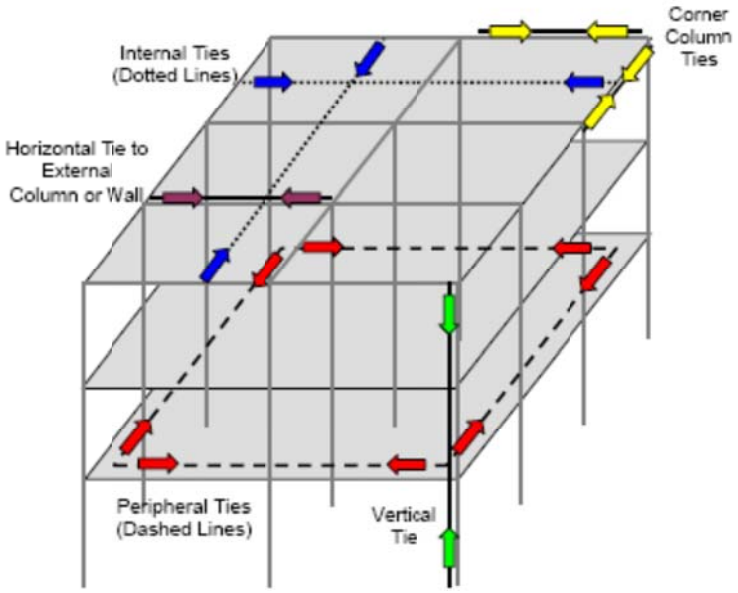

Figure 2.5.1: System of tie forces (DoD, 2004)

Table 2.5.1: Static load combinations for alternate load path analysis

Code	Static Load Combination
DoD (2004):	2 [(0.9 or 1.2)D + (0.5 L or 0.2S)]
DoD (2009):	Ω_N[(0.9 or 1.2)D + (0.5 L or 0.2S)]
GSA:	2(D+0.25L)

* $\Omega_N = 1.04 + 0.45 / (\theta pra/\theta y + 0.48)$

For a linear static analysis, the GSA guidelines use a demand-to-capacity ratio, generally 2, to account for inelastic deformations. The DoD guidelines require an iterative procedure to account for inelastic loads with acceptance criteria in the form of member deformation limits.

Both methods also include procedures for static inelastic analysis. The procedures allow for use of plastic deformation capacities and material over-strength factors. The inelastic analysis can also include geometric non-linearity, such as tension membrane or catenary action. However, the relative advantages and disadvantages of a catenary system that may hold a floor up compared to one that would break away to prevent damage to the rest of the structure must be evaluated (Figure 2.5.2). The acceptance criteria are based on member deformation limits. For example, GSA requires a reinforced concrete beam to have a rotation less than 6 degrees or 0.105 radians. DoD deformation requirements are similar. Both guidelines also include procedures for dynamic analysis of a structure.

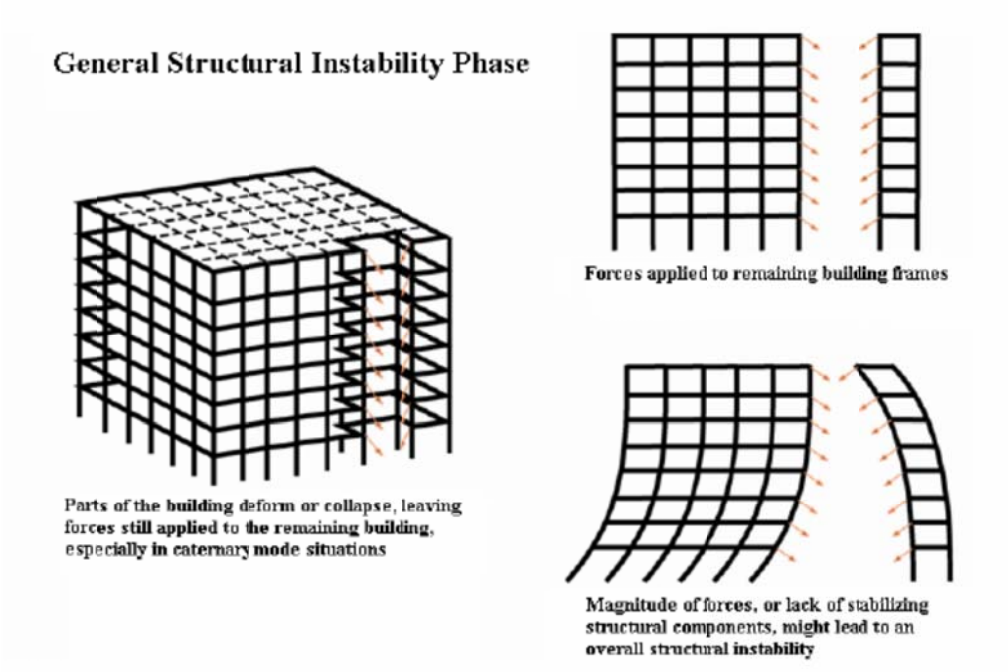

Figure 2.5.2: Forces on structure due to catenary loads (NIST, 2007)

One of the major problems with reinforced concrete structures and progressive collapse that is addressed in this research is the lack of continuity of reinforcement. The GSA

guidelines state "providing continuous bottom reinforcing steel across the connection is essential to accommodating the double span condition." However, many older buildings do not have continuous top or bottom reinforcing bars. The integrity of reinforcement provisions requiring continuous bottom bars were not added until the 1989 ACI building code. The current ACI 318 (2008) Chapter 7 integrity of reinforcement provisions are:

> *7.13.1—In the detailing of reinforcement and connections, members of a structure shall be effectively tied together to improve integrity of the overall structure.*
>
> *7.13.2.2—Beams along the perimeter of the structure shall have continuous reinforcement consisting of:*
>
> > *a) at least <u>one-sixth</u> of the tension reinforcement required for negative moment at the support, but not less than two bars; and*
> >
> > *b) at least <u>one-quarter</u> of the tension reinforcement required for positive moment at midspan, but not less than two bars.*

Furthermore, the commentary states that "by making a portion of the bottom reinforcement continuous, catenary action can be provided." However, these provisions are not designed to resist progressive collapse. They are just general "good building practices" for structural integrity. There is no assurance that continuity will provide catenary action or resist progressive collapse.

3. EXPERIMENT SETUP

This research considered 3 different frame designs to evaluate the capacity of the alternative resistance mechanisms as shown in Table 3.1.

Table 3.1: Test Frame Matrix

Test	Frame	Details
1	Discontinuous Reinforcement Frame	Control frame based on 1971 ACI code
2	Continuous Reinforcement Frame	Modern frame based on 2008 ACI code
3	Infill Wall Frame	Addition of infill walls

There were many stages within the process of this research. This chapter describes the design of the reinforced concrete test frames, construction of the test frames, design of the reaction frames, and construction of the reaction frames.

3.1. Design of the Full Scale Reinforced Concrete Frames

The first step in designing the test frames was to determine the design of typical office buildings designs in the United States. This building design will be used for the prototypical frame which will be quarter scaled down for the test frames. After looking at several examples, it was determined that our model building footprint would be 6 bays by 4 bays on 24 feet center-to-center spacing. The building would have 6 stories and each story would be 12 feet tall.

The reinforced concrete building would have one-way girders with joists. The concrete used would have a unit weight of 150 lbs/ft^3 and a compressive strength of 4,000 psi. The columns were designed as 22 in. by 22 in. square columns. The interior girders were designed as 36 in. by 18in. rectangular beams while the spandrel or exterior girders were designed as 24 in. by 12 in. rectangular beams. The joists were designed as 16 in. by 8 in. rectangular beams and the floors were designed as 6 in. thick slabs. All of the reinforcement was designed with yield strength of 60 ksi.

The model building was designed to withstand the loading conditions of a typical office building. Therefore, an additional dead load of 30 psf and a live load of 50 psf were applied to every floor. These were the only loading conditions considered for the purposes of this research. All of this information was placed into the structural modeling program RISA 3D as shown in Figure 3.1.1.

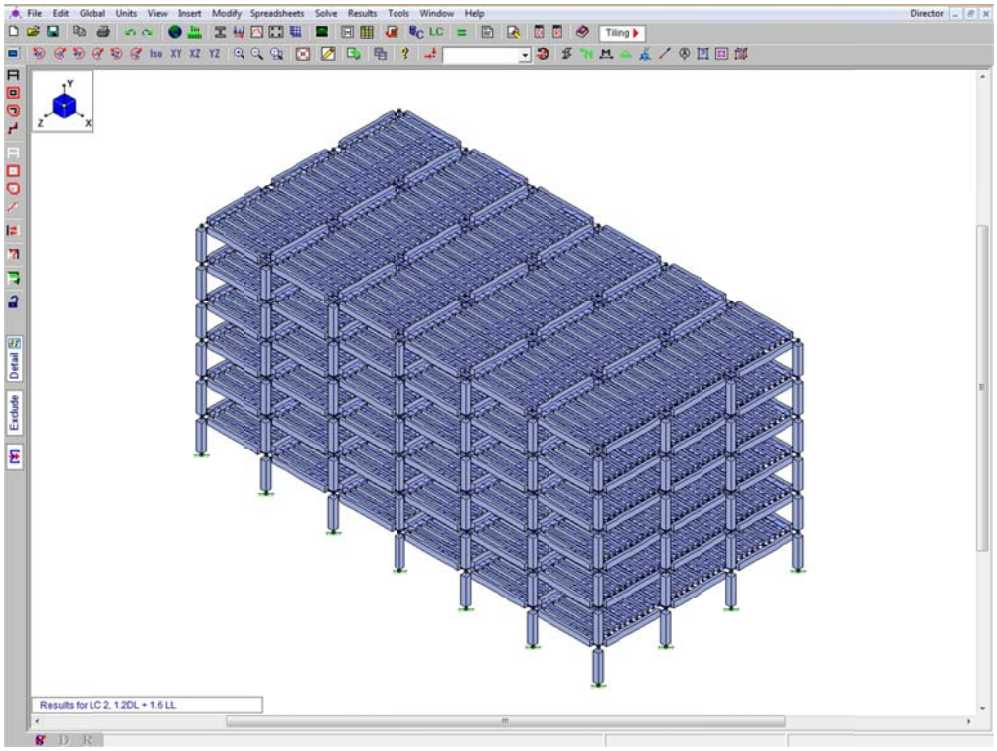

Figure 3.1.1: RISA model of a typical office building

Based on this RISA model and hand calculations, the shear and moment diagrams were determined for the exterior columns and spandrel beams. Based on this information, the reinforcement was determined as shown in Figure 3.1.2, Figure 3.1.3 and Figure 3.1.4. The columns consisted of 8 #10 longitudinal bars and #4 stirrups at 18 in. spacing. The beams consisted of 3 #8 bars for the positive moment and 4 #8 bars for the negative moment. Also, #3 stirrups would be placed every 6 in. as long as the shear required it which was 9 ft. from the face of the columns.

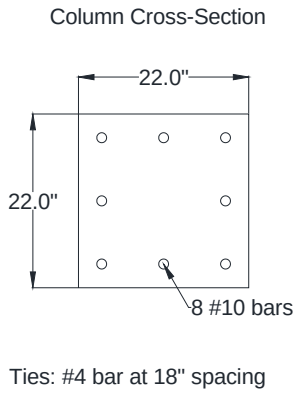

Figure 3.1.2: Column cross-section for full scale frame

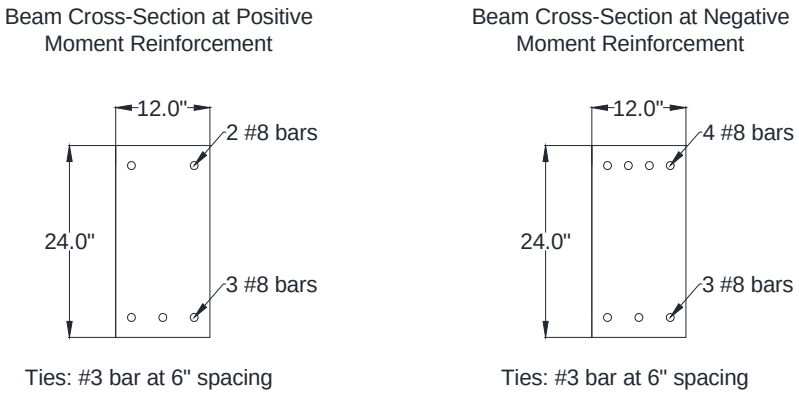

Figure 3.1.3: Beam cross-section for full scale frame

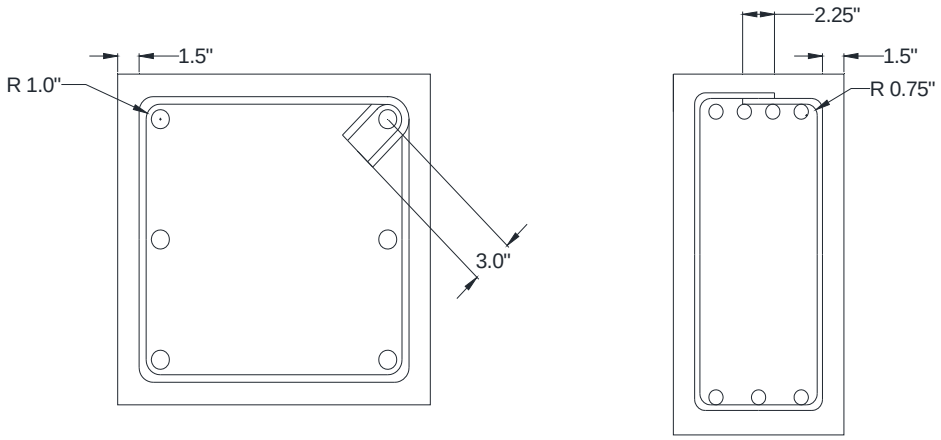

Figure 3.1.4: Transverse reinforcement detailing for full scale frame

These cross-sections are the full scale representation for all three of the test frames. The control specimen was based on the 1971 ACI code which called for different lengths of positive and negative reinforcement than the 2008 ACI code. The main difference between the two codes is that 1971 code did not require continuous reinforcement in perimeter frames. But the shear or transverse reinforcement for the beams was the same for both codes. Also, all of the column reinforcement requirements were the same for both codes.

The reinforcement layout for the full scale frame based on the 1971 ACI code is shown in Figure 3.1.5 and Figure 3.1.6. As stated before, the columns contained 8 #10 bars with 38 in. lap splices located just above the bottom beams. The positive moment reinforcement included 3 #8 bars for the middle 19.42 ft. of the beams with the 2 outer

bars extending 6 in. into the columns. The cutoff point for the middle #8 bar was determined by the inflection point location of the positive moment graph (7.92 ft.) plus d (21.5 in) as stated by the ACI code. Adding these two values together and doubling the length gave 19.42 ft. The 1971 ACI code did not call for the positive moment reinforcement to extend all the way through the columns. As for negative moment reinforcement, 2 #8 bars would extend 86 in. from the face of the column while the 2 outer #8 bars would only extend 49 in. The 86 in. value was determined from the inflection point location of the negative moment graph (63.84 in.) plus d (21.5 in.). The 49 in. value was determined from the location of the half-way point of the maximum of the negative moment graph (26.6 in.) plus d (21.5 in.). The 1971 ACI code did not call for any of the negative moment reinforcement to be continuous. The outer ends of these bars were extended and hooked 12 in. down into the outer columns. As for the shear reinforcement, the columns contained #4 stirrups every 18 in. The beams had 19 #3 stirrups in each end every 6 in. Thus, there were 38 stirrups in every beam.

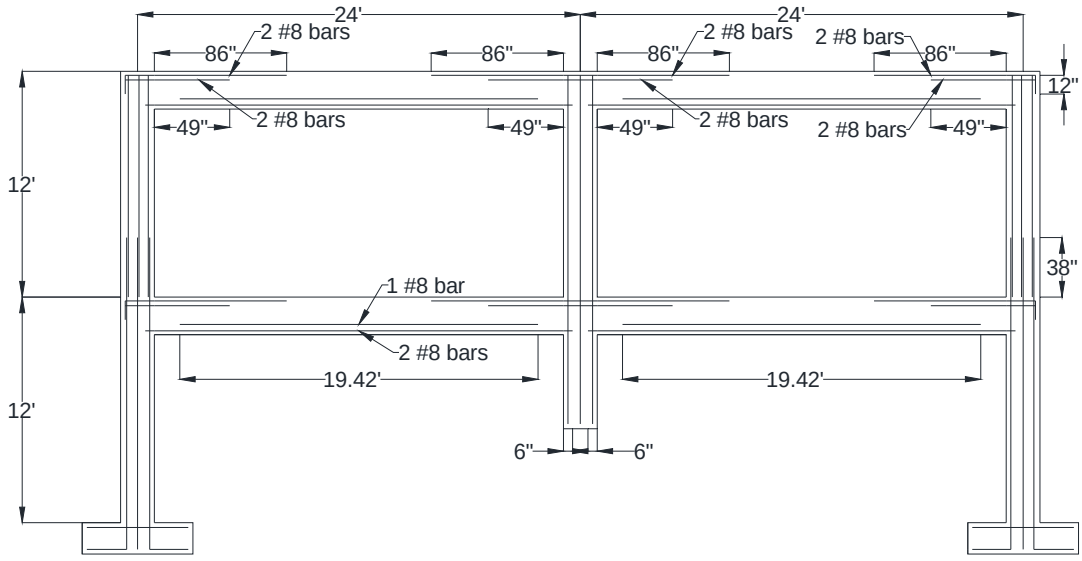

Figure 3.1.5: Longitudinal reinforcement layout for full scale discontinuous frame

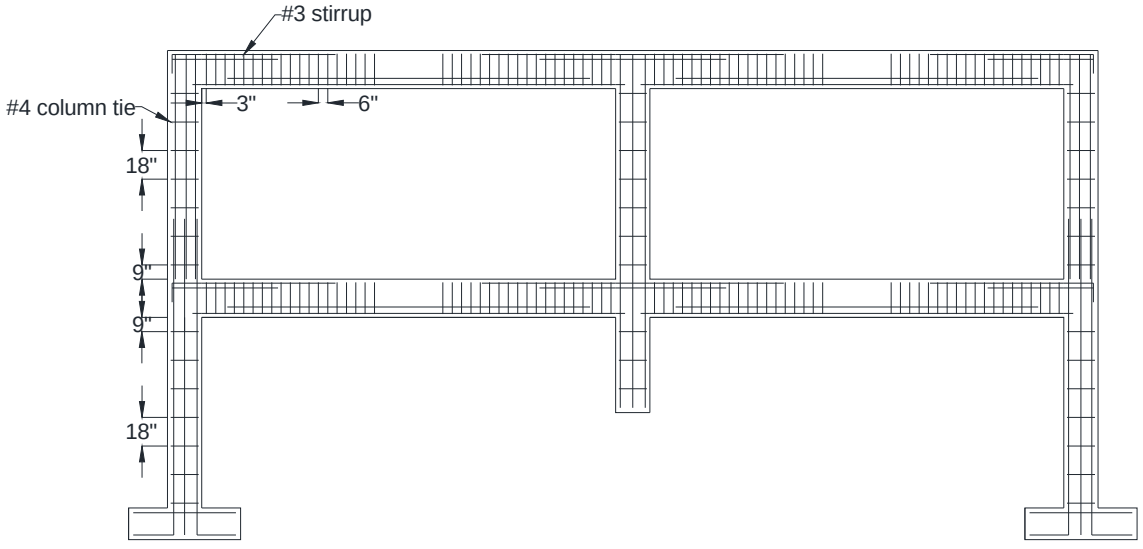

Figure 3.1.6: Transverse reinforcement layout for full scale discontinuous frame

3.2. Design of the Discontinuous Reinforcement Test Frame

At this point, the full scale frame had been designed and detailed according to the 1971 ACI code. The next step was to scale the frame to one-quarter of the size based on length. Thus the columns became 5.5 in. by 5.5 in. and the beams became 6 in. by 3 in. By quarter scaling the length, the area of concrete is scaled down to one-sixteenth of the original. As for the reinforcement, the scaling was based on the diameter of the bars. Unfortunately, the scaling of the bars was not as exact as the concrete due to the limited number of bar sizes. For the column reinforcement, the 8 #10 bars (1.27 in. diameter) were scaled to 6 #3 bars (0.375 in. diameter). For the beam reinforcement, all of the #8 bars (1.0 in diameter) were scaled to #2 or D5 bars (0.25 in. diameter). The cold drawing manufacture process of small reinforcing bars generally reduces their ductility and eliminates the yield plateau. Therefore, the #2 bars were all heat treated to preserve ductility, and their ultimate tensile strength was about 90 ksi. The #3 (0.375 in. diameter) and #4 bars (0.5 in. diameter) for the shear reinforcement were all scaled down to D2 bars. When it comes to area of the bars, the scaled beam bars were one-sixteenth the original, but the scaled column bars were about one-twelfth the original. These were the closest matches based on availability. The quarter scale cross-sections are shown in Figure 3.2.1, Figure 3.2.2 and Figure 3.2.3.

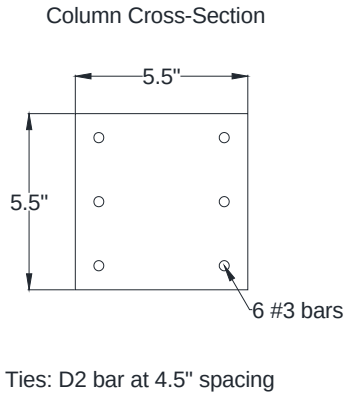

Figure 3.2.1: Column cross-section for quarter scale frame

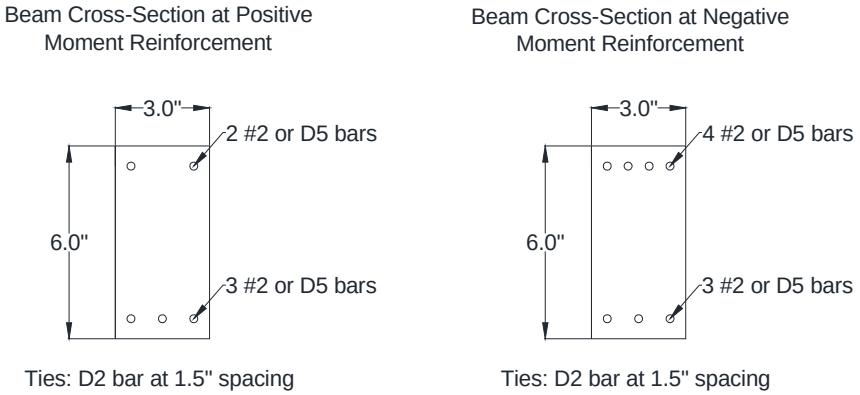

Figure 3.2.2: Beam cross-section for quarter scale frame

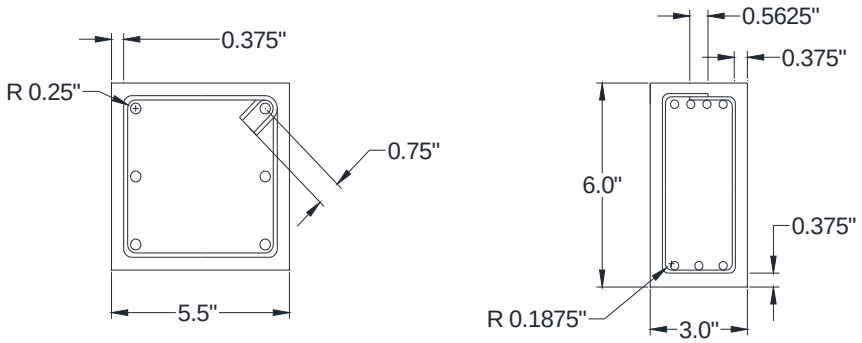

Figure 3.2.3: Transverse reinforcement detailing for quarter scale frame

The quarter scale discontinuous reinforcement frame is shown in Figure 3.2.4 and Figure 3.2.5. As with everything else, the length of the bars was scaled down to one-quarter of the length. The columns contained 6 #3 bars with 9.5 in. lap splices. The positive moment reinforcement included 3 #2 bars for the middle 58 in. of the beams with the 2 outer bars extending 1.5 in. into the columns. As for negative moment reinforcement, 2 #2 bars would extend 21.5 in. from the face of the column while the 2 outer #8 bars would only extend 12 in. The outer ends of these bars were extended and hooked 3 in. down into the outer columns. As for the shear reinforcement, the columns contained D2 stirrups every 4.5 in and the beams had 19 D2 stirrups on each end every 1.5 in.

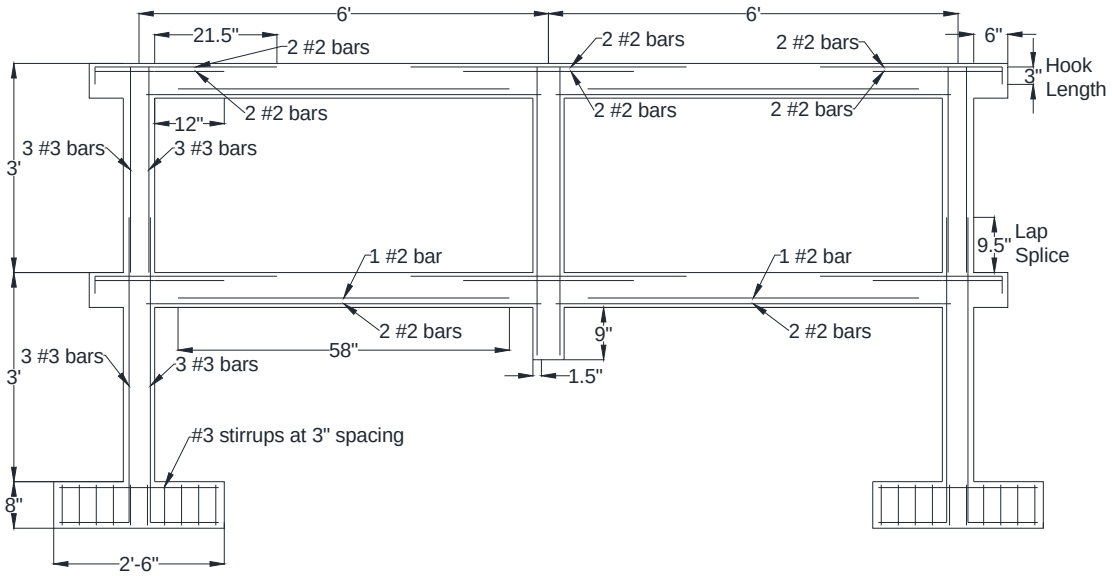

Figure 3.2.4: Design of discontinuous reinforcement test frame

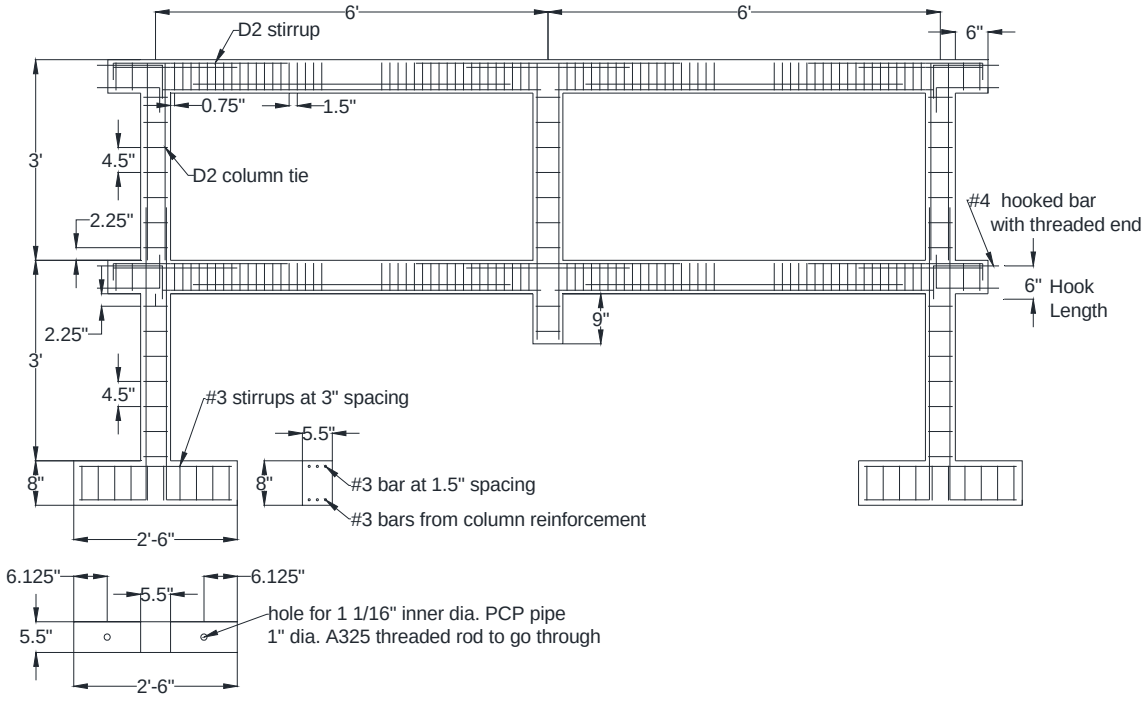

Figure 3.2.5: Transverse reinforcement layout for discontinuous reinforcement test frame

In order to attach the test frame to the reaction frame and provide the needed axial resistance, #4 threaded bars were extended out of the beams. One problem was that there was insufficient room for the development length of the hook. Thus, a 6 in. long knob was added to the outer end of each of the beams to solve the problem as shown in Figure 3.2.5. The beam reinforcement extended and hooked into the knobs. In order to provide moment resistance to the base of the columns, a 2 ft.-6 in. long by 8 in. high pedestal was added to the bottom of the two outer columns as shown in Figure 3.2.5. This pedestal was the same thickness as the columns (5.5 in.). The 6 #3 bars in each column extended and hooked through the bottom of the pedestals. Also, 3 #3 bars were placed in the longitudinally in the top of the pedestals. Stirrups made of #3 bars were placed in the pedestal at 3 in. spacing. Two PCP pipes of 1.0625 in. inner diameter were placed each of the pedestals to allow threaded rods to go through and anchor the test frame to the structural floor. The final modification of the test frames was that the bottom of the middle column was removed as shown in Figure 3.2.4. This was done to simulate that it had been irrevocably damaged or destroyed.

3.3. Design of the Continuous Reinforcement Test Frame

The next step was to design the test frame based on the 2008 ACI code. The column reinforcement for both the longitudinal and shear was not affected by this change. The area of steel for the beams also remained the same. The shear reinforcement for the beams remained the same as well. What did change was the length of the longitudinal reinforcement for the beams. While the 2 outer bars of the negative moment reinforcement were the same length as the previous frame, the 2 inner bars would extend

throughout the beams as called for in the 2008 ACI code. Since this length would surpass the common maximum length of bars (40 ft.), a lap splice of 62 in. would be used in the full scale frame. For the quarter scale frame, this would mean a 15.5 in. lap splice placed in the middle of the beams as shown in Figure 3.3.1. As for the positive moment reinforcement, the shorter inner bar was the same length as the previous frame, but the 2008 ACI code called for the outer 2 bars to extend continuously throughout the beams. Since this length also surpassed the common maximum length of bars, a lap splice would also be used. These 15.5 in. lap splices for the quarter scale frame would be placed at the columns as shown in Figure 3.3.1.

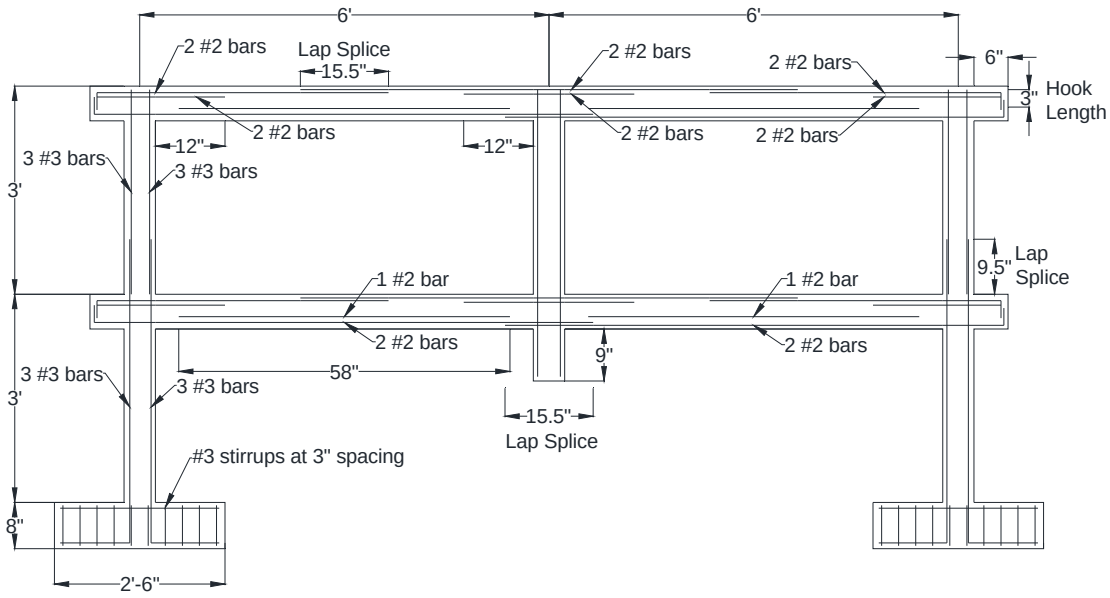

Figure 3.3.1: Design of continuous reinforcement test frame

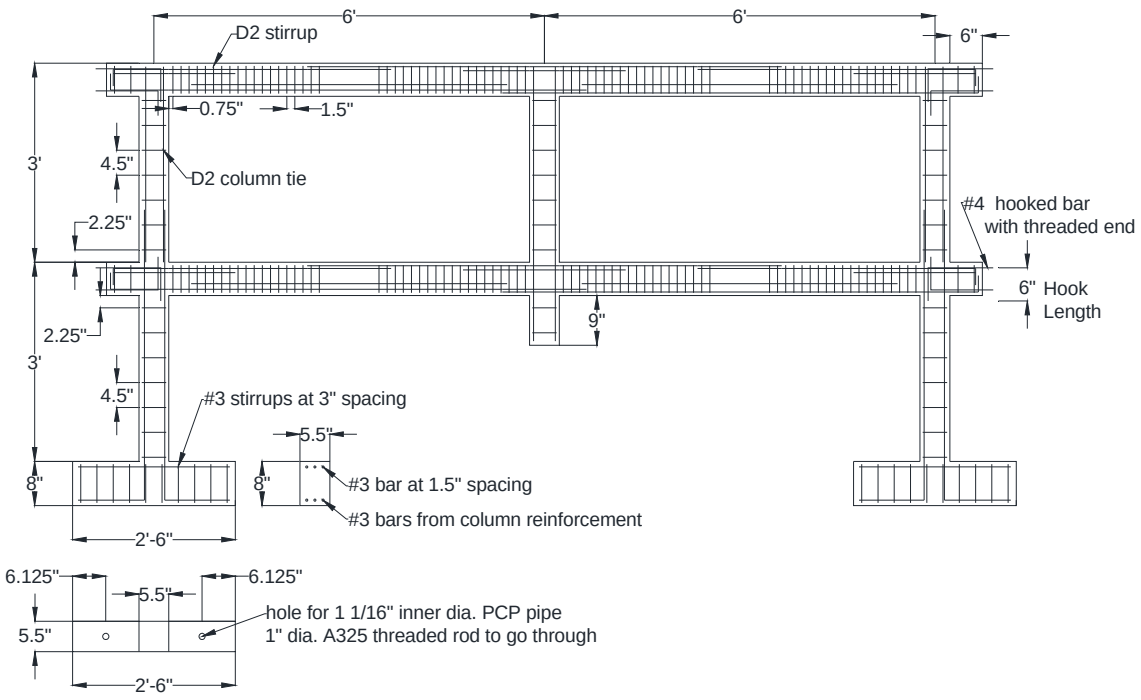

Figure 3.3.2: Transverse reinforcement layout for continuous reinforcement test frame

3.4. Design of the Infill Wall Test Frame

The infill wall test frame had the same reinforcement layout as the discontinuous reinforcement frame based on the 1971 ACI code. The difference was that this frame would also have an infill or shear wall placed in it as shown in Figure 3.4.1. The two top bays were filled with four rows of cinder blocks. This replicates frames with windows or parking garages with short walls. Each row had 14 cinder blocks that measured 4.5 in. long by 2.25 in. wide by 2.25 in. high (scaled down from typical cinder blocks of 16 in. by 8 in. by 8 in.). Type S mortar was used with a compressive strength of 1,800 psi. The walls were not grouted and the bed joints were approximately 0.25 in. thick.

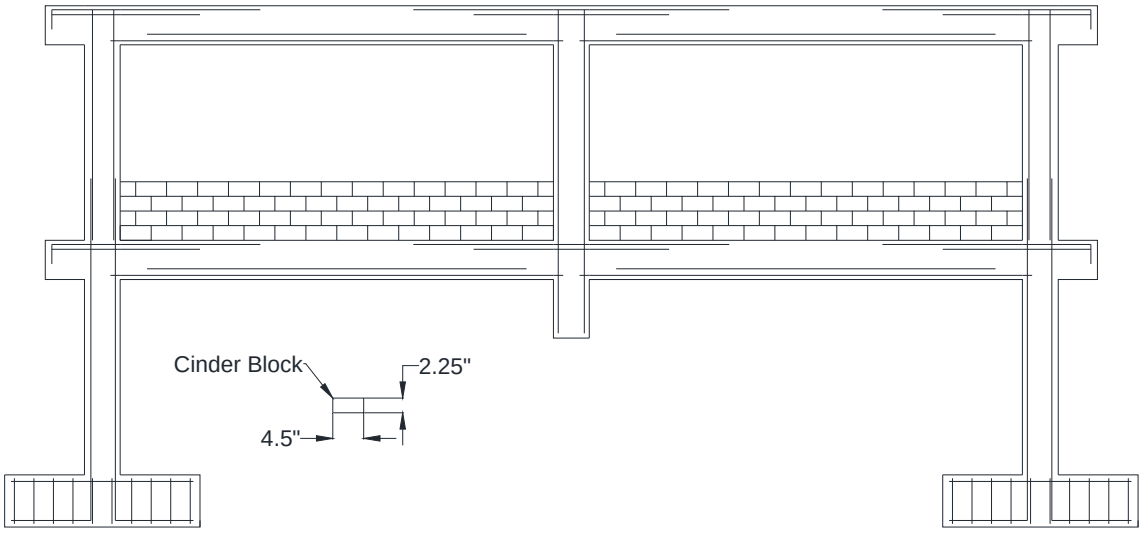

Figure 3.4.1: Test frame with infill wall

3.5. Construction of the Reinforced Concrete Test Frames

The first part of construction was making the formwork. The idea was to have the formwork be reusable for multiple frames. Therefore the formwork was designed so that it could be taken off without damaging the wood. The formwork was made out of ¾ in. plywood, ½ in. plywood and 2 by 4's. It was constructed and labeled according to Figure 3.5.1. The construction of the formwork is shown in Figure 3.5.2, Figure 3.5.3, Figure 3.5.4 and Figure 3.5.5.

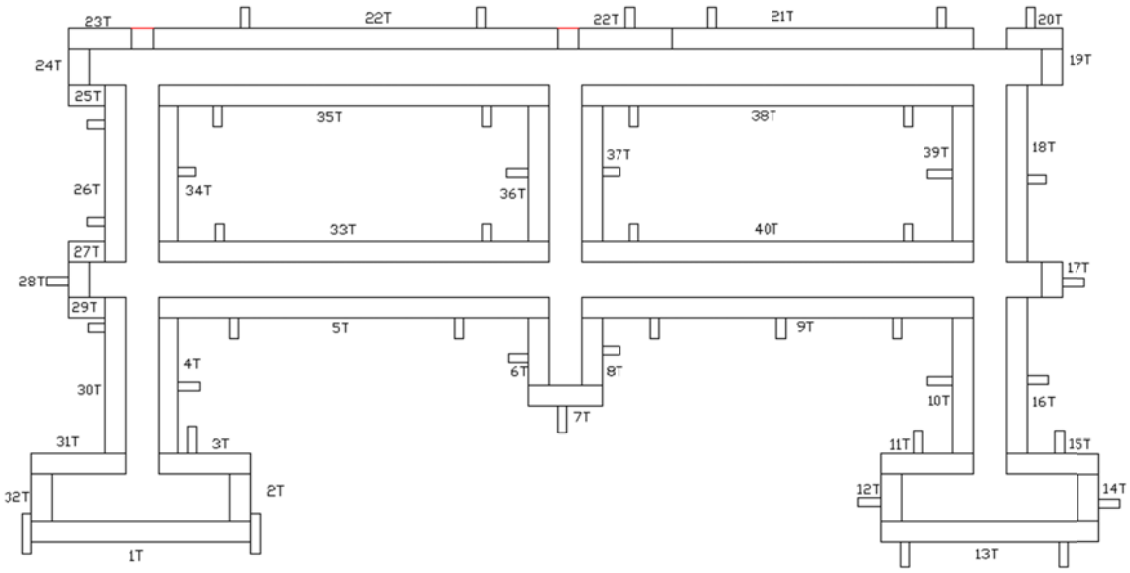

Figure 3.5.1: Design of formwork

Figure 3.5.2: Construction of formwork

Figure 3.5.3: Construction of formwork

Figure 3.5.4: Construction of formwork

Figure 3.5.5: Construction of formwork

After the formwork was constructed, the bars needed to be cut and bent to the specified dimensions. Jigs were constructed in order to bend the D2 size stirrups the same way each time as shown in Figure 3.5.6 and Figure 3.5.7. As for the #2 and #3 longitudinal bars, they were bent using a pipe and vice as shown in Figure 3.5.8. The final products are shown in Figure 3.5.9, Figure 3.5.10 and Figure 3.5.11.

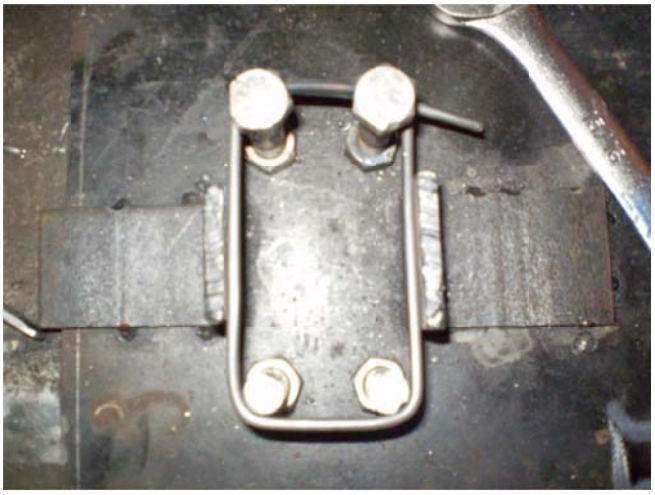

Figure 3.5.6: Bending of beam stirrup

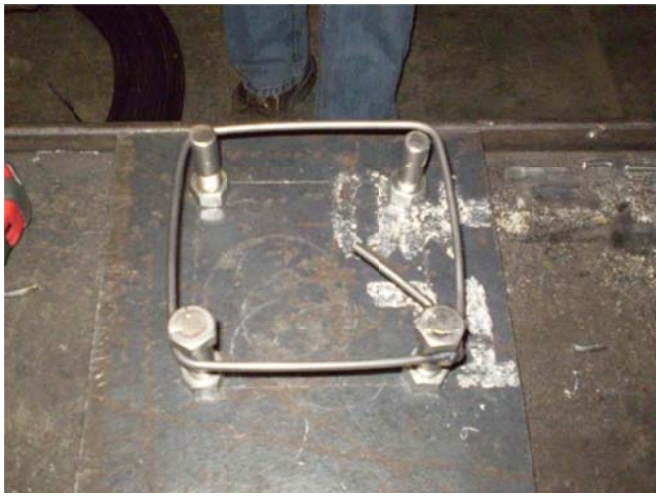

Figure 3.5.7: Bending of column stirrup

Figure 3.5.8: Bending of longitudinal bar

Figure 3.5.9: Beam stirrup

Figure 3.5.10: Column stirrup

Figure 3.5.11: Bent longitudinal bars

Before the reinforcement could be placed in the formwork, strain gages had to be attached to certain bars. These strain gages were attached according to the directions in the Vishay Measurements Group Education Division's "Student Manual for Strain Gage Technology". First the bars were grinded and wiped clean to look like the one in Figure 3.5.12. Then the strain gages were glued to the bars and covered like those in Figure 3.5.13.

Figure 3.5.12: Bars grinded and scrubbed clean

Figure 3.5.13: Strain gages on bars

Besides the basic layout, holes had to be cut throughout the formwork. Holes had to be cut out for the PCP pipes in the pedestals (Figure 3.5.14), for the hooked #4 end-threaded bars coming out of the outer ends of the beams (Figure 3.5.15), and for the lifting inserts in the top of each column (Figure 3.5.16). The PCP pipes were so that the 1 in. threaded rod could go through the pedestals. The hooked #4 end-threaded bars were for tying the concrete frame into the reaction frame. The lifting inserts were so that the frame could be lifted by a crane.

Figure 3.5.14: PCP pipe in pedestals

Figure 3.5.15: Hooked #4 end-threaded bars

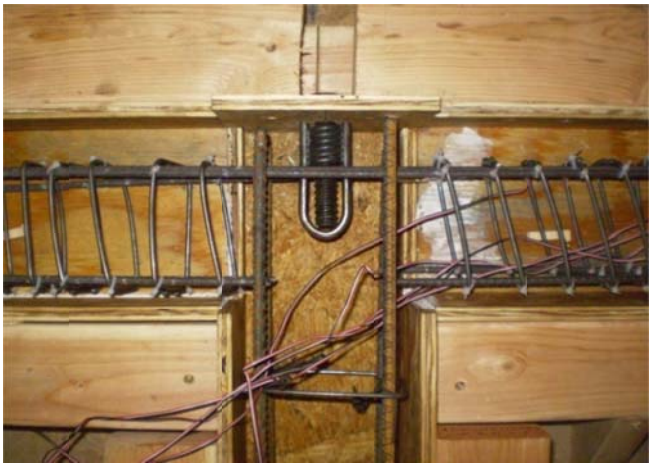

Figure 3.5.16: Lifting insert in the top of each column

The next step was to place the reinforcement in the formwork as shown in Figure 3.5.17, Figure 3.5.18 and Figure 3.5.19. The stirrups were connected to the longitudinal bars using bar ties. The reinforcement cages were held up off the bottom of the formwork by chairs made out of wood. The strain gage wires were pulled into a few different exit points.

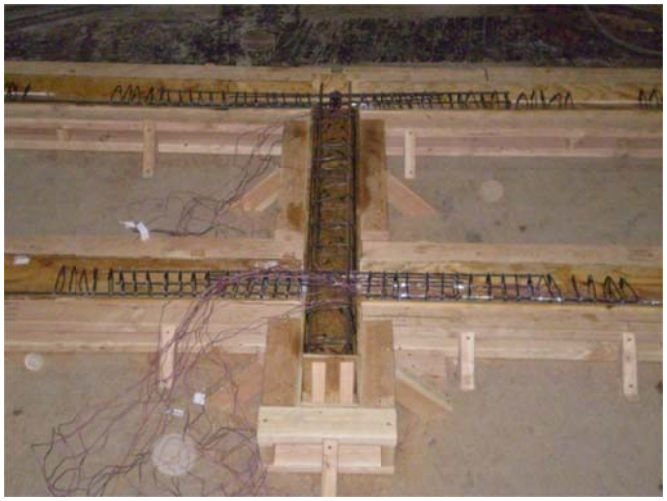

Figure 3.5.17: Middle column of the frame

Figure 3.5.18: Outer column of frame

Figure 3.5.19: Reinforcement tied into formwork

The final step in the construction of the test frames was the actual pouring of concrete. As stated before, the concrete used had a unit weight of 150 pcf and a compressive strength of 4,000 psi. It was made out of 3/8 in. limestone and was bought from a local supplier. After the concrete had been poured and vibrated (Figure 3.5.20), it was smoothed out using troughs (Figure 3.5.21). Once it was smoothed out, the frame looked like as show in Figure 3.5.22. Afterwards, cylinders (4 in. by 8 in.) were filled with concrete for future compression tests (Figure 3.5.23).

Figure 3.5.20: Pouring and vibrating concrete

Figure 3.5.21: Smoothing out the concrete

Figure 3.5.22: Poured concrete frame

Figure 3.5.23: Compression test cylinders

The concrete was covered with a plastic sheet and laid in place for about a week before the formwork was taken off. The frame was lifted about two weeks after pouring. The concrete was allowed to cure for at least 28 days. The finished product can be seen in Figure 3.5.24, Figure 3.5.25 and Figure 3.5.26.

Figure 3.5.24: Lifting insert and end-threaded bars

Figure 3.5.25: PCP pipes in pedestals

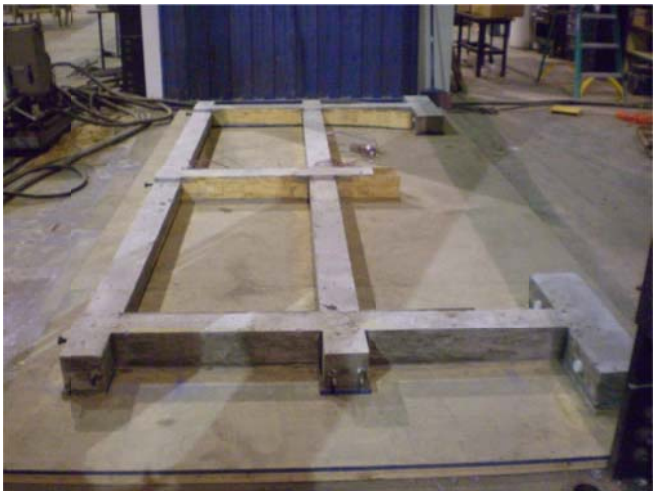

Figure 3.5.26: Finished concrete frame

3.6. Design and Construction of Test Setup

The design of the test setup involved designing the reaction frame, the floor anchors, the collar for the center column, and the connection to the actuator. The reaction frame was the most critical part of the test setup. It is designed to represent the reactions from the rest of the building. After all of the building dimensions and load were placed into a RISA model, the column and portions of the floor were removed to simulate that it had

been destroyed. Based on the cause of the initial column removal, there are different areas to represent as damaged or removed in the RISA model. The two main variables were how much of the column to remove and how much of the floor remove. Either one floor of the column could be removed or two floors could be removed. For the floor itself, none, half or the entire floor encompassing the two surrounding bays could be removed. The situation that was used was when the column was removed for two floors and half of the floor was removed as shown in Figure 3.6.1.

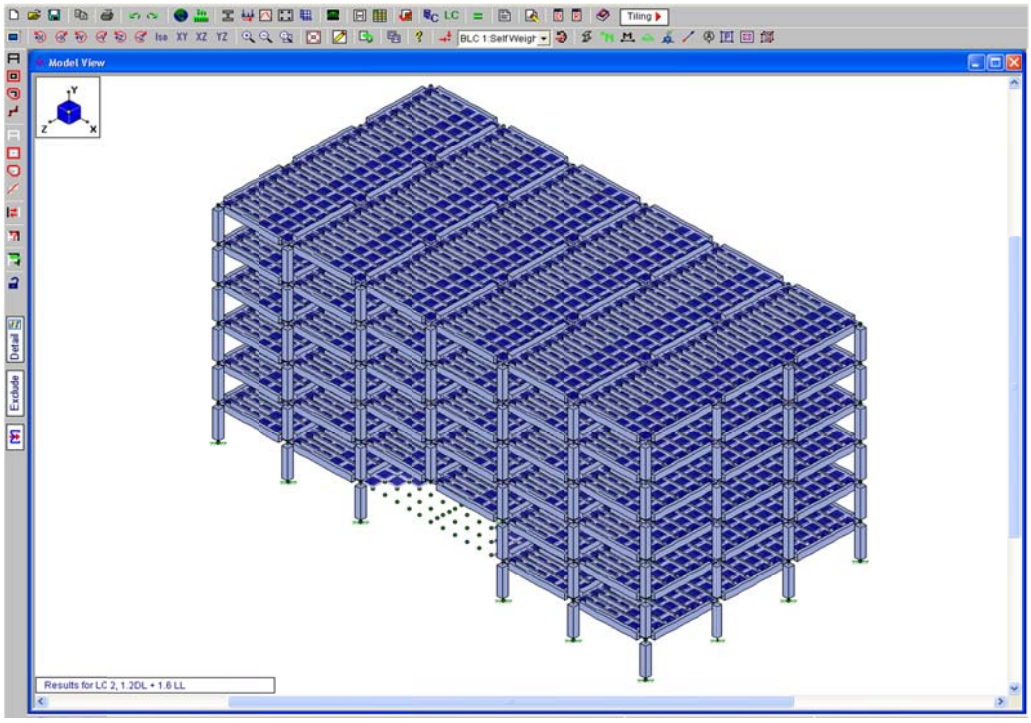

Figure 3.6.1: RISA model with missing column

From this model, the lateral stiffness of the surrounding frame could be calculated and used to design the stiffness of the reaction frame. Fictitious horizontal loads were placed on the two exterior columns on each side of the missing column at the top of the first

floor. These loads were perpendicular to the missing column and placed in the same plane as the other exterior columns. After inputting the loads, the displacement at those two points were found and the desired stiffness could be calculated. Based on this model, the stiffness of the outer columns were approximately 5000 kips/in. This would correlate to a stiffness of 1250 kips/in for the quarter scale test frame. Therefore, the reaction frame had to mimic the building by having a stiffness of 1250 kips/in.

The reaction frame was designed to be bolted into the structural floor just like the column pedestals. Using W shapes and tubes, the reaction frame was designed to have a stiffness of 1250 kips/in. Each side of the reaction frame consisted of two W14x22's that were welded together, an HSS4.5x4.5x5/16 tube, an HSS3.5x3.5x1/4 and a number of plates as shown in Figure 3.6.2. The reaction frame was built so that it could be taken apart and put back together. The tubes were welded to plates which bolted into the W shapes and the floor anchors as shown in Figure 3.6.3, Figure 3.6.4 and Figure 3.6.5. The concrete test frame tied into the reaction frame using the #4 end-threaded bars sticking out. Plates connected to extensions of the reaction frame were bolted onto the threaded bars as shown in Figure 3.6.6. Included in each of these extensions was a hinge. The point of the hinges was to protect the load cells (discussed later in this chapter). They were located at the inflection point where a concrete beam (if there was one) would form a hinge.

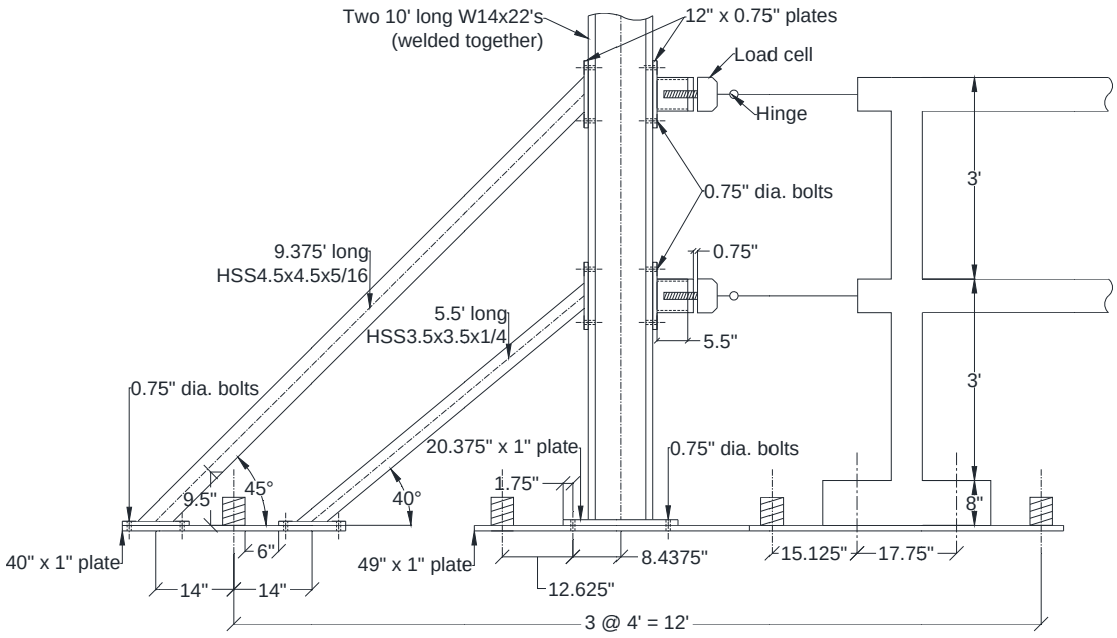

Figure 3.6.2: Design of reaction frame

Figure 3.6.3: Reaction frame

Figure 3.6.4: Reaction frame

Figure 3.6.5: Reaction frame bolted into the structural floor

Figure 3.6.6: Reaction frame tied into the concrete frame

In conjunction with the reaction frame were the pedestals for the outer columns. The pedestals of the test frames represent the anchorage of the columns into the foundation and provide moment resistance at the base of the column. The floor where the testing took place was a structural floor with bolt holes on a 4 ft. by 4 ft. grid. Steel plates with tubes would connect the test frame to the structural floor as shown in Figure 3.6.7, Figure 3.6.8 and Figure 3.6.9. The concrete pedestals were bolted to the steel plates with 1 in. diameter threaded rods that went through the PCP pipes. The threaded rods screwed into the plate and a nut was used to tie down the pedestals. The steel plates were bolted down into the structural floor using 3.5 in. diameter threaded rods. Nuts were twisted until they were tight against the pipes that were welded to the plates. The HSS4x4x1/4 tubes welded on the sides of the plate were there for extra support.

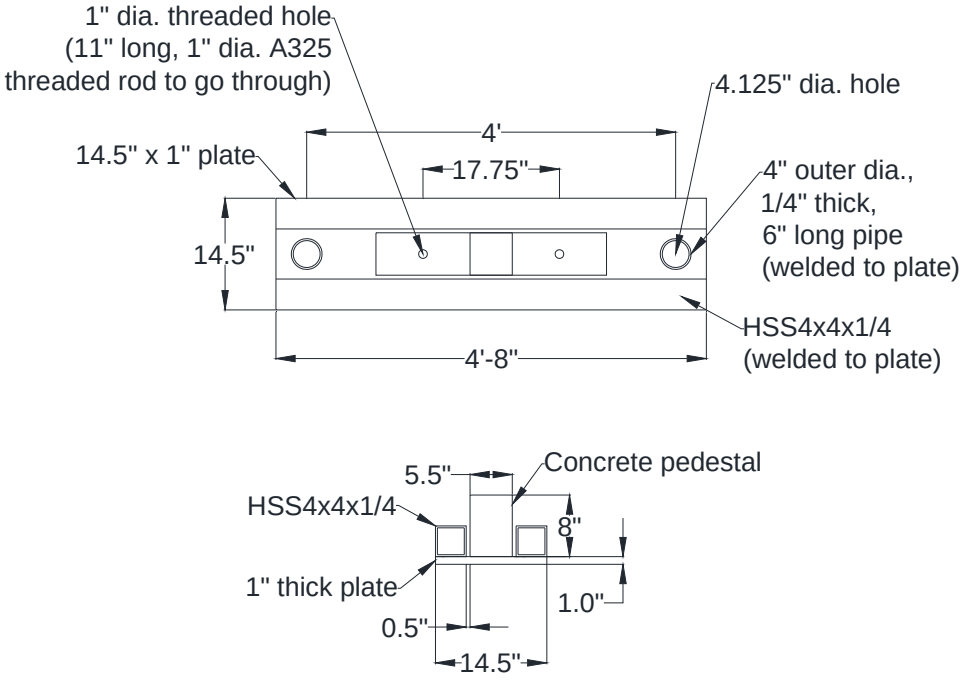

Figure 3.6.7: Design of anchors for the pedestals

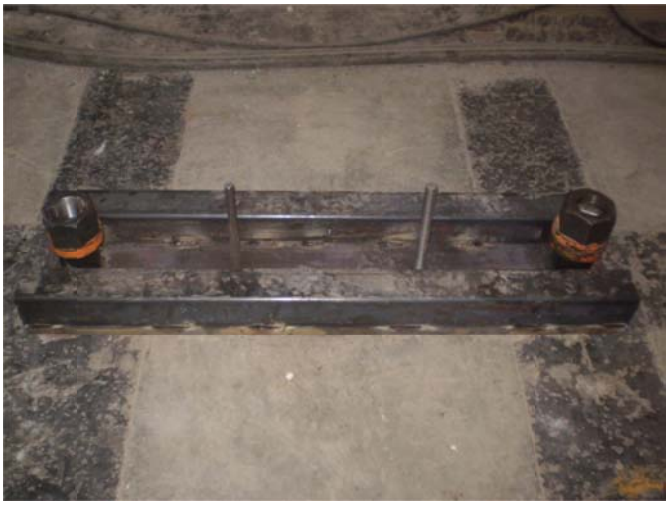

Figure 3.6.8: Anchor for the pedestal

Figure 3.6.9: Pedestal anchored to the floor

Another part of the test setup was the collar for the center column. This collar was would only allow the center column to move vertically as shown in Figure 3.6.10. The collar was made out of HSS6x6x1/4 tubing and ½ in. plates as shown in Figure 3.6.11. The collar was in four pieces that bolted together tightly around the center column. Linear ball bearings were bolted on two sides of the collar. These bearings would slide down

shafts as the frame was pushed down as shown in Figure 3.6.13 and Figure 3.6.14. These shafts were bolted to W4x13's which were welded to out-of-plane frames. These frames were made of HSS6x2x1/4 tubing and welded to plates which were connected to anchored W sections.

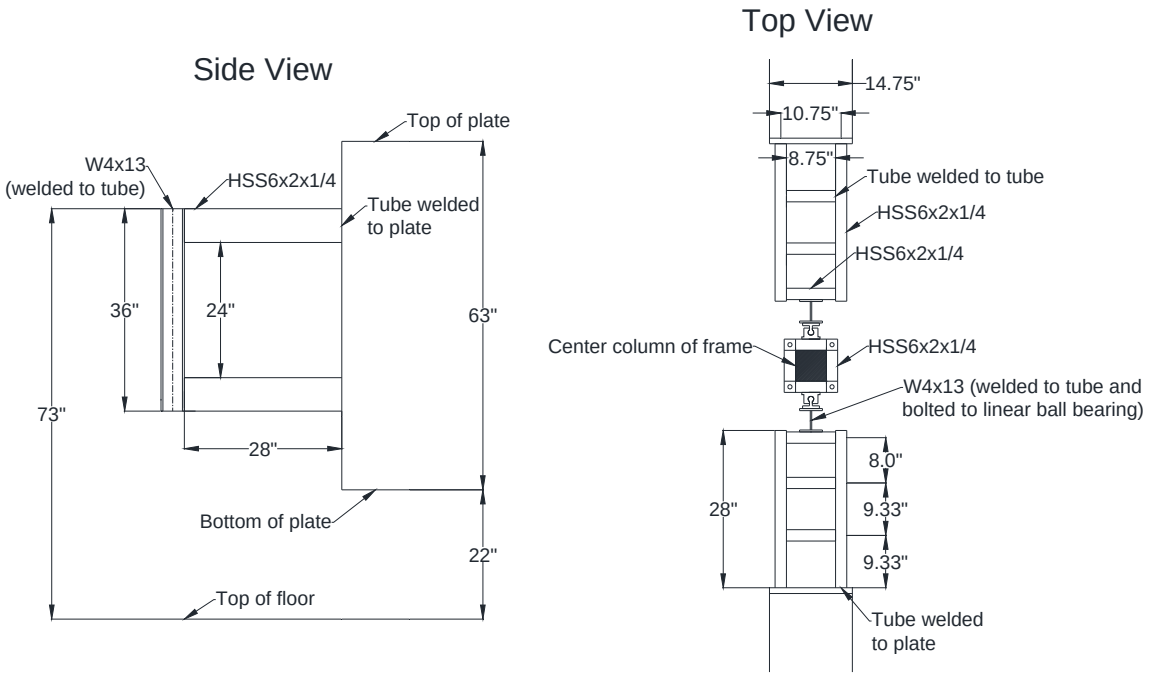

Figure 3.6.10: Design of the collar for the center column

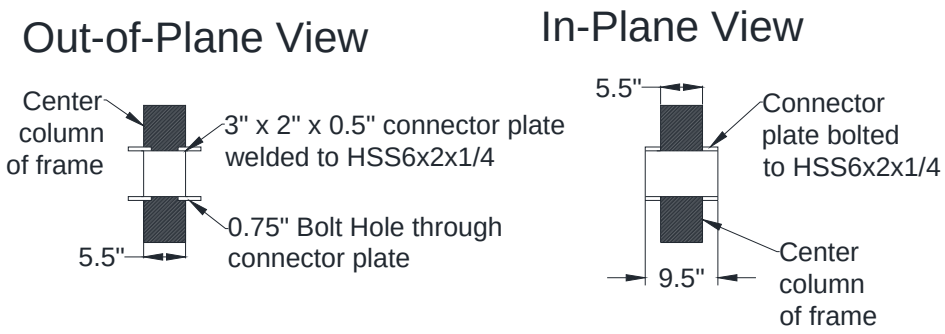

Figure 3.6.11: Details of the collar

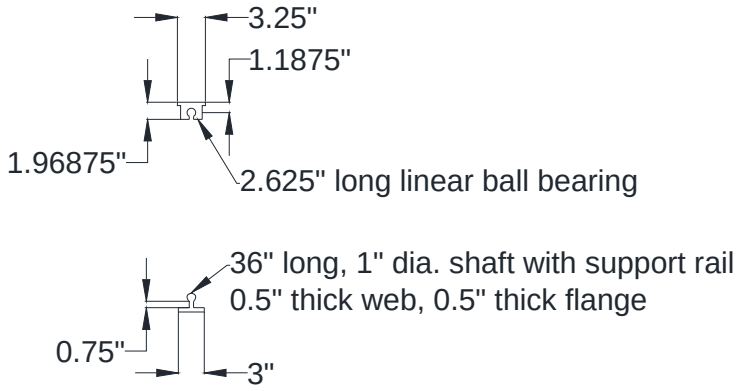

Figure 3.6.12: Details of the linear ball bearings

Figure 3.6.13: Collar for the center column

Figure 3.6.14: Collar for the center column

The last part of the test setup involving a connection was the connection to the actuator. The point of this connection was so that the actuator would stay square on the center of the concrete frame. The actuator was an MTS model capable of 110 kips. An extension was attached to this actuator in order reach the desired displacement. At the end of this

extension was a swivel head had a plate at the bottom with four holes. The concrete frame was connected by threaded rods through these holes as shown in Figure 3.6.15. Plates were underneath the top beams for the threaded rods to bolt through. Nuts at each end of the threaded rods were used to tighten the connection as shown in Figure 3.6.16.

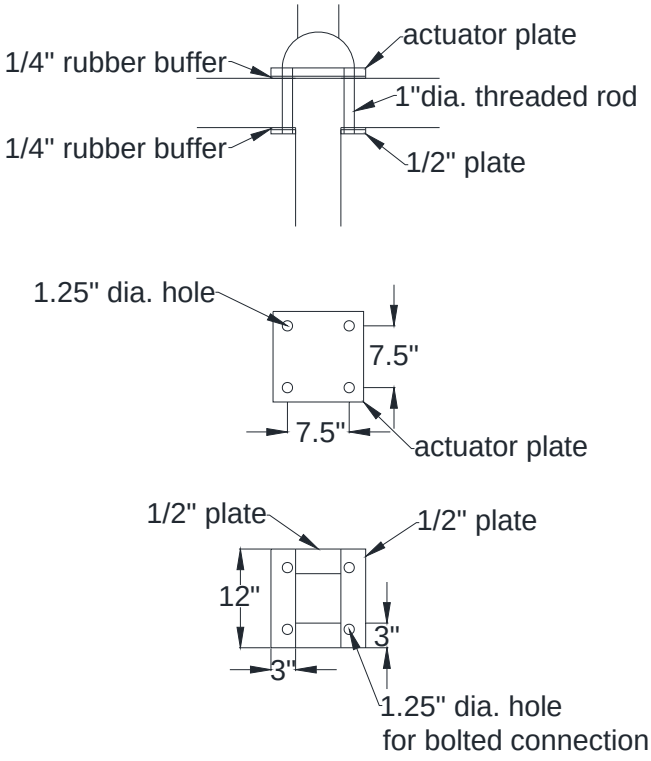

Figure 3.6.15: Design of the connection to the actuator

Figure 3.6.16: Connection to the actuator

Figure 3.6.17: Connection to the actuator

3.7. Instrumentation

Besides the test setup, there was also instrumentation such as strain gages, load cells, LVDT's (Linear Variable Differential Transformer), a string pot, and a load actuator. All of these measurement devices were hooked up to a data acquisition system where all of the data was recorded (Figure 3.7.1). The purpose of recording all this data is to compare

the various tests within this research and to compare against tests from other research. These values can show how much more the effective the resistance mechanisms are.

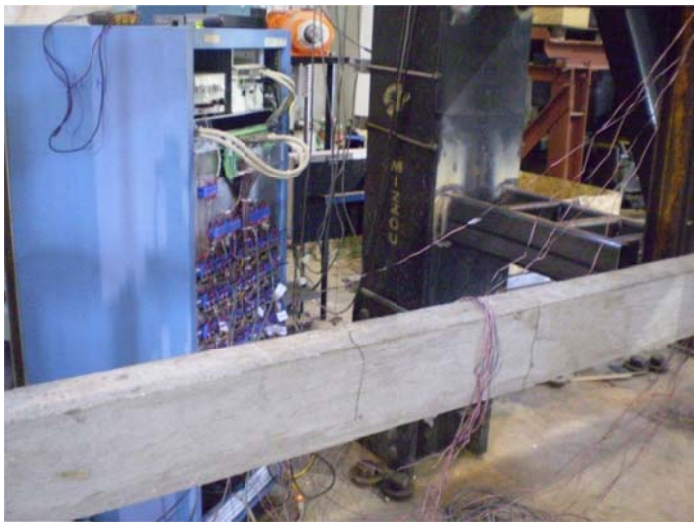

Figure 3.7.1: Data acquisition system

One design aspect of the instrumentation was the placement of the strain gages. Strain gages were located on one side of the test frames on both the positive and negative moment reinforcement. Some were placed at the maximum positive (middle of beams) and negative moment (end of beams) points. Others were placed throughout the beams to see the strain across the beams. Redundant strain gages were added in case some malfunctioned. The strain gage layout for the test frames with the discontinuous reinforcement is shown in Figure 3.7.2. There were 16 strain gages used in each of these test frames. The naming system is such that "T" stands for those in the top beam and "B" stands for those in the bottom beam. Also, "P" stands for those in the positive moment region and "N" stands for those in the negative moment region. The strain gage layout for the test frame with the continuous reinforcement is shown in Figure 3.7.3. There

were 21 strain gages used in this test frame. The naming system was the same for this frame.

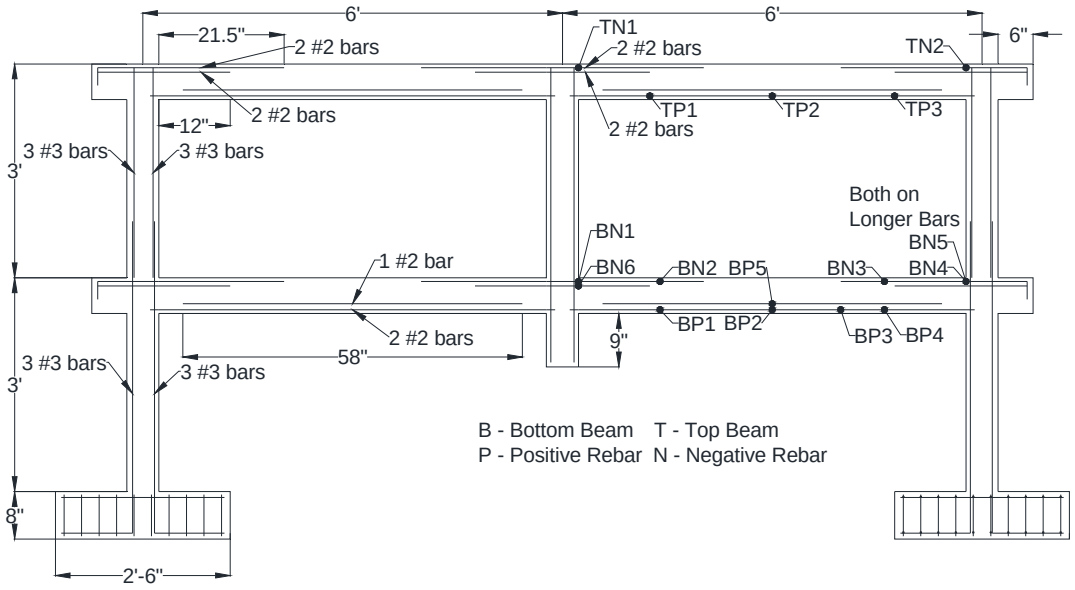

Figure 3.7.2: Strain gage layout for test frames with discontinuous reinforcement

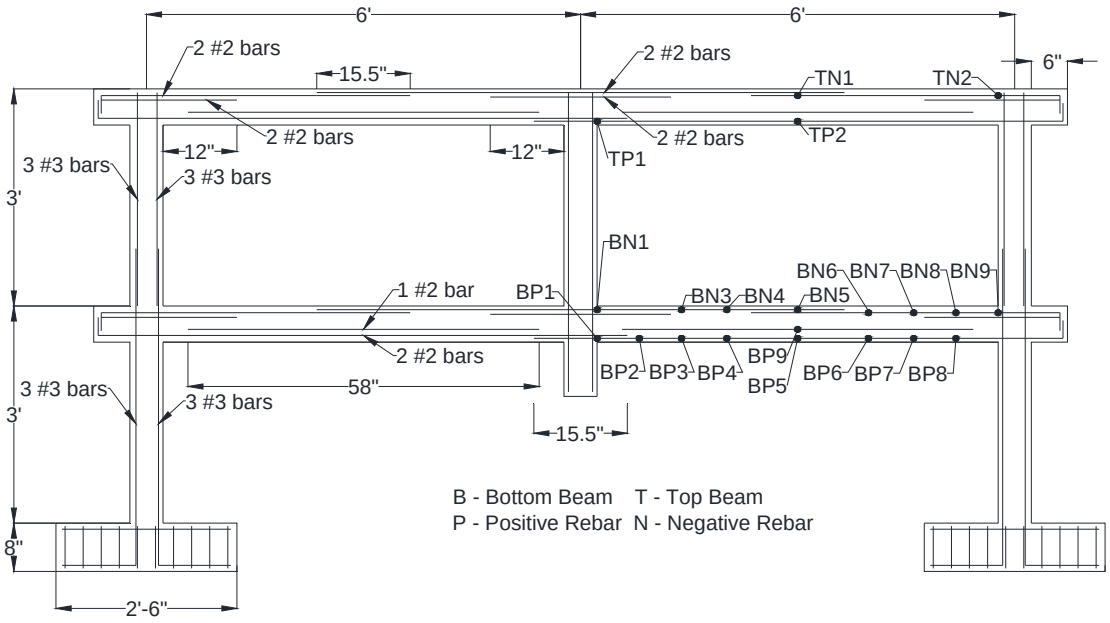

Figure 3.7.3: Strain gage layout for test frame with continuous reinforcement

Two Interface 1200 Standard Load Cells were connected to one side of the reaction frame using threaded rods as shown in Figure 3.7.4 and Figure 3.7.5. The loads cells were connected to the concrete frame by an extension made of W4x13's. At the end of these extensions were welded plates that were bolted to the concrete through the #4 end-threaded bars sticking. These load cells would measure the horizontal reaction force caused by compressive arch and catenary tension.

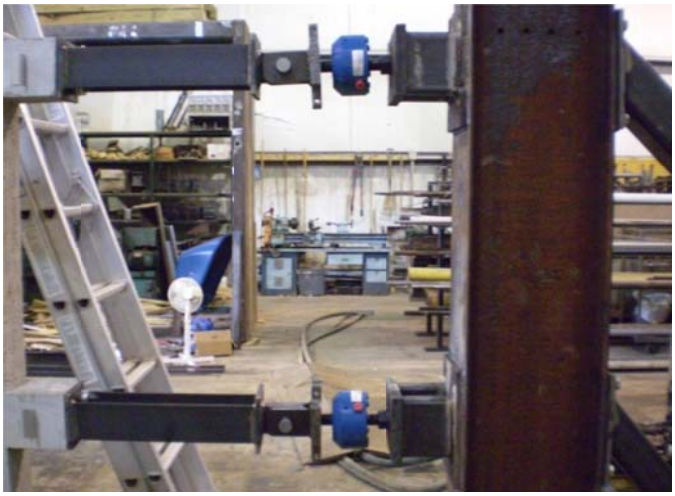

Figure 3.7.4: Load cells

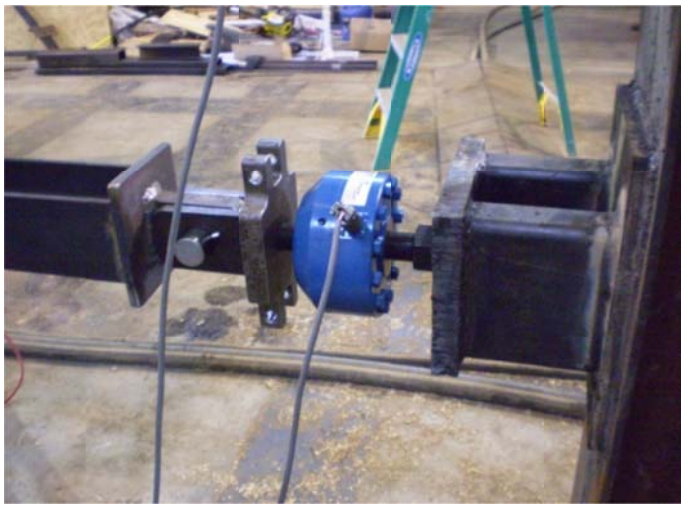

Figure 3.7.5: Load cell

Two LVDT's (Linear Variable Differential Transformers) were on the same side as the load cells as shown in Figure 3.7.6. Each one was placed at the center of the beams. Both were attached to a separate structure so that their values would be independent of the reaction frame. A couple small angles were glued to the concrete so that the rods in the LVDT's would have a resting place (Figure 3.7.7). The purpose of the LVDT's was to measure the lateral deflection of the concrete frame.

Figure 3.7.6: LVDT's

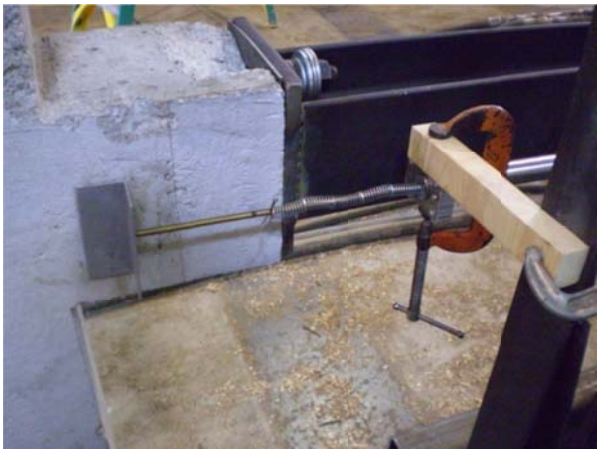

Figure 3.7.7: LVDT

The other measuring instrument was the string pot underneath the center column of the frame (Figure 3.7.8). This device measured the vertical deflection of the middle of the concrete frame and gave a backup measurement of the displacement recorded in the MTS actuator.

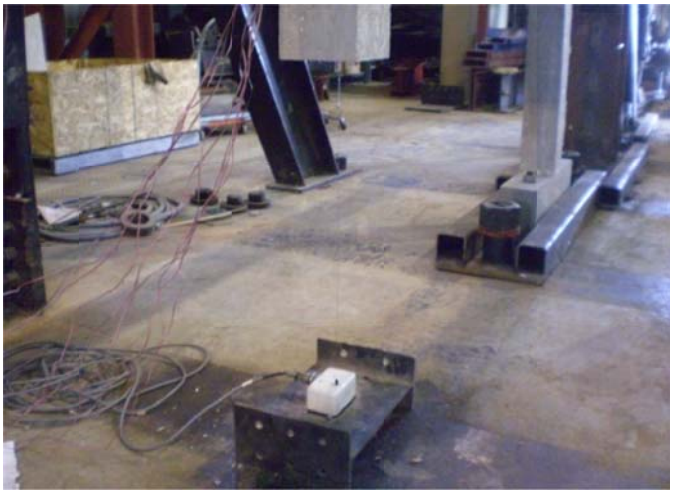

Figure 3.7.8: String pot

The final component was the device that loaded the test frames. An MTS force transducer or load actuator applied load at the center of the frame as shown in Figure 3.7.9. This load actuator would operate at a rate of 1/300 in/sec for the first 2 in. and 1/120 in/sec for the remainder of the test. A load cell in the actuator recorded the vertical load applied to the frame.

Figure 3.7.9: Load actuator

3.8. Material Properties

Material properties were determined according to ASTM (American Society of Testing and Materials) standards. Compression tests for the concrete cylinders (Table 3.8.1) were performed according to ASTM C39. The concrete's specified strength was 4000 psi. Due to variations in concrete batch and time of testing, the actual cylinder strength varied from 3417 psi to 6283 psi. The tension tests for the reinforcing bars (Table 3.8.2 and Table 3.8.3) were performed according to ASTM A370. Examples of these reinforcing bar tension tests are shown in Figure 3.8.1 and Figure 3.8.2. The specified yield point of the #3 column bars was 60,000 psi or 6,600 lbs. Due to variations in steel quality, the actual tensile strength of the #3 bars varied from 6,251 lbs to 6,587 lbs. The specified ultimate tensile strength of the #2 beam bars was 90,000 psi or 4,500 lbs. The loss of a well defined yield plateau was due to the #2 bars being cold drawn. The actual tensile strength of the #2 bars varied from 4,639 lbs to 4,848 lbs. All of these results were within acceptable ranges. The #2 bars were heat treated so that they had a similar ductility as larger reinforcing bars. The approximate Young's Modulus was calculated to be 17,500 ksi for the #2 bars and 13,300 ksi for the #3 bars. The elongation at break of the #2 bars was 2.55 and 2.73 for the #3 bars.

Table 3.8.1: Concrete cylinder compression tests

	Cylinder	Applied Load (lbs)	Strength (psi)
Discontinuous Frame	1	53970	4295
	2	56760	4517
	3	54900	4369
	4	54240	4316
	5	53320	4243
	6	58920	4689
	Average		4405
Continuous Frame	1	45930	3655
	2	42945	3417
	3	45420	3614
	4	45855	3649
	5	46005	3661
	6	46620	3710
	Average		3618
Infill Wall Frame	1	74160	5901
	2	78960	6283
	3	78420	6240
	4	76080	6054
	5	71940	5725
	6	75495	6008
	Average		6035

Table 3.8.2: Column #3 bar tension tests

Column #3 Bar	Yield Point (lbs)	Ultimate Load (lbs)
1	6251	10579
2	6504	10844
3	6587	10863
4	6446	10759
5	6262	10610
Average	6410	10731

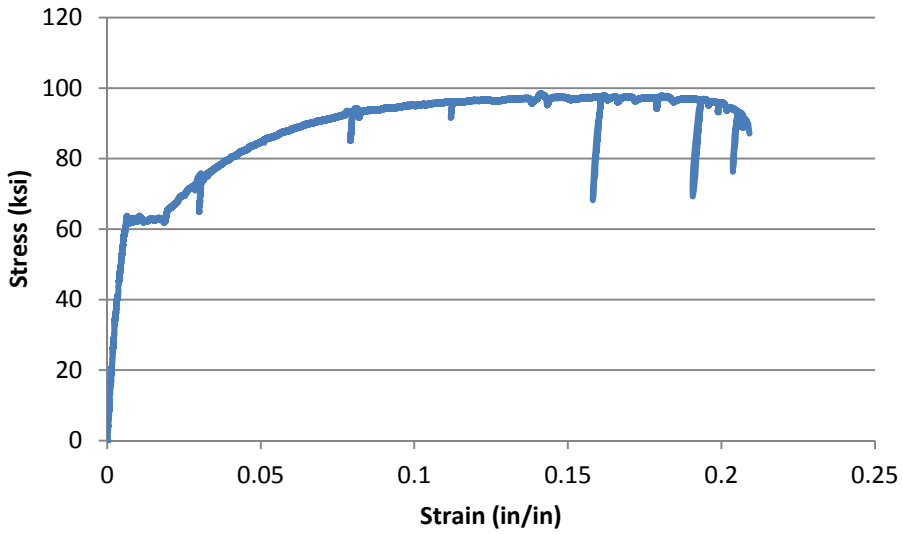

Figure 3.8.1: Stress vs. strain graph for column #3 bar

Table 3.8.3: Beam #2 bar tension tests

	Beam #2 Bar	Yield Point (lbs)	Ultimate Load (lbs)
Discontinuous Frame	1	4116	4817
	2	4125	4796
	3	4028	4660
	4	4045	4664
	5	4123	4836
	Average	4087.4	4754.6
Continuous Frame	1	4166	4848
	2	4117	4731
	3	4283	4736
	4	4160	4793
	5	4111	4749
	Average	4167.4	4771.4
Infill Wall Frame	1	4036	4666
	2	4041	4728
	3	4027	4639
	4	4189	4844
	5	4090	4780
	Average	4076.6	4731.4

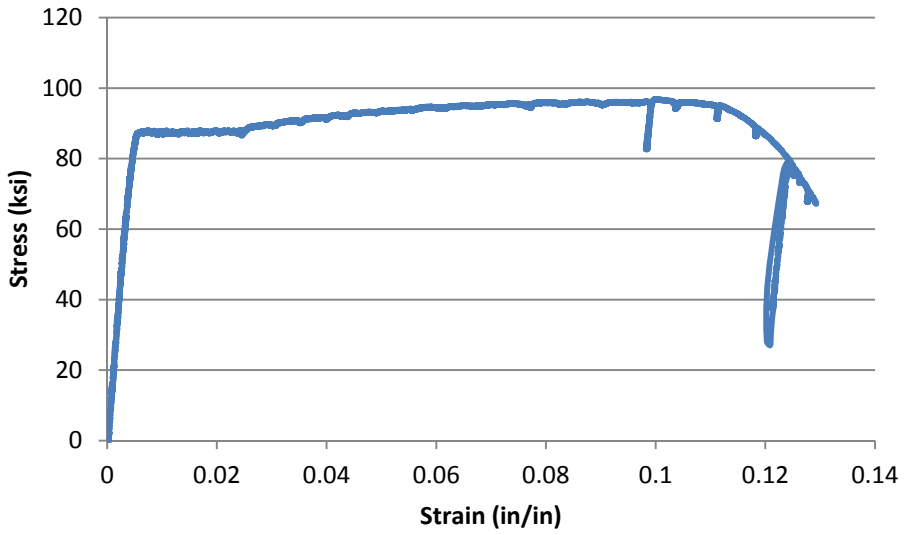

Figure 3.8.2: Stress vs. strain graph for beam #2 bar

The rest of the material property tests were related to the infill wall. The mortar cubes compression tests (Table 3.8.4) were performed according to ASTM C109. The single prisms compression tests (Table 3.8.5) and the dual-layer prisms compression tests (Table 3.8.6) were performed according to ASTM C1314. The stacked prisms flexural four-point bending tests (Table 3.8.7) were performed according to ASTM E518. The stacked prism flexural tests give an indication of the tensile strength of the mortar joints. Based on the tests, the average tensile strength of the mortar joints was 189 psi. All of these results were within acceptable ranges.

Table 3.8.4: Mortar cubes compression tests

Mortar Cubes Compression		
Specimen	**Applied Load (lbs)**	**Compressive Strength (psi)**
1	5045	1261
2	3030	758
3	3645	911
4	2100	525
Average		864
*Cross Sectional Area = 4 in^2		

Table 3.8.5: Single prisms compression tests

Single Prisms Compression			
Specimen	**Applied Load (lbs)**	**Compressive Strength (psi)**	**Failure Mode**
1	8625	1356	Semi Conical Break
2	21480	3377	Conical Break
3	14850	2335	Conical Break
4	18895	2971	Conical Break
Average		2510	
*Cross Sectional Area = 6.36 in^2			

Table 3.8.6: Dual-layer prisms compression tests

Dual-Layer Prisms Compression			
Specimen	**Applied Load (lbs)**	**Compressive Strength (psi)**	**Failure Mode**
1	18375	2889	Conical Break
2	9705	1526	Cone and Shear Break
3	15835	2490	Cone and Split Break
4	16755	2634	Conical Break
5	17850	2807	Conical Break
Average		2469	
*Cross Sectional Area = 6.36 in^2			

Table 3.8.7: Stacked prisms flexural tests

Stacked Prisms Flexural	
Specimen	**Ultimate Load (psi)**
1	232.6
2	166.5
3	167.2
Average	188.8

4. TEST RESULTS

The three tests (discontinuous reinforcement frame, continuous reinforcement frame and infill wall frame) will be shown and the results will be presented in this chapter. Furthermore, this chapter will discuss and compare the results of the three tests.

4.1. Discontinuous Reinforcement Frame

The control frame was based on the 1971 ACI code and thus had discontinuous reinforcement throughout the beams. Once the frame was set in place and ready to be tested, the actuator applied load to the center of the frame over the location of the lost column. Due to a technical error, the first 12 in. of displacement was loaded at a rate of 3 in/sec. The remaining part was tested at a rate of 1/300 in/sec and then 1/120 in/sec. Upon loading, the frame initially responded in an elastic manner. At a load of around 200 to 250 lbs, cracks began to form at the locations of discontinuous reinforcement (Figure 4.1.2). As the load increased, the cracks widened and hinges began to form as shown in Figure 4.1.3. The ultimate failure point was when the negative moment bars tore out of the last stirrup as shown in Figure 4.1.4.

Figure 4.1.1: Discontinuous frame before loading

Figure 4.1.2: Discontinuous frame forming cracks

Figure 4.1.3: Discontinuous frame forming hinges

Figure 4.1.4: Discontinuous frame at failure

A closer look at a particular beam will show details of the cracking and hinge formations. At a about a load of 200 to 250 lbs, cracks formed at the discontinuous ends of the reinforcement (Figure 4.1.5). This correlated well to the predicted cracking moment of the beams (8.532 kip-in) which translated to a load of 237 lbs. These cracks occurred at the discontinuous ends of the negative reinforcement which ended 21.5 in. from the face of the outer columns. On this particular beam, the crack started 22.5 in. from the column as shown in Figure 4.1.6. This was similar to all four beams. Because no reinforcement crossed these cracks, they continued to open widely and formed hinges (Figure 4.1.7) with little further cracking in the rest of the beam. The only other significant cracking in the beams took place at the discontinuous ends of the negative moment reinforcement coming from the center column (21.5 in. from the face). These cracks formed secondary hinges as shown in Figure 4.1.3.

Figure 4.1.5: Initial cracking

Figure 4.1.6: Crack at end of negative reinforcement

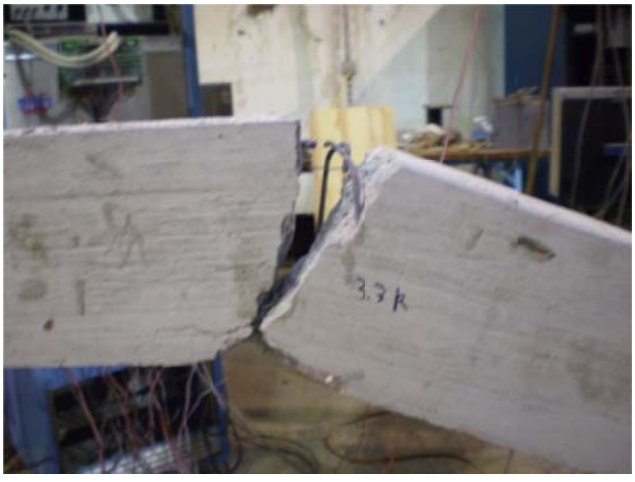

Figure 4.1.7: Formation of hinge

In addition to the hinges within the beams, there was damage where the beams connected with the center column. This was especially true for the bottom beams (Figure 4.1.8). These cracks occurred because the discontinuous positive reinforcement only extended 1.5 in. into the columns. These cracks widened and formed hinges as shown in Figure 4.1.9. At failure, the negative moment bars tore out of the stirrups as shown in Figure 4.1.10.

Figure 4.1.8: Formation of cracks at the center column

Figure 4.1.9: Formation of hinges at the center column

Figure 4.1.10: Longitudinal bars breaking out of the stirrups

The beams of this frame experienced two phases of resistance mechanism actions. After cracking and hinge formation, compressive arch action occurred as the end corners of the beam blocks were being crushed (Figure 4.1.11). Once these end corners were crushed, catenary action took over as the bars in the beams were placed in axial tension. These bars were pulled to the point that they tore out of the stirrups.

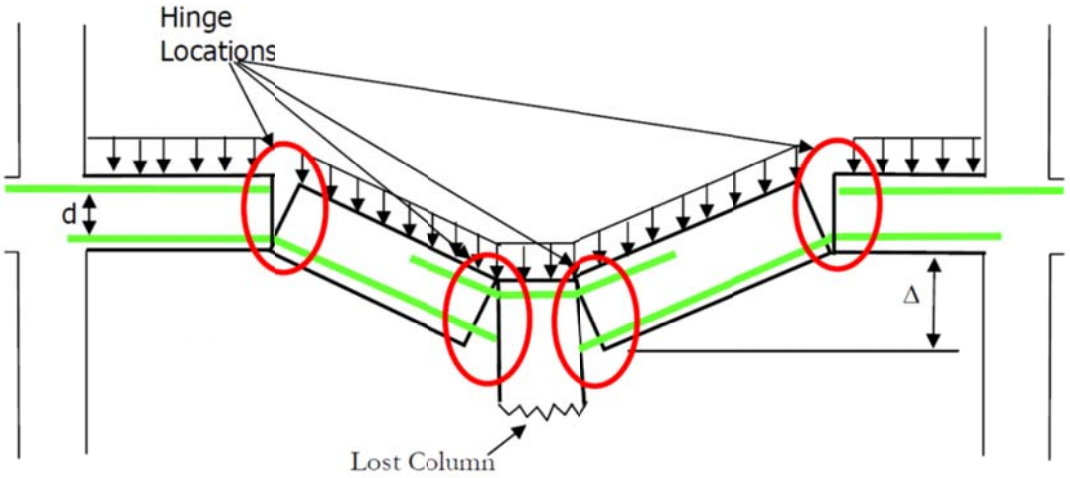

Figure 4.1.11: Diagram of compressive arch action (Orton, 2007)

Figure 4.1.12 shows the vertical load vs. displacement graph. From this graph, one can see the compressive arch action, the catenary action, and where the top bars tore out of the stirrups. Despite having only 237 lbs in load capacity according to flexural beam theory (based on the cracking moment of the beams), the frame was able to reach 2.34 kips in compressive arch action. As stated before, this strength comes from the compression arch effect as the beam blocks try to rotate. The high stresses at the end corners of the beam blocks eventually caused the concrete to crush and lose the compressive arch resistance. After the compressive arch phase, the frame continued to deflect with little increase of load until about 6.70 in. of displacement. Once this displacement was reached, any further deflections caused tensile strains in the beam blocks and catenary action began. At the end of the catenary action phase, the frame was able to reach a maximum load of 8.19 kips. At this level of load, the negative moment reinforcement tore out of the stirrups. The stirrups, as described earlier, were lapped 90 degrees at the top and were pulled out by the longitudinal bars.

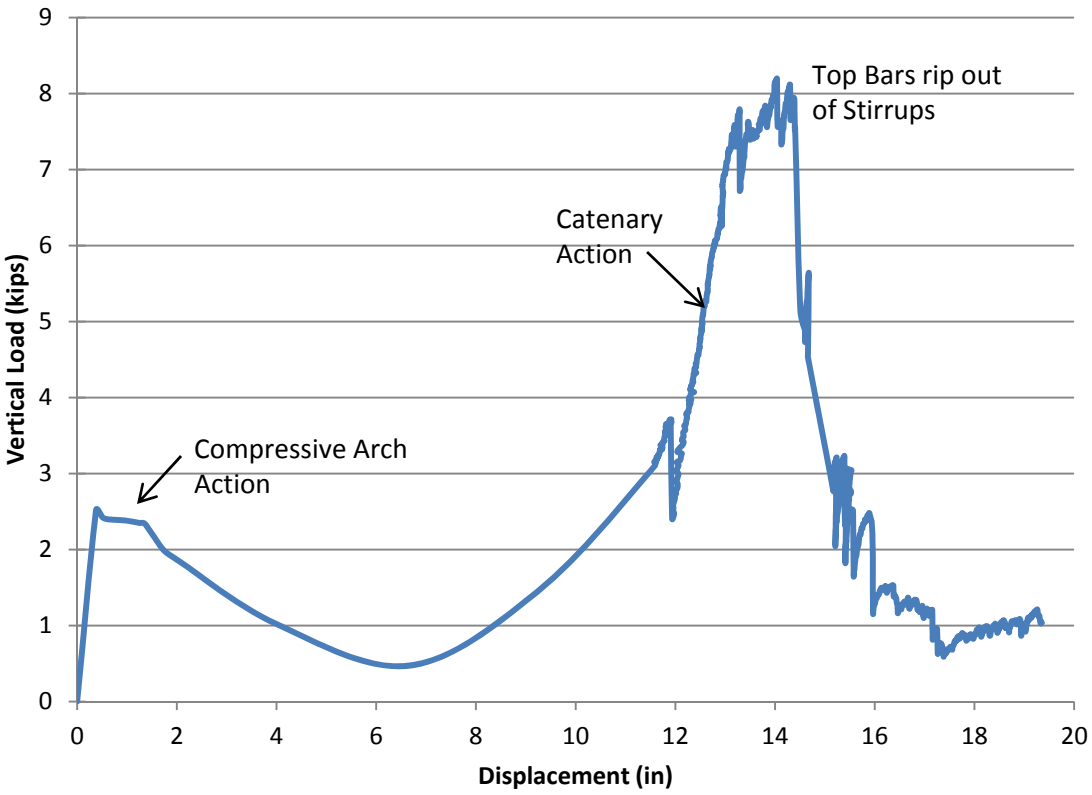

Figure 4.1.12: Vertical load vs. displacement graph

Horizontal load data was also recorded at the ends of the beams. The top load cell reached a maximum tensile load of 9.23 kips at the end of the catenary action phase while the bottom load cell only reached 7.64 kips (Figure 4.1.13). In the compressive arch action phase, the bottom load cell experienced a compressive load of 2.30 kips while the top load cell experienced almost none. The lack of compressive load in the top load cell may be due to insufficient tightening of the connections before the test.

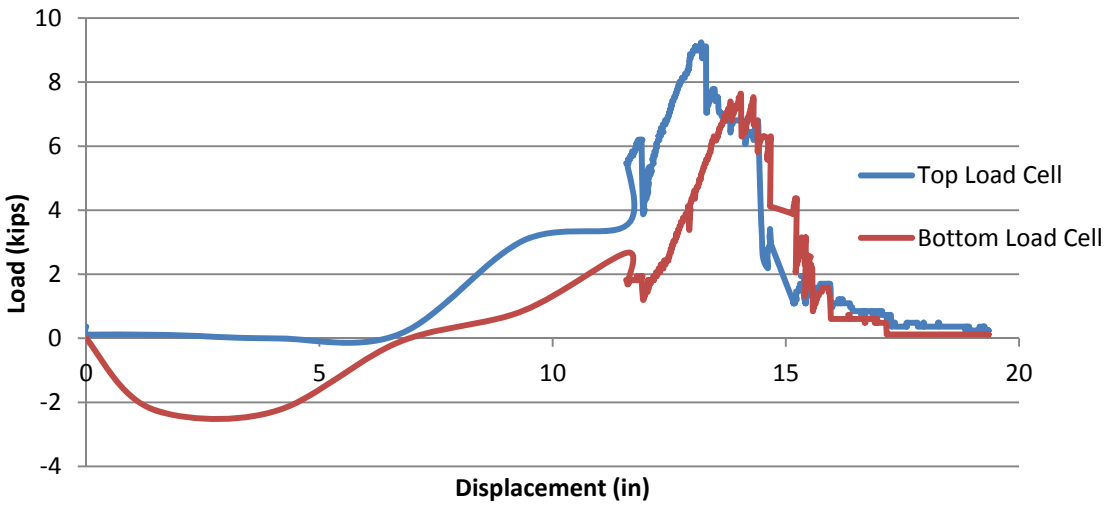

Figure 4.1.13: Load cell vs. displacement graph

Horizontal displacement data was recorded through LVDT's (Linear Variable Differential Transformers) at the ends of the beams. The top LVDT reached a maximum tensile displacement of 0.54 in. while the bottom LVDT only reached 0.28 in. (Figure 4.1.14). This was much higher than expected and was probably due to slop in the connections to the reaction frame. In the compressive arch phase, the top LVDT experienced a maximum compressive displacement of 0.127 in. while the bottom LVDT experienced only 0.104 in. This would indicate that the top connection was allowed to move more and therefore did not develop compressive loads as indicated in the load cell data.

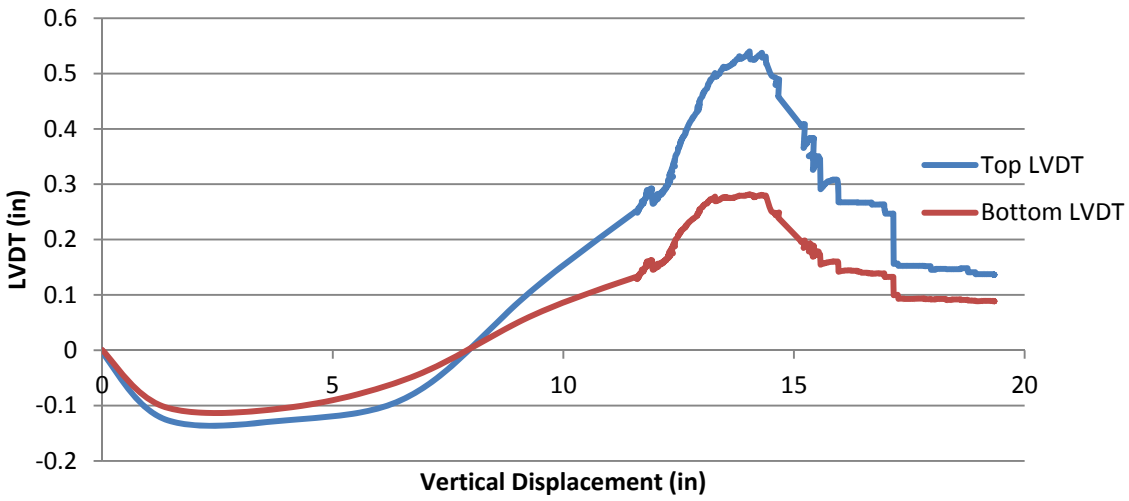

Figure 4.1.14: LVDT vs. vertical displacement graph

Besides the previous data, there was data from the 16 strain gages throughout two of the beams. The following graphs (Figure 4.1.15 through Figure 4.1.18) have strain points for each gage that didn't malfunction. The green dots represent the strain at the peak compressive arch action load (2.34 kips). The blue dots represent the strain at the peak catenary action or ultimate load (8.19 kips). At the peak compressive arch load, the strain in the positive moment bars increased towards the middle column while the strain in the negative moment bars increased towards the outer column which was expected. At the peak catenary action load, the highest strains for the negative moment bars were at the ends of the beams and the highest for the positive moment bars were at the middle of the beams which was also expected. The middle of the positive moment bars reached a stress of 56.7 ksi (BP2) which translated to 8.5 kips of load as compared to the 7.64 kips felt by the bottom load cell. The ends of the negative moment bars reached a stress of 33.3 ksi (TN2) which translated to 6.7 kips of load as compared to the 9.23 kips felt by the top load cell.

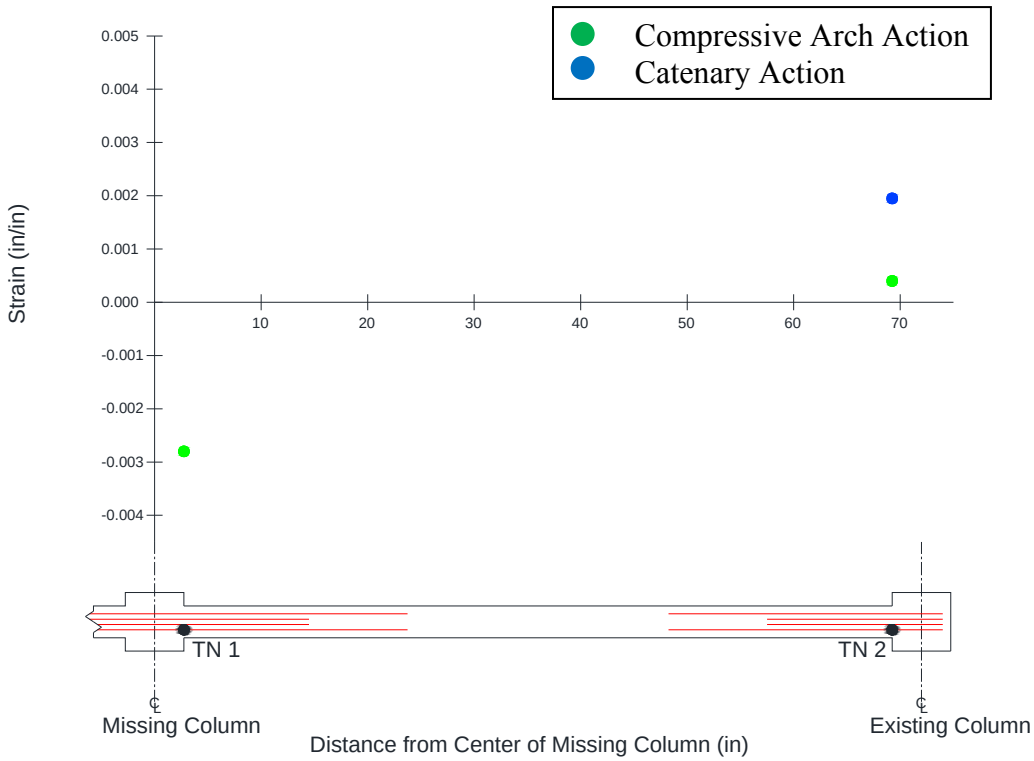

Figure 4.1.15: Strain gages in negative moment region of top beam

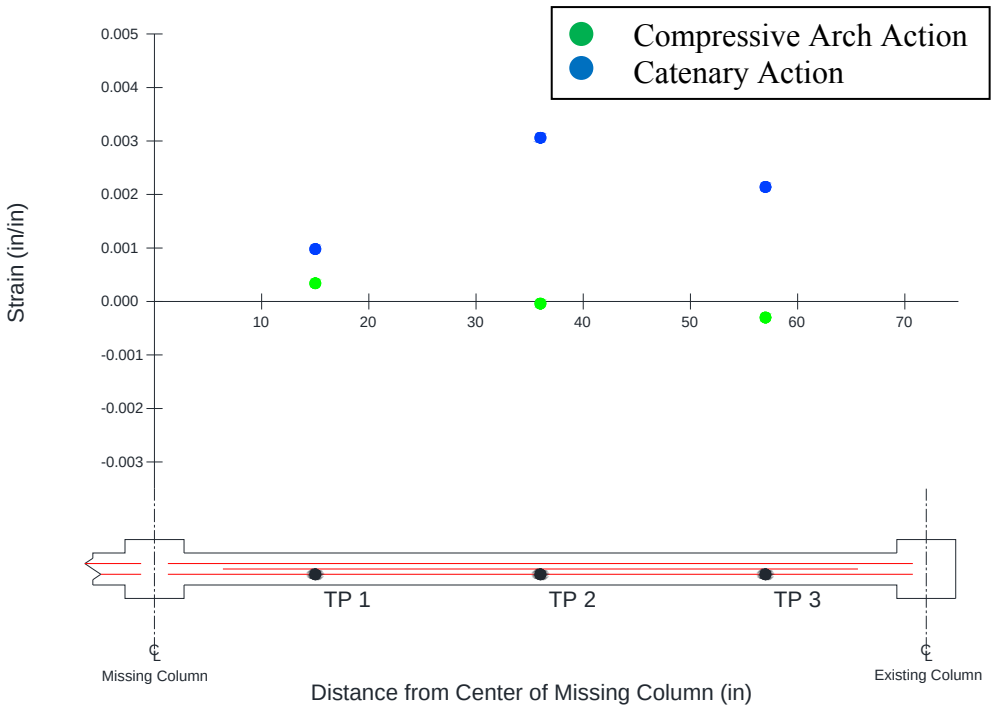

Figure 4.1.16: Strain gages in positive moment region of top beam

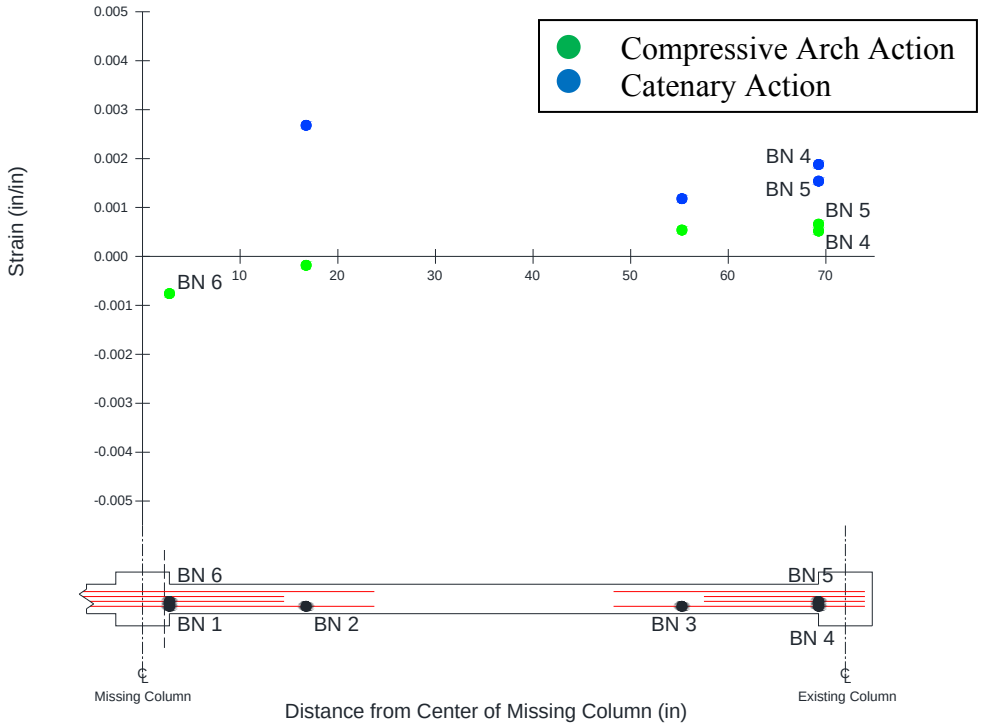

Figure 4.1.17: Strain gages in negative moment region of bottom beam

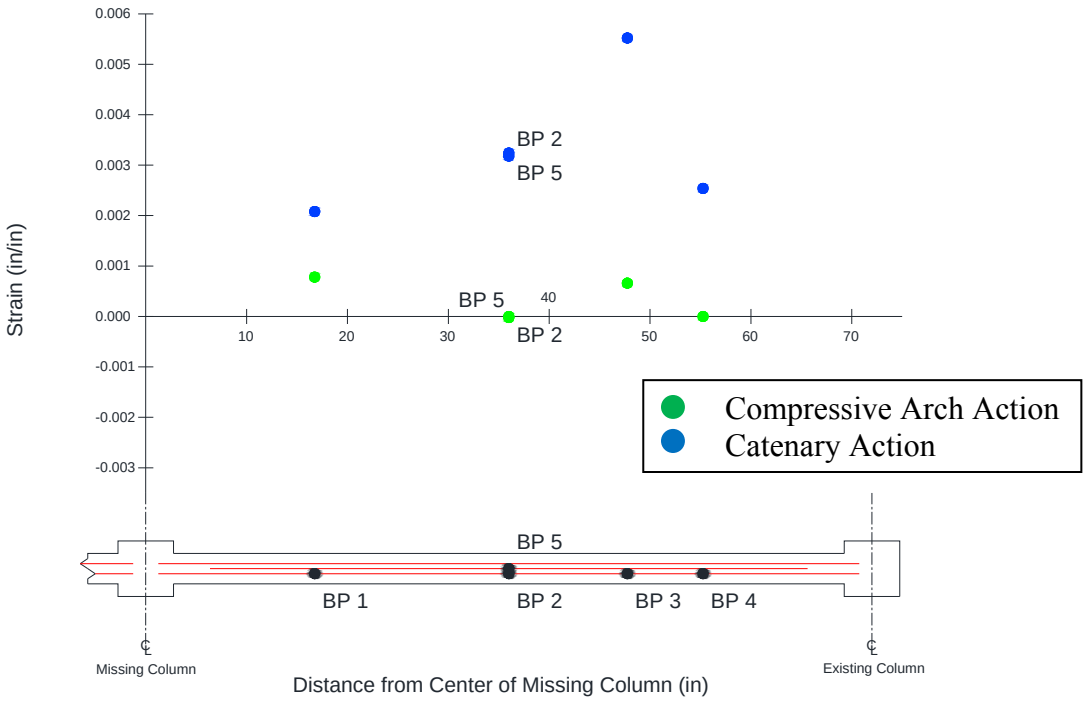

Figure 4.1.18: Strain gages in positive moment region of bottom beam

4.2. Continuous Reinforcement Frame

This frame was designed according to the 2008 ACI code which called for continuous reinforcement throughout beams. As with the discontinuous frame test, the actuator applied load to the center of the frame over the location of the lost column. Upon loading, the frame initially responded in an elastic manner. At a load of around 200 to 250 lbs, cracks began to form at the locations where the shorter bars of the negative moment reinforcement ended (Figure 4.2.2). As the load increased, the cracks widened and hinges began to form as shown in Figure 4.2.3. The ultimate failure point was when all the longitudinal bars in one area completely fractured as shown in Figure 4.2.4.

Figure 4.2.1: Continuous frame before loading

Figure 4.2.2: Continuous frame forming cracks

Figure 4.2.3: Continuous frame forming hinges

Figure 4.2.4: Continuous frame at failure

A closer look at a particular beam will show details of the cracking and hinge formations. At a about a load of 200 to 250 lbs, cracks formed at the ends of the shorter two bars of the negative moment reinforcement (Figure 4.2.5). This correlated well to the predicted cracking moment of the beams (8.532 kip-in) which translated to a load of 237 lbs. These cracks occurred at the ends of the shorter negative reinforcement bars which ended 12 in. from the face of the outer columns. On this particular beam, the crack started 11.5 in. from the column as shown in Figure 4.2.6. This was similar to all four beams. These cracks continued to open widely and formed hinges (Figure 4.2.7) with little further cracking in the rest of the beam. Next, the concrete near the hinge broke and fell off (Figure 4.2.8). At this point, all that was holding up the beam was the two longer negative moment bars until they fractured (Figure 4.2.9).

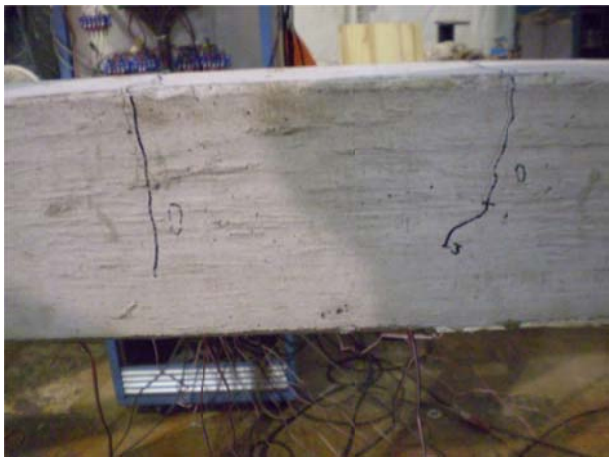

Figure 4.2.5: Initial cracking

Figure 4.2.6: Widening of cracks

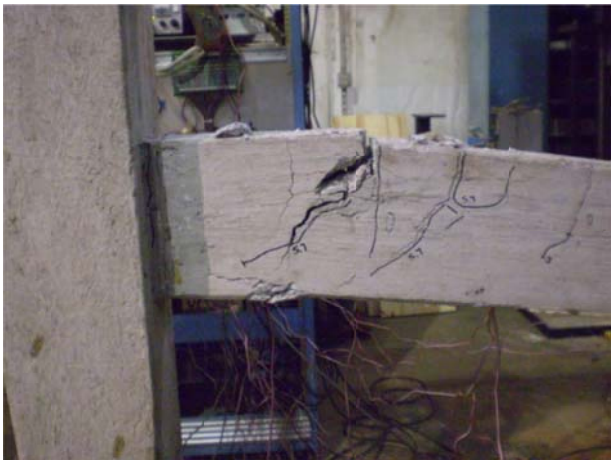

Figure 4.2.7: Formation of hinge

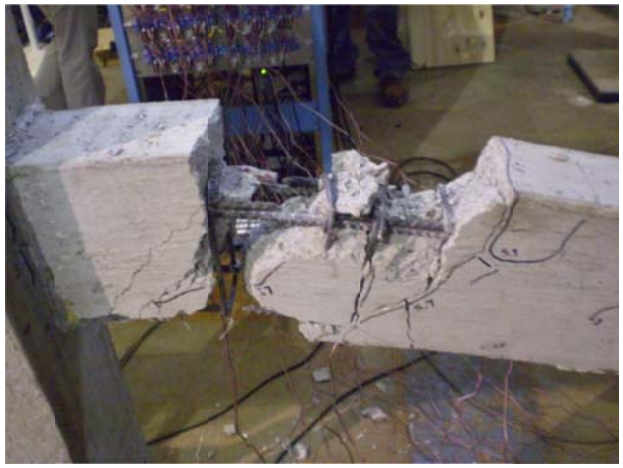

Figure 4.2.8: Concrete falling off

Figure 4.2.9: Failure of beam

In addition to these hinges, hinges also formed near the center column. Cracks formed about 5 in. from the face of the center column (Figure 4.2.10). They occurred at the location of the end of the lap splice. These cracks widened and formed hinges as shown in Figure 4.2.11. When the positive moment bars fractured (Figure 4.2.12), the negative moment bars were all that was left to carry the load.

Figure 4.2.10: Crack forming near center column

Figure 4.2.11: Hinge forming near center column

Figure 4.2.12: Bars fracturing near center column

The beams of this frame experienced two phases of resistance mechanism actions. After cracking and hinge formation, compressive arch action occurred as the end corners of the beam blocks were being crushed. Once these end corners were crushed, catenary action took over as the bars in the beams were placed in axial tension. These bars were pulled to the point that they completely fractured.

Figure 4.2.13 shows the vertical load vs. displacement graph. From this graph, one can see the flexural action (combined with the compressive arch action of the beam), the catenary action, and the ultimate failure when all of the bars in one area had fractured. According to plastic flexural theory, the frame would be able to carry a load of 4.7 kips when the hinges develop. During testing, the frame was able to reach 5.81 kips before formation of hinges, indicating that there may have been some contribution from compressive arch action. Once hinges formed, the frame continued to deflect with little increase of load until about 7.60 in. of displacement. Once this displacement was reached, the rotational capacity of the hinges was exhausted and the tensile reinforcement fractured. After fracture of the reinforcement, the frame was still able to carry load via catenary action. At the end of the catenary action phase, the frame was able to reach a maximum load of 8.30 kips. At this level of load, all the bars at one location had completely fractured.

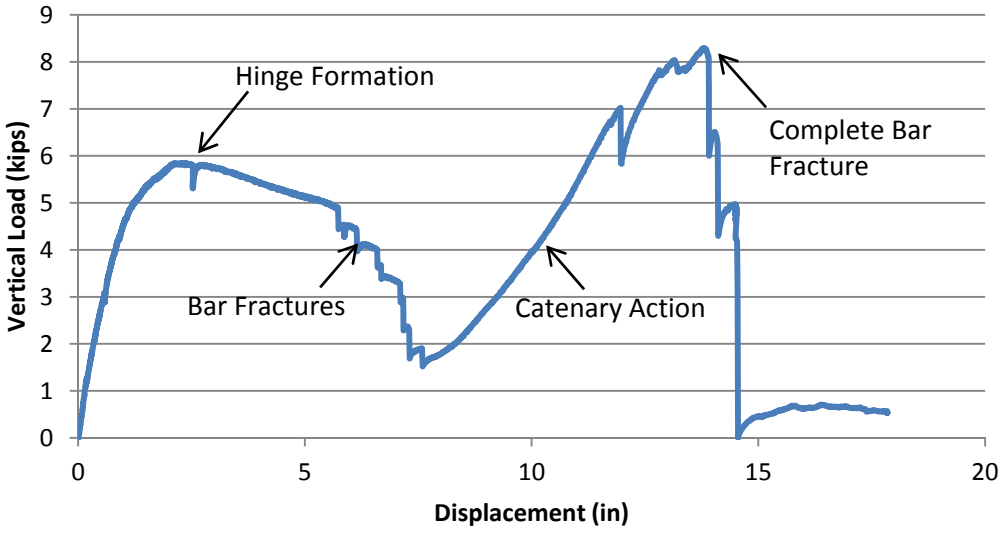

Figure 4.2.13: Vertical load vs. displacement graph

Horizontal load data was also recorded at the ends of the beams. The top load cell reached a maximum tensile load of 12.49 kips during the catenary action phase while the bottom load cell only reached 5.95 kips (Figure 4.2.14). In the compressive arch phase, the bottom load cell experienced a compressive load of 1.94 kips while the top load cell experienced only 0.97 kips.

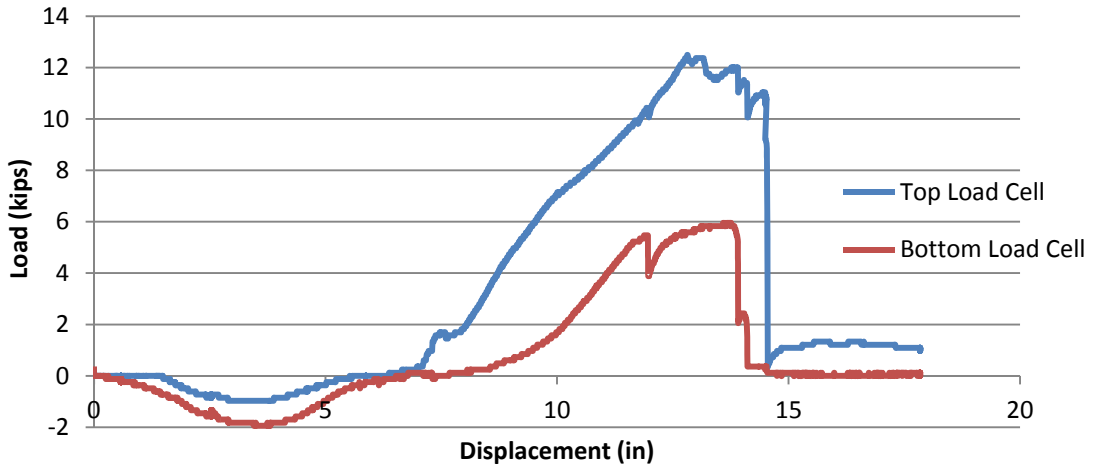

Figure 4.2.14: Load cell vs. displacement graph

Horizontal displacement data was recorded through LVDT's (Linear Variable Differential Transformers) at the ends of the beams. The top LVDT reached a maximum tensile displacement of 0.56 in. while the bottom LVDT only reached 0.35 in. (Figure 4.2.15). Like the discontinuous frame, this was much higher than expected and was probably due to slop in the connections to the reaction frame. In the compressive arch phase, the top LVDT experienced a maximum compressive displacement of 0.078 in., but the bottom LVDT was able to experience 0.088 in. The errors of the bottom LVDT graph are due to a lack of springs on the rod which kept the rod from moving out during

the tension phase. The LVDT was moved at about 14 in. of vertical displacement in order to give a deflection reading for the bottom LVDT.

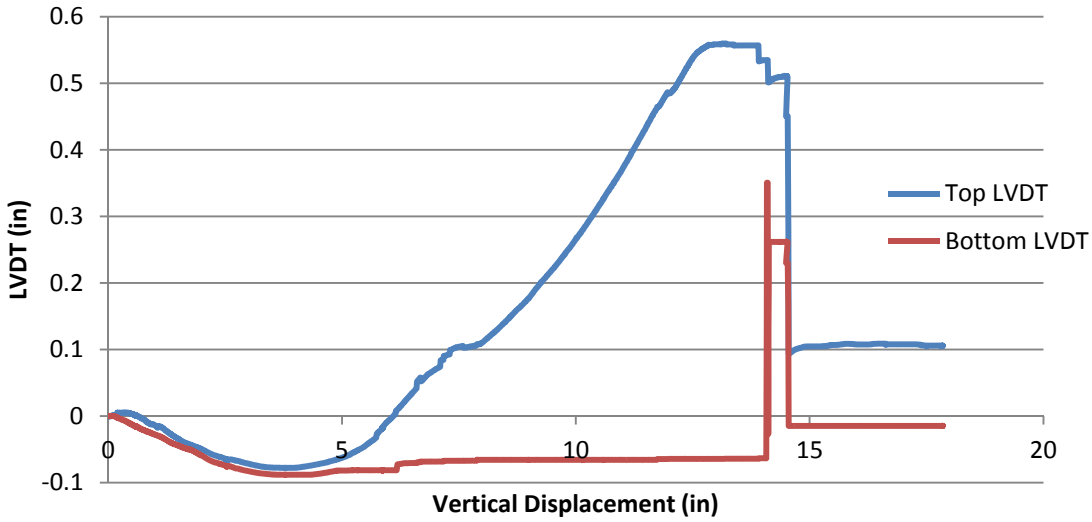

Figure 4.2.15: LVDT vs. vertical displacement graph

Besides the previous data, there was data from the 21 strain gages throughout two of the beams. The following graphs (Figure 4.2.16 through Figure 4.2.19) have strain points for each gage that didn't malfunction. Like the previous strain gage graphs, the green dots represent the strain at the peak flexural action load (5.81 kips) and the blue dots represent the strain at the peak catenary action or ultimate load (8.30 kips). At the peak flexural action load, the strain in the positive moment bars increased towards the middle column while the strain in the negative moment bars increased towards the outer column which was expected as these were the locations of the tension sides of the hinges. At the peak catenary action load, the strain in the positive moment bars increased towards the outer

column while the strain in the negative moment bars increased towards the middle column which was also expected. Only the negative moment steel was continuous in through the middle column, so it had to carry the entire catenary tension load. Only the positive moment steel was continuous at the outer columns, so the catenary tension load was transferred from the negative moment steel to the positive moment steel and then into the columns. This transfer is clearly indicated by the slopes of the strain readings. The middle of the positive moment bars reached a stress of 38.5 ksi (TP2) which translated to 5.8 kips of load as compared to the 12.49 kips felt by the top load cell. The ends of the negative moment bars also reached a stress of 50.8 ksi (BN1) which translated to 10.2 kips of load as compared to the 5.95 kips felt by the bottom load cell.

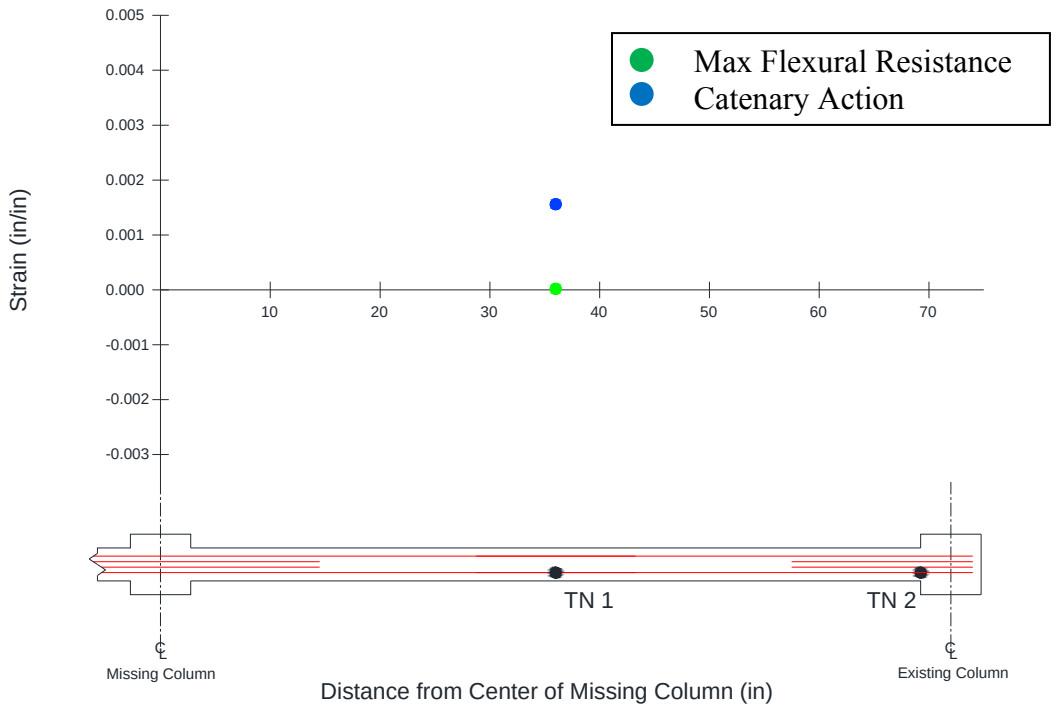

Figure 4.2.16: Strain gages in negative moment region of top beam

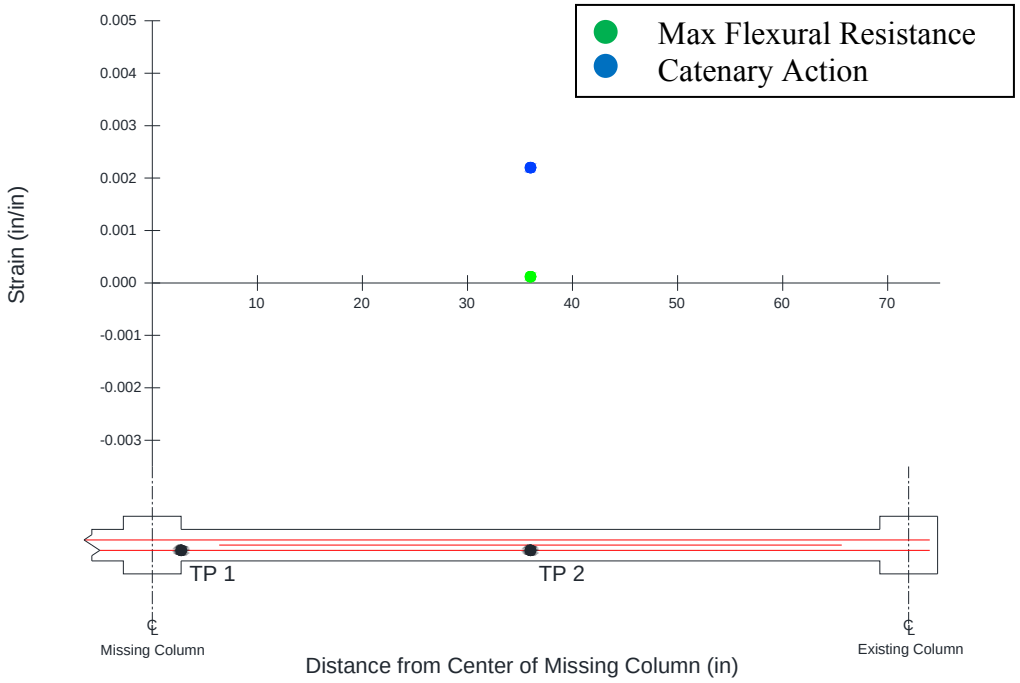

Figure 4.2.17: Strain gages in positive moment region of top beam

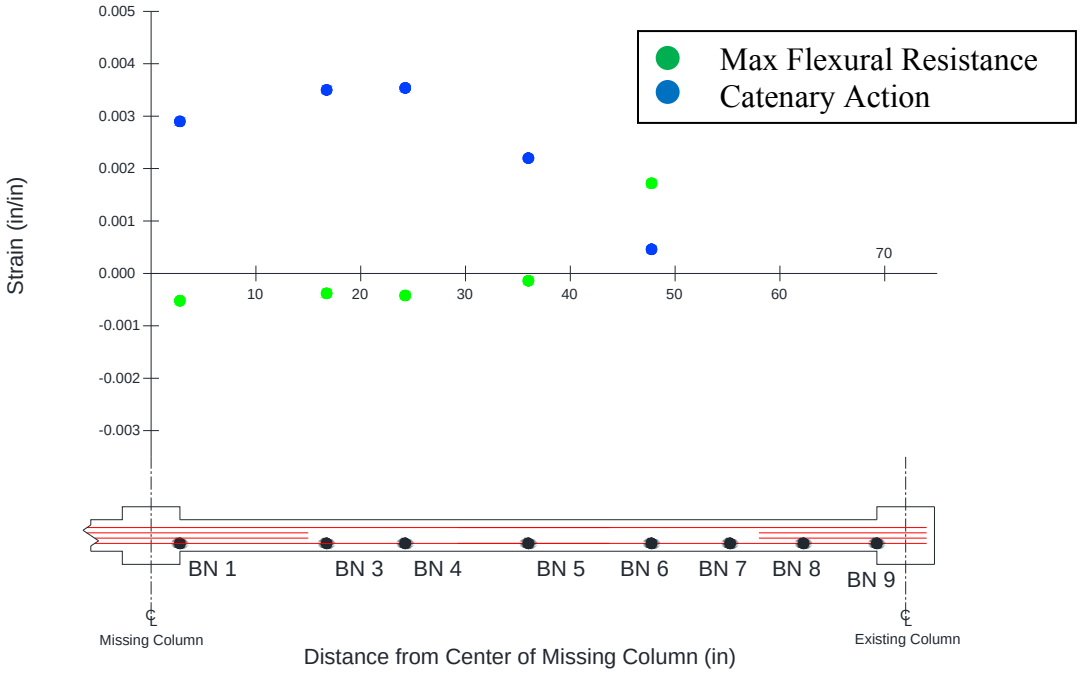

Figure 4.2.18: Strain gages in negative moment region of bottom beam

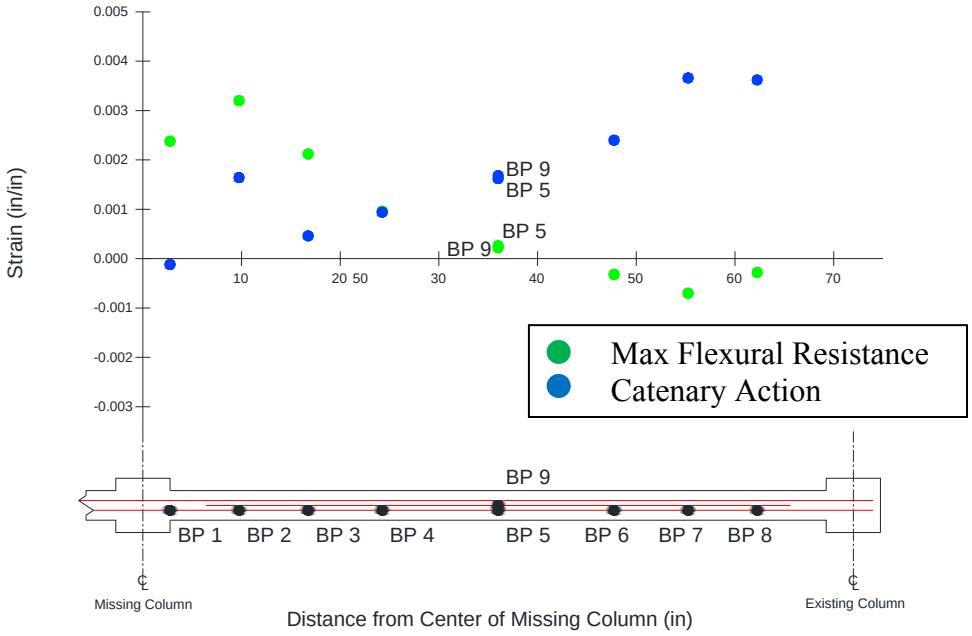

Figure 4.2.19: Strain gages in positive moment region of bottom beam

4.3. Infill Wall Frame

The last frame had the same reinforcement layout as the discontinuous reinforcement frame from the 1971 ACI code, but it had an infill or shear wall in the upper bays as shown in Figure 4.3.1 and Figure 4.3.2. Another feature of this frame was that there was a third LVDT going diagonal along the infill wall (Figure 4.3.3) that measured the compression of the infill wall.

Figure 4.3.1: Side view of infill wall

Figure 4.3.2: Top view of infill wall

Figure 4.3.3: Diagonal LVDT

Once the frame was set in place and the masonry had been given time to cure, the actuator applied load to the center of the frame over the location of the lost column. Upon loading, the frame initially responded in an elastic manner. At a load of around 200 to 250 lbs, cracks began to form at the locations of discontinuous reinforcement (Figure 4.3.4). As the load increased, the cracks widened (Figure 4.3.5) and hinges began to form (Figure 4.3.6). The cracks propagated through the beam and infill wall (Figure 4.3.7) and then the ultimate failure point was reached when the negative moment bars tore out of the last stirrup (Figure 4.3.8).

Figure 4.3.4: Infill wall frame forming cracks

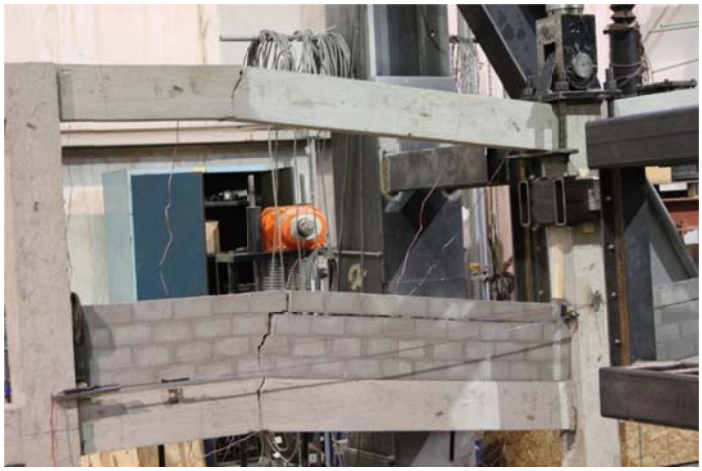

Figure 4.3.5: Infill wall frame cracks widening

Figure 4.3.6: Infill wall frame forming hinges

Figure 4.3.7: Infill wall separating from beam

Figure 4.3.8: Infill wall frame at failure

Looking at the other side of the frame, one can see the propagation of the damage. At a about a load of 200 to 250 lbs, a crack occurred in the infill wall (Figure 4.3.9). This correlated well to the predicted cracking moment of the beams (8.532 kip-in) which translated to a load of 237 lbs. These cracks occurred at the discontinuous ends of the negative reinforcement which ended 21.5 in. from the face of the outer columns as shown in Figure 4.3.13. This was similar to all four beams. Because no reinforcement crossed these cracks, they continued to open widely (Figure 4.3.10) and formed hinges (Figure

4.3.11) with little further cracking in the rest of the beam. As the load increased, the infill wall separated from the beam (Figure 4.3.12) and fell off. The frame reached ultimate failure when the negative moment bars tore through the stirrups (Figure 4.3.14).

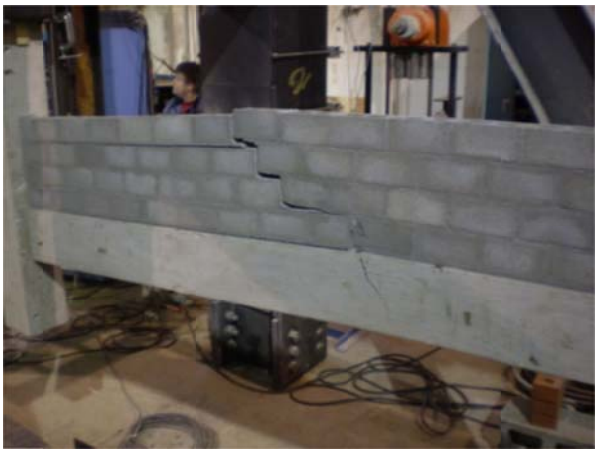

Figure 4.3.9: Crack forms in infill wall

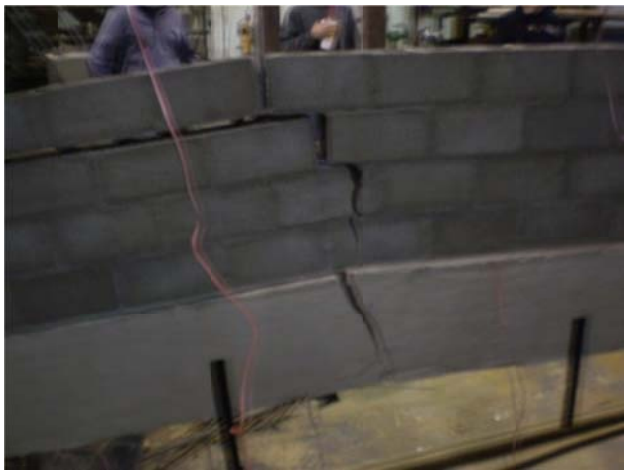

Figure 4.3.10: Crack propagates through beam

Figure 4.3.11: Crack widens and forms hinge

Figure 4.3.12: Infill wall is separated from beam

Figure 4.3.13: Crack formed where negative moment bars end

Figure 4.3.14: Negative moment bars have break through stirrups

In addition to the hinges within the beams, there was damage where the beams connected with the center column as shown in Figure 4.3.15. This was especially true for the bottom beams. These cracks occurred because the discontinuous positive reinforcement only extended 1.5 in. into the columns. These cracks widened and formed hinges as shown in Figure 4.3.16. Eventually, this will assist with the infill wall falling off the beam as shown before.

Figure 4.3.15: Initial crack near the center column

Figure 4.3.16: Crack propagates through beam and forms a hinge

The beams of this frame experienced two phases of resistance mechanism actions. After cracking and hinge formation, compressive arch action occurred as the end corners of the beam blocks were being crushed. This compressive arch action was enhanced by the presence of the infill wall. Once these end corners were crushed, catenary action took over as the bars in the beams were placed in axial tension. These bars were pulled to the point that they tore out of the stirrups.

Figure 4.3.17 shows the vertical load vs. displacement graph. From this graph, one can see the compressive arch action, the catenary action, and the ultimate failure when the top bars tore out of the stirrups. Despite having only 237 lbs in load capacity according to flexural beam theory (based on the cracking moment of the beams), the frame was able to reach 2.87 kips in compressive arch action. As stated before, this strength comes from the compression arch effect as the beam blocks try to rotate. This was aided by the presence of the infill wall. The high stresses at the end corners of the beam blocks eventually caused the concrete to crush and lose the compressive arch resistance. After

the compressive arch phase, the frame continued to deflect with little increase of load until about 5.76 in. of displacement. Once this displacement was reached, any further deflections caused tensile strains in the beam blocks and catenary action began. At the end of the catenary action phase, the frame was able to reach a maximum load of 7.42 kips. At this level of load, the negative moment reinforcement tore out of the stirrups.

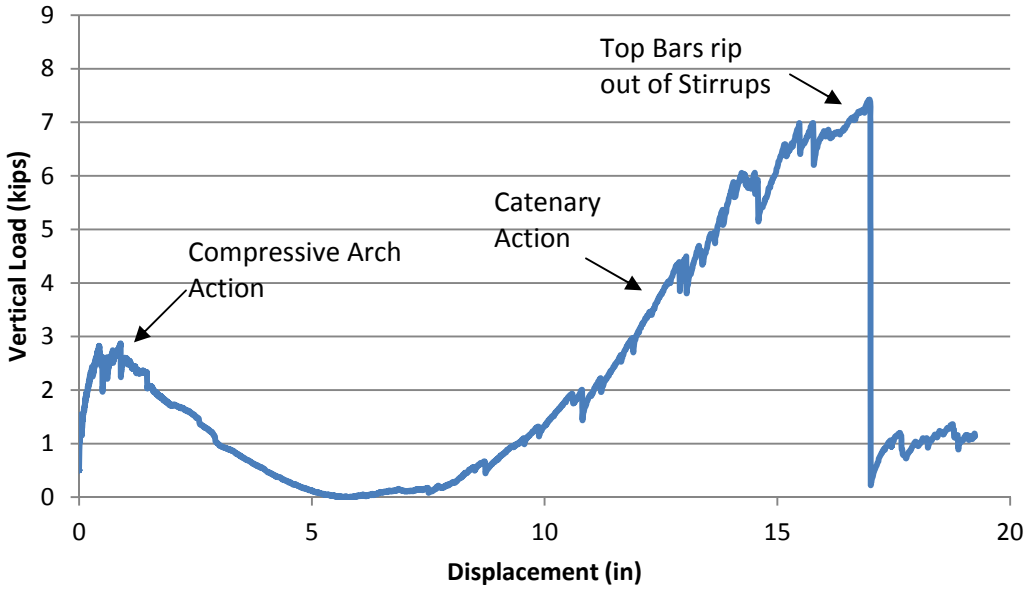

Figure 4.3.17: Vertical load vs. displacement graph

Horizontal load data was also recorded at the ends of the beams. The top load cell reached a maximum tensile load of 12.25 kips at the end of the catenary action phase while the bottom load cell only reached 1.09 kips (Figure 4.3.18). The lack of tensile load in the bottom load cell may be due to insufficient tightening of the connections before the test. In the compressive arch action phase, the bottom load cell experienced a compressive load of 3.16 kips while the top load cell experienced only 1.94 kips.

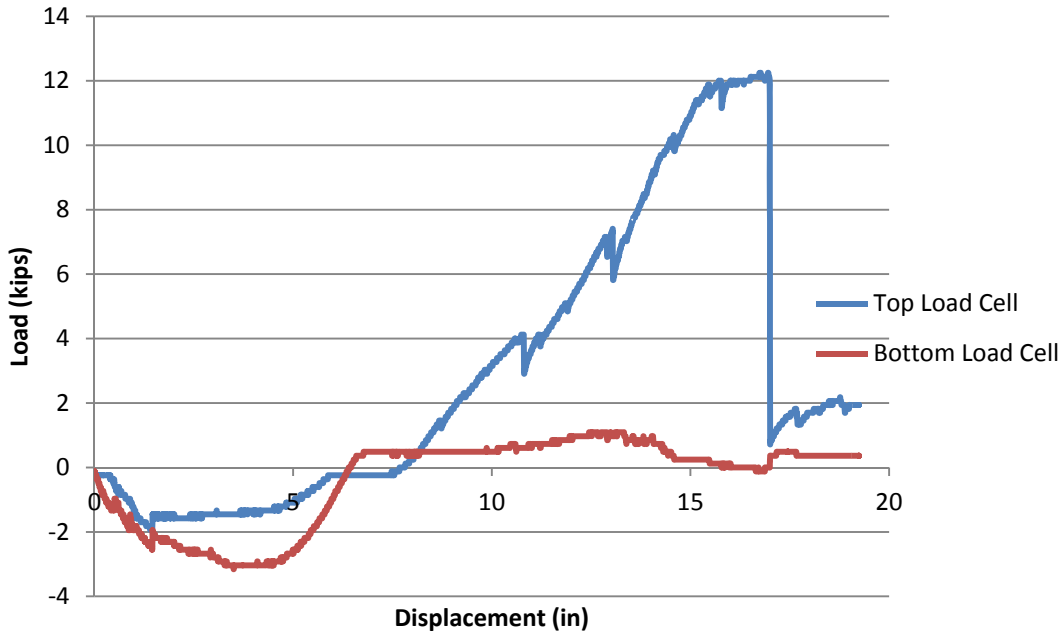

Figure 4.3.18: Load cell vs. displacement graph

Horizontal displacement data was recorded through LVDT's (Linear Variable Differential Transformers) at the ends of the beams. The top LVDT reached a maximum tensile displacement of 0.52 in. while the bottom LVDT only reached 0.28 in. (Figure 4.3.19). This was much higher than expected and was probably due to slop in the connections to the reaction frame. In the compressive arch phase, the top LVDT experienced a maximum compressive displacement of 0.159 in. while the bottom LVDT experienced only 0.089 in. The diagonal LVDT reached a compressive load of 1.71 in. before it ran out of displacement (Figure 4.3.20).

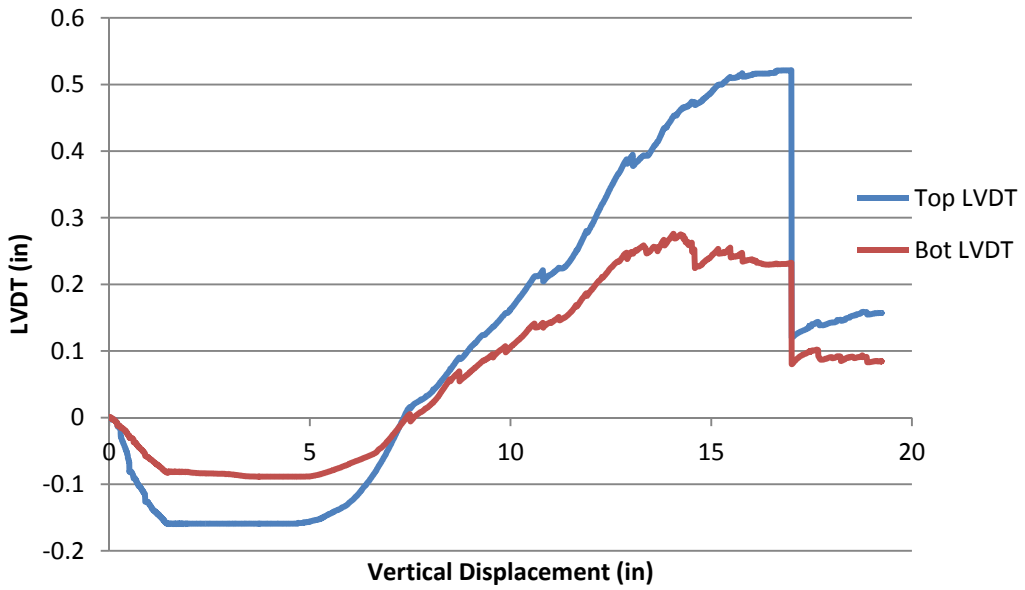

Figure 4.3.19: LVDT vs. vertical displacement graph

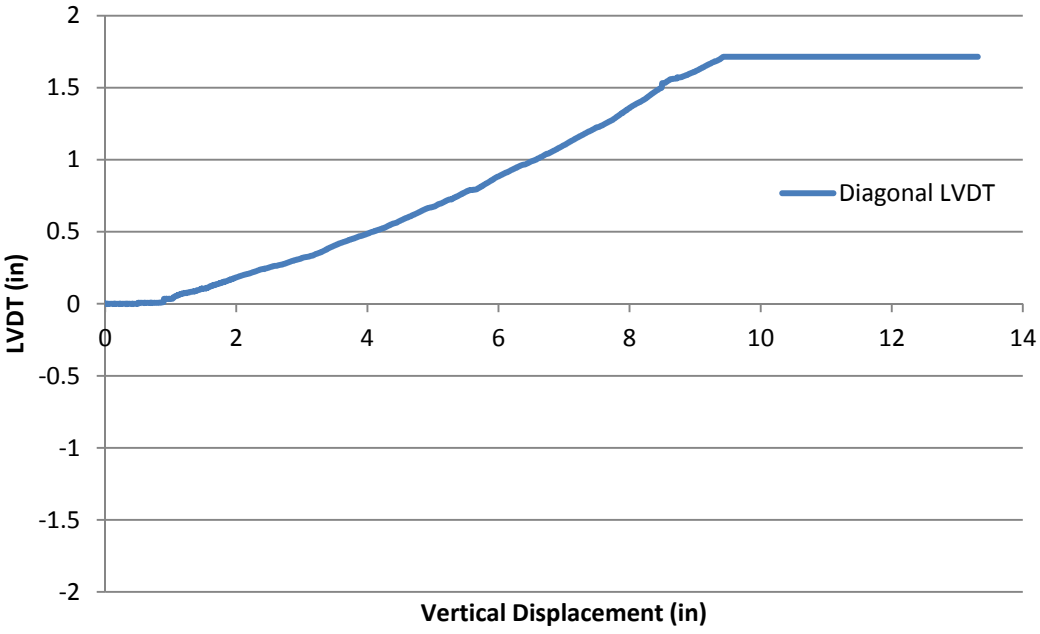

Figure 4.3.20: Diagonal LVDT vs. vertical displacement graph

Besides the previous data, there was data from the 16 strain gages throughout two of the beams. The following graphs (Figure 4.3.21 through Figure 4.3.24) have strain points for each gage that didn't malfunction. The green dots represent the strain at the peak compressive arch action load (2.87 kips). The blue dots represent the strain at the peak catenary action or ultimate load (7.42 kips). At the peak compressive arch load, the strain in the positive moment bars increased towards the middle column while the strain in the negative moment bars increased towards the outer column which was expected. At the peak catenary action load, the highest strains for the negative moment bars were at the ends of the beams and the highest for the positive moment bars were at the middle of the beams which was also expected. The middle of the positive moment bars reached a stress of 16.8 ksi (BP2) which translated to 2.5 kips of load as compared to the 1.09 kips felt by the bottom load cell. The ends of the negative moment bars reached a stress of 36.8 ksi (TN2) which translated to 7.4 kips of load as compared to the 12.25 kips felt by the top load cell.

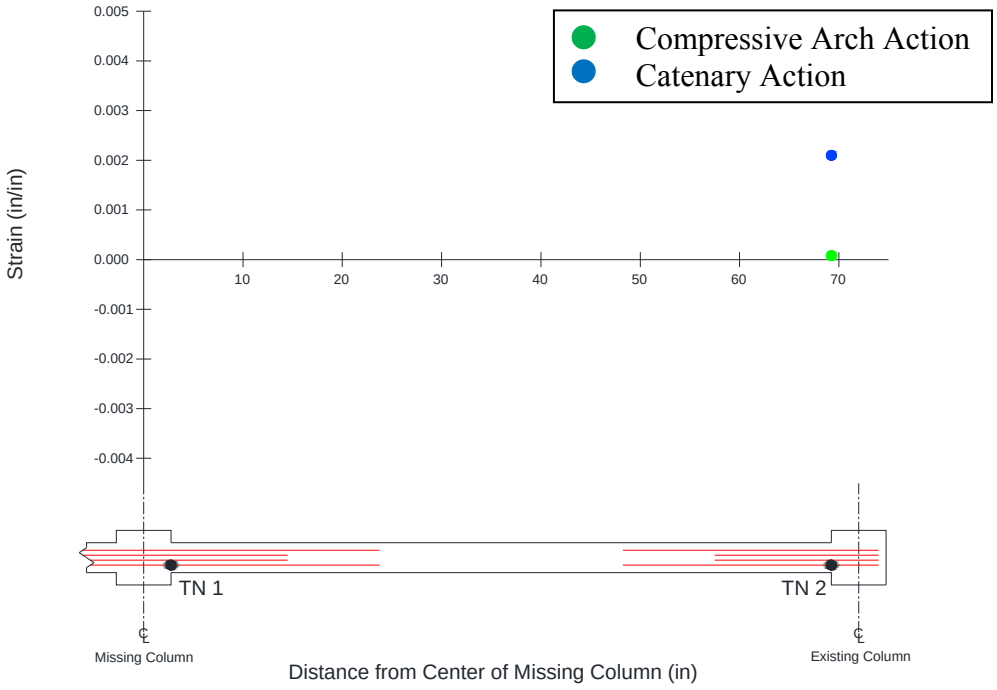

Figure 4.3.21: Strain gages in negative moment region of top beam

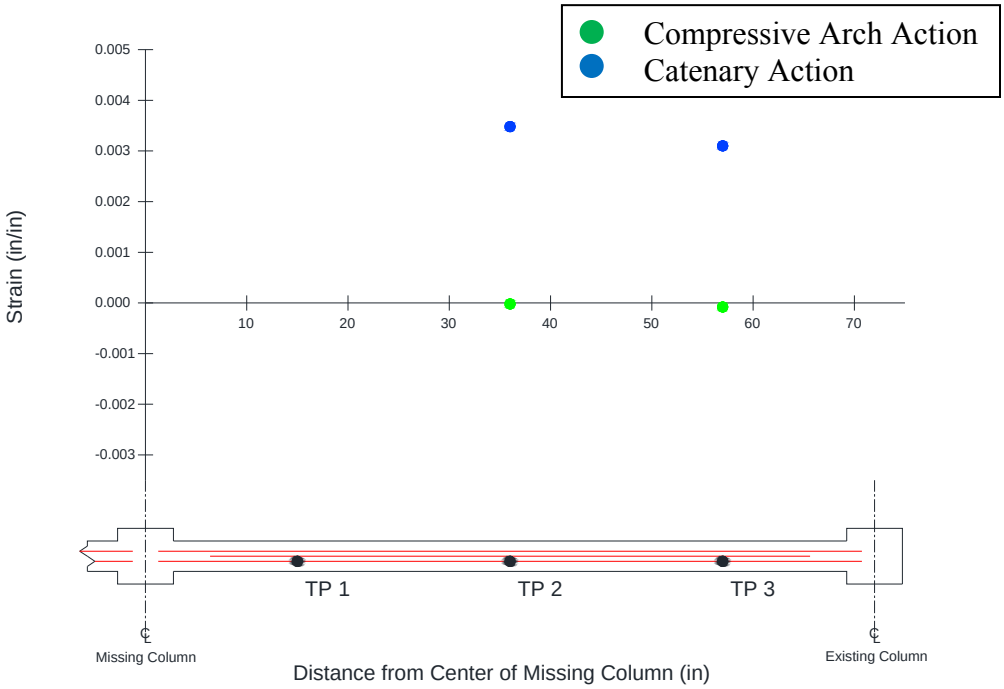

Figure 4.3.22: Strain gages in positive moment region of top beam

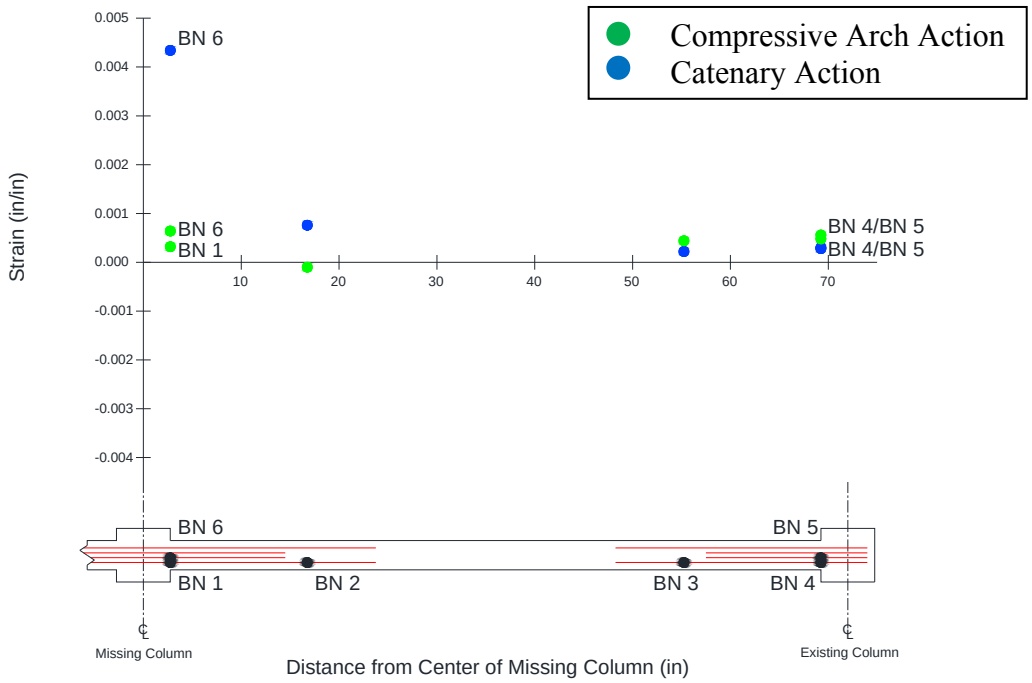

Figure 4.3.23: Strain gages in negative moment region of bottom beam

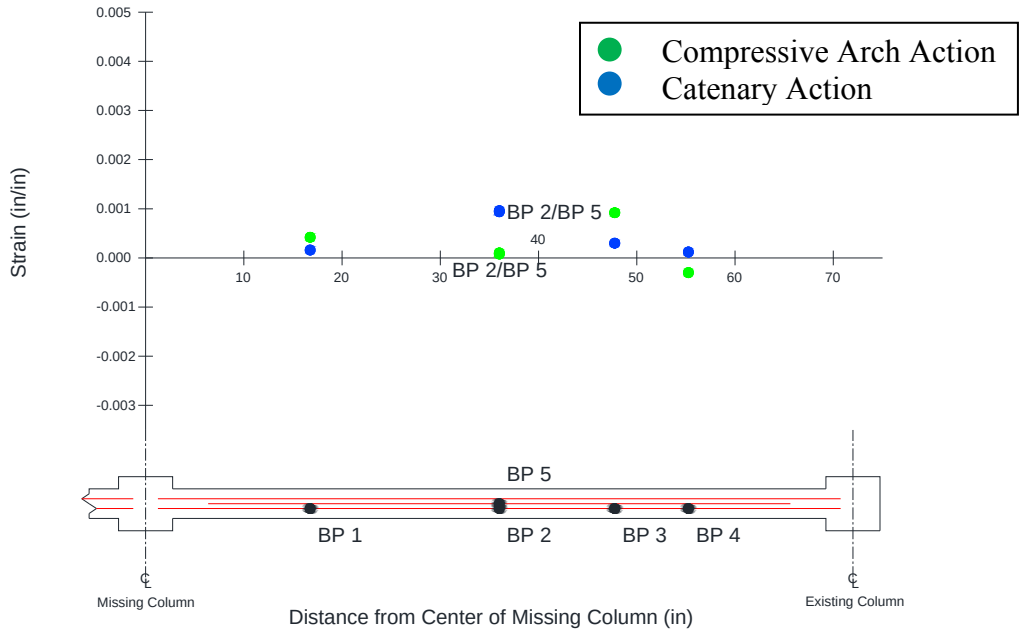

Figure 4.3.24: Strain gages in positive moment region of bottom beam

4.4. Combined Results and Discussion

Figure 4.4.1 shows the vertical load vs. displacement graph for all three tests. The continuous reinforcement frame had a higher load carrying capacity at low deflections (less than 6") due to flexural action that was about twice as much as the other two frames. This higher strength before the catenary action phase may be enough to resist collapse if that was all that it needed. Also, the continuous reinforcement frame retained its load carrying capacity for the longest displacement illustrating the ductility of the flexural action. Finally, the continuous reinforcement frame was able to reach the highest load of 8.30 kips during catenary action, but this was not much more than the 8.19 kips from the discontinuous reinforcement frame. Adding continuous reinforcement did not increase capacity in the catenary action phase. This is because the continuous reinforcement fractured due to limited rotational ductility of the hinge regions. The infill wall frame had a higher deflection at ultimate failure than the other two frames. This may be due the decreased stiffness from the horizontal support (bottom load cell did not experience high tension in catenary action phase) or the presence of the infill wall may have delayed the secondary hinge formation changing the deflected shape of the beam.

Looking at the area under the MTS load graphs, which is the strain (kinetic) energy dissipated by the frames, the continuous reinforcement frame was able to dissipate the most energy at 70.99 kips*in and thus provided better collapse resistance. The discontinuous reinforced frame (40.13 kips*in) and the infill wall frame (40.87 kips*in) dissipated just over half of that. All of the critical values from the MTS load, load cell and LVDT graphs are summarized in Table 4.4.1, Table 4.4.2 and Table 4.4.3.

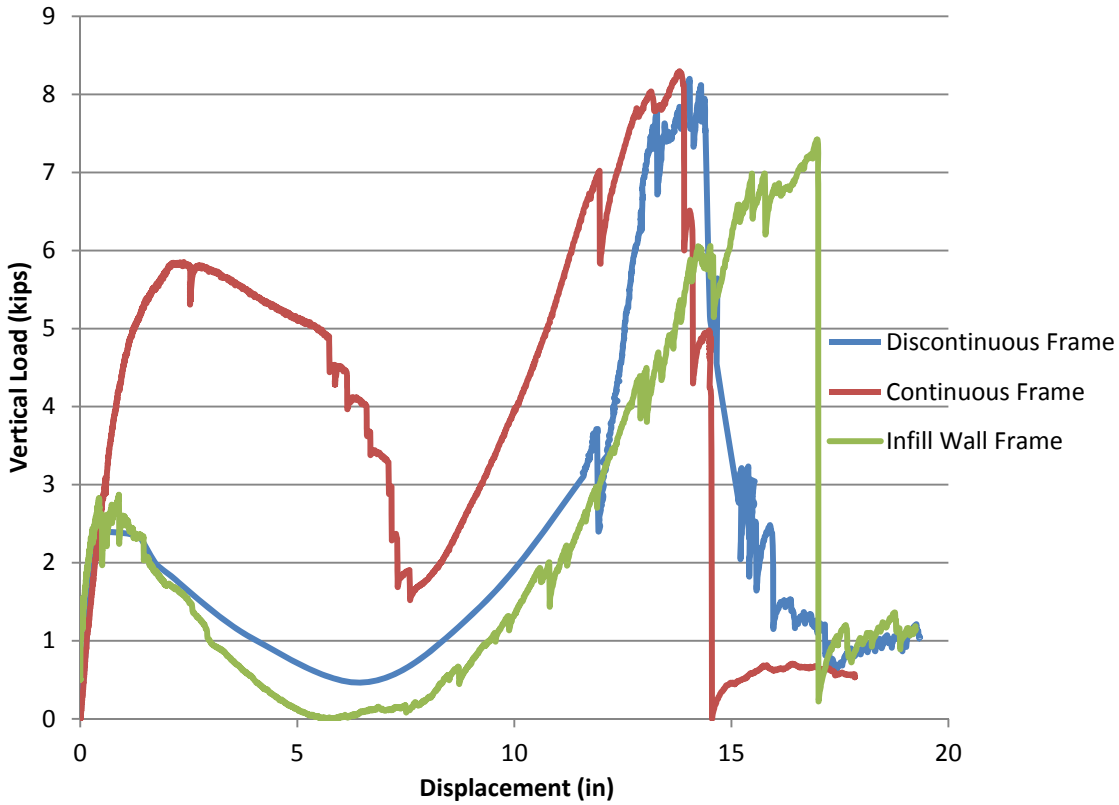

Figure 4.4.1: Combined vertical load vs. displacement graph

Figure 4.4.2 and Figure 4.4.3 show the horizontal load data from all three tests. As can be seen in the graphs, the axial load behavior for all three tests is similar, with the exception of the bottom load cell in the infill frame test. Furthermore, the infill wall frame experienced a higher compressive load for both the top and bottom load cells due to a slightly increased compressive arch effect. The continuous reinforcement frame and the infill wall frame had almost the same maximum tensile load for the top while the discontinuous reinforcement frame was about 3 kips lower. The difference in the values may be simply due to minor differences in the connection tightness or specimen properties.

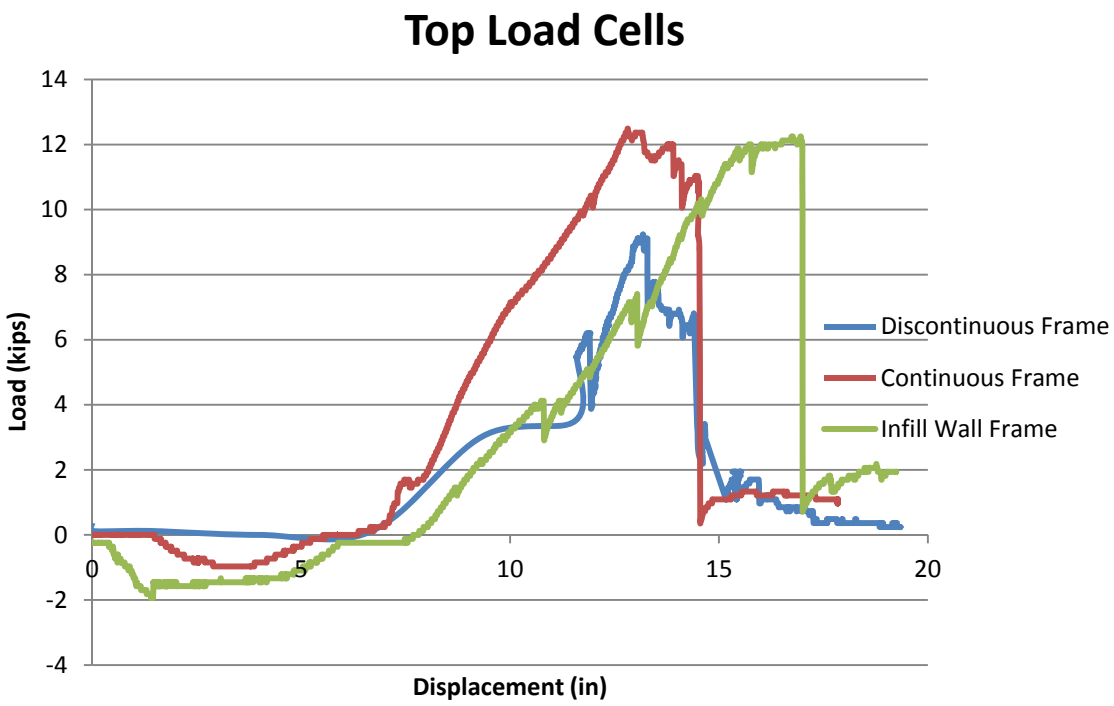

Figure 4.4.2: Combined top load cell vs. displacement graph

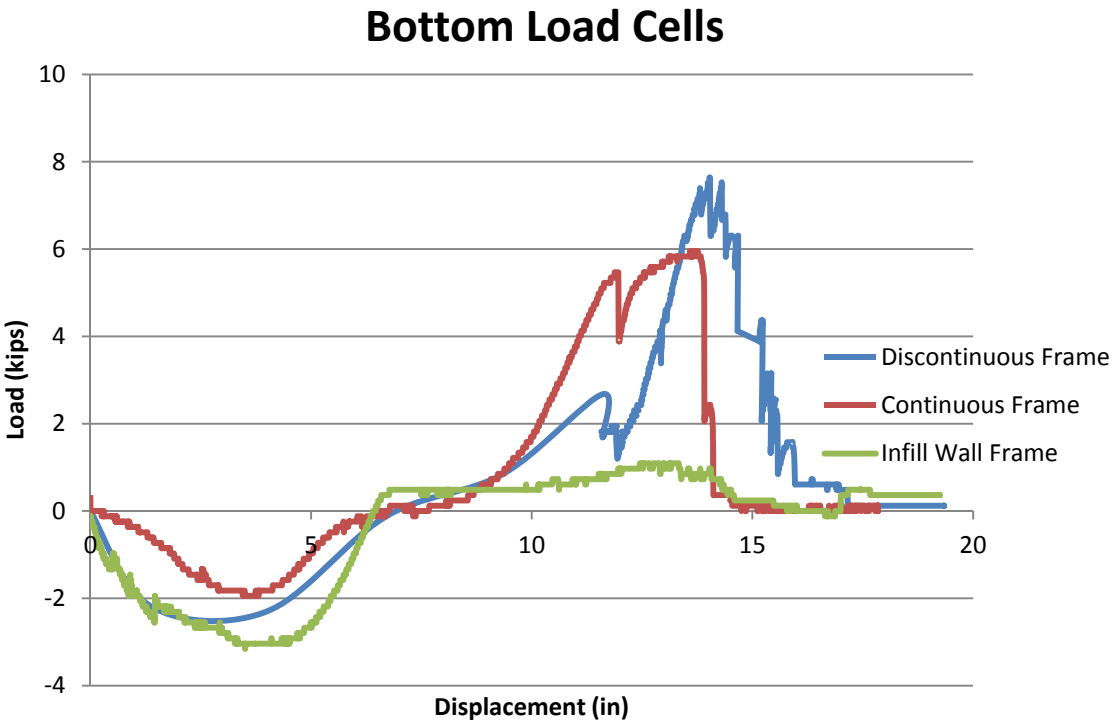

Figure 4.4.3: Combined bottom load cell vs. displacement graph

Figure 4.4.4 and Figure 4.4.5 show the horizontal displacement data from all three tests. Again the displacement data for all three tests is similar. The infill wall frame experienced a higher compressive displacement in the top LVDT, but the discontinuous reinforcement frame experienced a higher compressive displacement in the bottom LVDT. All of the maximum top LVDT values were within 0.04 in. of each other with the continuous reinforcement frame exhibiting the most horizontal displacement. In the bottom LVDT's, two of the frames had the same lateral displacement, but the continuous reinforcement frame had the most displacement.

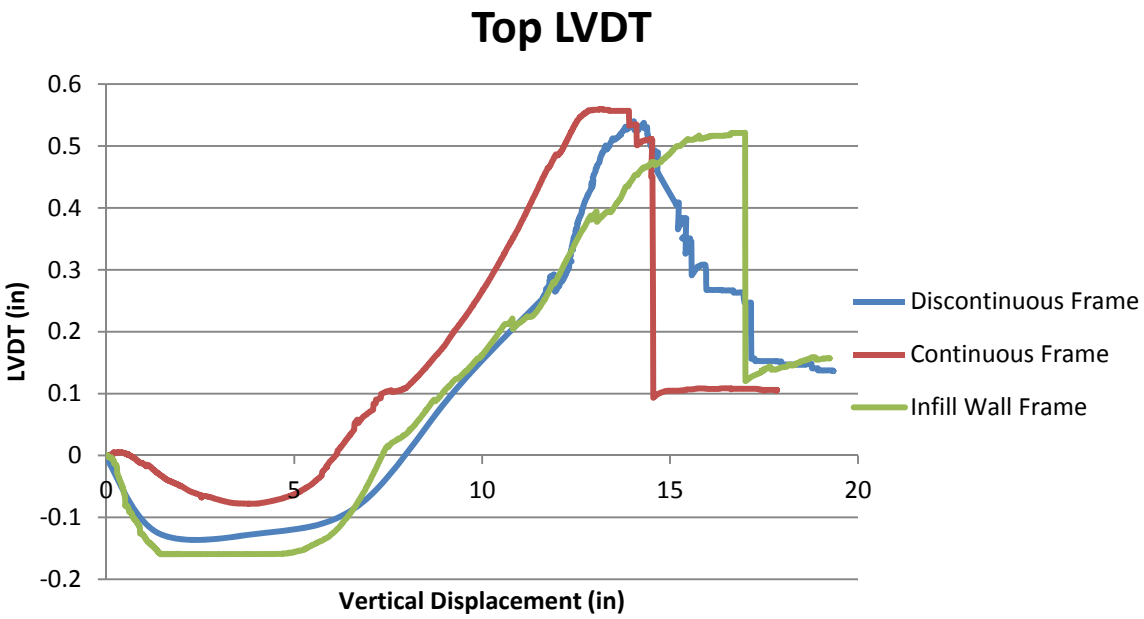

Figure 4.4.4: Combined top LVDT vs. vertical displacement graph

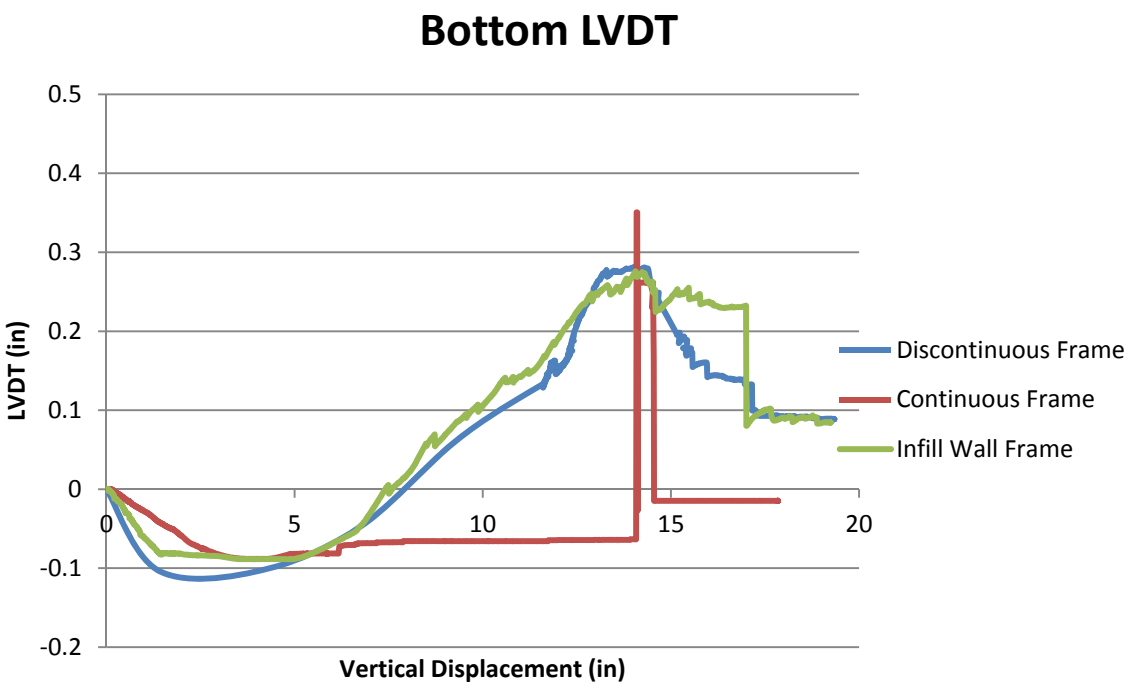

Figure 4.4.5: Combined bottom LVDT vs. vertical displacement graph

Table 4.4.1: Combined MTS load results

	Peak Catenary MTS Load (kips)	Peak Compressive Arch MTS Load (kips)	End of Compressive Arch Phase (in)
Discontinuous Frame	8.19	2.34	6.70
Continuous Frame	8.30	5.81	7.60
Infill Wall Frame	7.42	2.87	5.76

Table 4.4.2: Combined load cell results

	Top Load Cell Peak Tensile Load (kips)	Top Load Cell Peak Compressive Load (kips)	Bottom Load Cell Peak Tensile Load (kips)	Bottom Load Cell Peak Compressive Load (kips)
Discontinuous Frame	9.23	0	7.64	2.30
Continuous Frame	12.49	0.97	5.95	1.94
Infill Wall Frame	12.25	1.94	1.09	3.16

Table 4.4.3: Combined LVDT results

	Top LVDT Peak Tensile Disp (in)	Top LVDT Peak Compressive Disp (in)	Bottom LVDT Peak Tensile Disp (in)	Bottom LVDT Peak Compressive Disp (in)
Discontinuous Frame	0.54	0.127	0.28	0.104
Continuous Frame	0.56	0.078	0.35	0.088
Infill Wall Frame	0.52	0.159	0.28	0.089

As stated before, there were 16 strain gages in both the discontinuous reinforcement and infill wall frames, and there were 21 gages in the continuous reinforcement frame. Table 4.4.4 shows the peak forces determined from the strain readings developed in the reinforcing bars at peak catenary action. With a ultimate tensile strength of 90 ksi, the force at fracture for two reinforcing bars is 9 kips, which is comparable to the force derived from the strain readings when the two negative moment bars fractured at the end of the catenary action phase of the continuous frame test. The forces in the negative

moment bars at the end of the catenary phase for the discontinuous and infill frame test were only 6.7 and 7.4 kips. This indicates that the bars were nearing fracture load when they tore out of the stirrups. Furthermore, in the discontinuous frame there is a high tensile load also in the positive moment bars. This indicates that the tensile load from the catenary action is fully transferred from the negative moment to the positive moment bars.

Table 4.4.4: Combined strain gage results

	Tensile Load of Middle Positive Bars at Peak Catenary (kips)	Tensile Load of End Negative Bars at Peak Catenary (kips)
Discontinuous Frame	8.5	6.7
Continuous Frame	5.8	10.2
Infill Wall Frame	2.5	7.4

5. CONCLUSION

As stated above, the main objective of this research is to better understand the collapse resistance mechanisms of reinforced concrete buildings and determine their capacities. The alternative collapse resisting mechanisms that were evaluated in this research included catenary action, compressive arch action, and contributions from infill walls. By better understanding the effects of these various resistance mechanisms, we can move closer to the ultimate goal of creating a set of guidelines on how to best resist progressive collapse.

Although flexural theory would predict that the frame with discontinuous reinforcement had little load carrying capacity (moment capacity of hinge regions only due to cracking moment), the discontinuous reinforcement frame was able to reach a load of 2.34 kips under compressive arch action and 8.19 kips under catenary tension. The significant increase in capacity alone is a reason to consider these resistance mechanisms in collapse design.

The frame with continuous reinforcement reached a load of 5.81 kips under the flexural action (combined with compressive arch action) and 8.30 kips under catenary tension. The resistance under flexural action (along with compressive arch action) for a continuously reinforced frame may be sufficient to resist collapse. However, that resistance comes with a limited ductility. The hinge regions on the continuous reinforcement frame exhausted their rotational ductility at about 6 in. of displacement and

the reinforcement fractured. However, even after reinforcement fracture, the frame was able to carry 8.30 kips of load in catenary tension, which is slightly higher to the load carried by the frame with discontinuous reinforcement. Therefore, continuous reinforcement in a frame may not be effective in resisting collapse if the force and deformation demands cause fracture of the reinforcement. However, the frame still has significant capacity under catenary tension.

The frame with the infill wall reached a load of 2.87 kips under compressive arch action and 7.42 kips under catenary tension. The compressive arch action load is slightly higher than the frame with discontinuous reinforcement. This indicates that the infill wall may have contributed to the resistance of the frame, but the weak mortar joints in the non-grouted wall fractured and caused the wall to break up rather than contributing significantly to the compressive arch action. If the infill wall was composed of grouted or reinforced cells, had a higher strength mortar, or was the full height of the wall, the contribution from the infill could be much more significant. Although the infill wall frame was 23 % more effective in the compressive arch phase than the discontinuous reinforcement frame, it performed worse in the catenary action phase. Because the frames were of the same design and the infill wall was mostly destroyed before catenary tension, the difference in the results is likely due to minor differences in the connection of the frame to the test setup, material properties, or locations of hinges.

In order to compare the results of the frames to the requirements of the United Facilities Criteria (UFC) and other test data, it is necessary to scale up the results to the full scale

frame. In order to adjust the point load to represent an equivalent uniform load, the point load was divided by the combined length of the four beams (24 ft.) and multiplied by a factor of two to match the same area under the moment diagram as the distributed load (Figure 5.1). Since these test frames were quarter scale models, the distributed load was multiplied by a scale factor of four to give a peak catenary action load of 2.73 kips/ft for the discontinuous reinforcement frame and 2.76 kips/ft for the continuous reinforcement frame. Doing the same for the compressive arch action load gives 0.78 kips/ft for the discontinuous reinforcement frame and 1.93 kips/ft for the continuous reinforcement frame for flexural action.

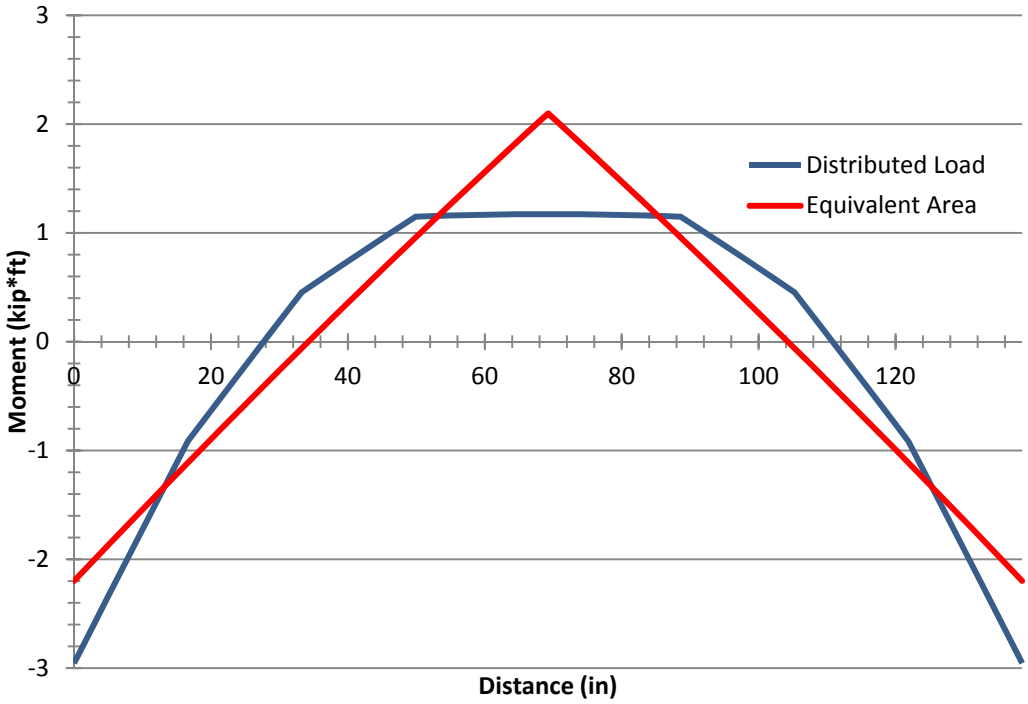

Figure 5.1: Moment diagram for frame

According to the DoD document *Design of Buildings to Resist Progressive Collapse* (2009), the increased load of the adjacent bays due to immediate removal of a column creates a uniform load along the beams of 2.36 kips/ft. The capacities reached by the test frames in catenary tension were 2.76 kips/ft. This indicates that the frame would be able to survive a collapse.

As stated before, Orton (2007) performed similar tests for two half scale beams of nearly the same design. The continuous reinforcement beam reached approximately 1.3 kips/ft of load scaled to full size beams in flexural action. The discontinuous reinforced beam reached a load of 1.8 kips/ft in catenary tension. These loads are less than the loads reached in the frame tests. The difference may be due to the different test setups and scales or the presence of a second beam in the frame test. Yi and Kunnath (2008) also performed a similar test on a four bay by three story continuous reinforcement one-third scale frame. This frame reached a maximum load of approximately 2.03 kips/ft in catenary tension.

The conclusions drawn from the results of this research are:

- The implementation of continuous reinforcement throughout beams can greatly enhance the flexural action resistance over discontinuous reinforcement. However, the increased flexural resistance has a limited ductility due to the limited ductility of the hinge regions. Once this ductility is reached, the frame essentially behaves like a discontinuously reinforced frame. Therefore, continuous reinforcement may improve the collapse resistance of a frame, but if

the collapse loads are high, it will not exhibit a significantly better resistance than a discontinuously reinforced frame. Therefore, current ACI provisions that require continuous reinforcement in perimeter beams are not sufficient to resist progressive collapse of the frame.

- The specimen with partial height infill walls did not perform significantly better than the specimen without it. Therefore, partial height non-grouted walls may not be significant in increasing the collapse resistance of a frame.
- Both compressive arch and catenary action are viable resistance mechanisms in frames under a collapse loading. Compressive arch action in a discontinuous frame was only able to provide 40 % of the strength of the flexural action in a continuously reinforced frame, while catenary tension was able to provide approximately the same amount of the strength for both. Therefore, if methods are developed to determine these capacities, they can be incorporated into design guidelines and could reduce the required sizes and reinforcement of structural members.

The test results and conclusions highlight the need for the following future research that can be performed in this field:

- More tests need to be done on the same frame designs as were in this research in order to verify the results. One test per frame design does not guarantee accurate results.
- Tests need to be performed on frames that combine continuous reinforcement and infill walls to determine how effective they can be together.

- Tests need to be performed on frames with infill walls of different heights and reinforcement to determine how much this affects the compressive arch action capacity.
- Dynamic tests need to be performed to replicate the actual loading conditions under collapse and compared with the static tests' results.
- Tests need to be performed on full scale frames in order to get more accurate results. When testing scaled down models, it is impossible to tell how much scaling affects the performance.
- Tests need to be conducted that include a reinforced concrete slab to compare to those without a slab.
- Analysis methods need to be developed to predict the capacities of compressive arch action and catenary tension.

REFERENCES

American Concrete Institute. (1971). "Building Code Requirements for Reinforced Concrete (318-71)." Detroit, MI.

American Concrete Institute. (1989). "Building Code Requirements for Structural Concrete (318-89)." Farmington Hills, MI.

American Concrete Institute. (2008). "Building Code Requirements for Structural Concrete (318-08)." Farmington Hills, MI.

American Society of Civil Engineers (ASCE). (2005). "Minimum Design Loads for Buildings and Other Structures (SEI/ASCE 7/05)." Reston, VA.

American Society of Testing and Materials (ASTM). (2008). "Standard Test Methods." West Conshohocken, PA.

Breen, J.E. (1975). "Summary Report Research Workshop on Progressive Collapse of Building Structures." Austin TX, November 18-20, 1975.

Corley, G.W. (2004). "Lessons learned on Improving Resistance of Buildings to Terrorist Attacks." *Journal of Performance of Constructed Facilities*, May 2004, pp 68-78.

Crawford, J.E. (2002). "Retrofit Measures to Mitigate Progressive Collapse." *NIST/NIBS Multihazard Mitigation Council National Workshop on Prevention of Progressive Collapse*, Chicago, IL, July 2002.

Department of Defense (DoD). (2004). "Design of Buildings to Resist Progressive Collapse." Unified Facilities Criteria (UFC) 4-023-03, July 2004.

Department of Defense (DoD). (2009). "Design of Buildings to Resist Progressive Collapse." Unified Facilities Criteria (UFC) 4-023-03, July 2009.

General Services Administration (GSA). (2003). "Progressive Collapse Analysis and Design Guidelines." General Services Administration, June 2003.

Mlakar, P.F., Dusenberry, D.O., Harris, J.R., Haynes, G.A., Phan, L.T., and Sozen, M.A. (2003). "The Pentagon Building Performance Report." *American Society of Civil Engineers*, Reston, VA, 2003.

Nair, R.S. (2004). "Progressive Collapse Basics." February 2, 2006, <http://www.aisc.org/Content/ContentGroups/Documents/ePubs_Conference_Proceedings/ProgressiveCollapsBasics.pdf>.

National Institute of Standard and Technology (NIST). (2007). "Best Practices for Reducing the Potential for Progressive Collapse in Buildings." NISTIR 7396, February 2007.

Orton, Sarah. (2007). "Development of a CFRP System to Provide Continuity in Existing Reinforced Concrete Buildings Vulnerable to Progressive Collapse." Dissertation, 2007.

Pearson, C. and Delatte, N. (2005). M.ASCE2 "Ronan Point Apartment Tower Collapse and its Effect on Building Codes" *Journal of Performance of Constructed Facilities*, Vol. 19, No. 2, May 1, 2005.

Regan, P.E. (1975). "Catenary Action in Damaged Concrete Structures." *Industrialization in Concrete Building Construction, ACI SP-48*, 1975. pp191-225.

Ruth, P., Marchand, K. A., and Williamson, E. B. (2006). "Static Equivalency in Progressive Collapse Alternate Path Analysis: Reducing Conservatism While Retraining Structural Integrity." *Journal of Performance of Constructed Facilities*, 20 (4), 2006, pp. 349-364.

Sasani, M. and Kropelnicki, J. (2007). "Progressive Collapse Anslysis of an RC Structure." The Structural Design of Tall and Special Buildings (in press), Wiley Interscience, 2007.

Sasani, M. and Sagiroglu, S. (2007). "Progressive Collapse Resistance of Hotel San Diego." *Journal of Structural Engineering*, 134 (4), March 2007, pp. 478-488.

Sucuoglu, H., Citipitioglu, E., and Altin, S. (1994). "Resistance Mechanisms in RC Building Frames Subjected to Column Failure." *Journal of Structural Engineering*, 120 (3), March 1994, pp. 765-782.

Su, Y., Tian, Y., and Song, X. (2009). "Progressive Collapse Resistance of Axially-Restrained Frame Beams." *ACI Structural Journal*, 106 (5), 2009, pp. 600-607.

Vishay Measurements Group Education Division. (1992). "Student Manual for Strain Gage Technology." Raleigh, NC, 1992.

Wong, L.H. (2002). "Design and Detailing for Catenary Action." January 17, 2004, <http://www.eptc.com.sg/E-Learning/Catenary_Design.pdf> .

Yi, W.J., He, Q.F., Xiao, Y., and Kunnath, S.K. (2008). "Experimental Study on Progressive Collapse-Resistant Behavior of Reinforced Concrete Frame Structures." *ACI Structural Journal*, V.105, No. 4, July-August 2008, pp. 433-439.